**UNIVERSITÀ DEGLI STUDI DI CATANIA**

**IN CONVENZIONE CON**

**UNIVERSITÀ DEGLI STUDI DI PALERMO**

---

**DOTTORATO DI RICERCA IN**

**SCIENZA DEI MATERIALI E NANOTECNOLOGIE - XXX CICLO**

---

EMANUELE LUIGI SCIUTO

# *DEVELOPMENT OF INNOVATIVE TECHNOLOGIES FOR DNA EXTRACTION AND DETECTION*

TUTOR: DOTT.SSA SABRINA CONOCI

TUTOR DIDATTICO: PROF.SSA MARIA GRAZIA GRIMALDI

COORDINATORE: PROF.SSA MARIA GRAZIA GRIMALDI

---

TESI PER IL CONSEGUIMENTO DEL TITOLO DI DOTTORE DI RICERCA

# SUMMARY

# 1. INTRODUCTION

DNA is the code of life for every living being. However, the scientific knowledge about the structure and functioning of DNA is quite recent. Only in the 1950's, James Watson and Francis Crick discovered its chemical structure and were awarded the Nobel Prize for Medicine in 1962. Since then, the research on this molecule has been multiplied exponentially. Today, thanks to these discoveries, we have achieved fundamental progress in the diagnosis and treatment of many diseases.

In 2000, the International Consortium of the Human Genome Project announced the decoding of the whole nucleic acid sequence of human DNA or, in other words, the sequencing of the human genome. So today we know the exact order of succession of “bases” in the whole sequence, which is about three billion bases long for human being. Nowadays the sequence of thousands of genomes is known and this number is enormously increased in the last years. According to data reported in the GeneBank data-base (*GeneBank* *https://www.ncbi.nlm.nih.gov/nucgss/* ) the sequencing of about 2350 viruses, 14800 bacteria and 2100 Eukaryote organisms (included our specie, homo sapiens) has been reached, with an active propulsion in this direction achieved in the last five years (Fig. 1). This has impressively made progresses in many fields including anthropology, forensic and, particularly, medicine. In fact, the molecular analysis of nucleic acids (DNA, RNA) operated a real disruptive innovation in healthcare area being effective in early diagnosis, personalized therapy and preventive cancer screening, helping healthcare professionals to prescribe accurate therapeutic interventions. This opened innovative medical perspectives in many fields of medicine including infectious diseases, oncology, pharmacogenomics, genetic

diseases, diabetes, forensic, and neurological, cardiovascular diseases, going towards a deep revolution in terms of high throughput pathologies characterization and personalized therapies.

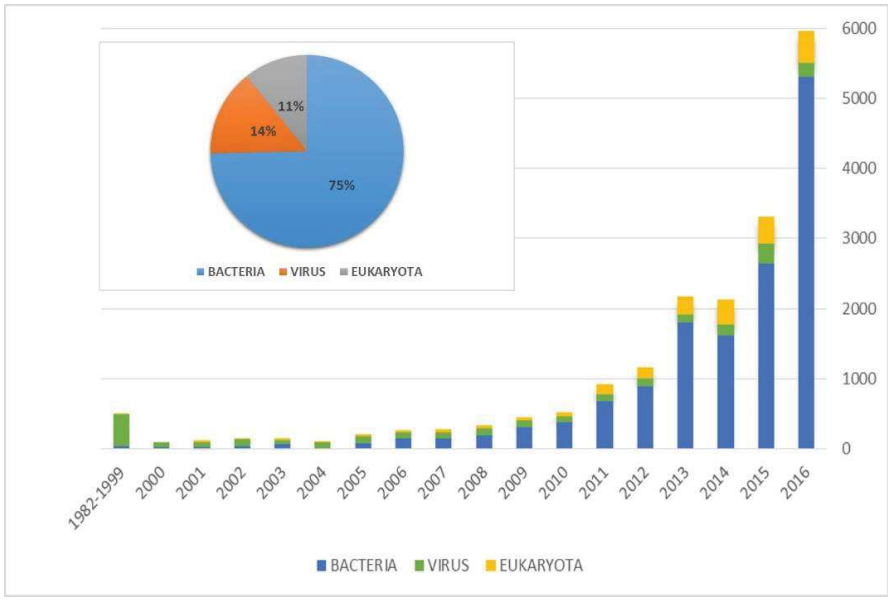


**Fig.1.** Number of sequenced genomes submitted to NCBI for Virus (green bar), Bacteria (blue bar) and Eukaryotic kingdoms (yellow bar). (*GeneBank* https://www.ncbi.nlm.nih.gov/nucgss/)

In last decade, the DNA analysis for molecular diagnosis evolved from genomic to epigenetic analysis.

DNA analysis can address different applicative approaches:

- *Analysis of SNPs* (Single Nucleotide Polymorfism). SNP is a difference in a single nucleotide in a specific target gene (for example, a SNP may replace the nucleotide cytosine (C) with the nucleotide thymine (T)). They are very important being correlated with some human genetic diseases (i.e. sickle cell anaemia) together with prediction of an individual's response to certain drugs, susceptibility to environmental factors such as toxins, and risk of developing particular diseases.
- *Analysis of gene expression*. It consists in the analysis of the DNA sequences (genes) expressed (translated in mRNA) in the cell. This type of analysis (usually carried out by

microarray biochip [1], focusing the finding of expression level of target genes, related to some specific intracellular pathway.

- *Identification of unknown sequences*. It is particular relevant in the diagnosis of infectious diseases where the DNA analysis offers the advantages to know the specific bacteria specie o mutated virus.

Whatever would be the application, experimental techniques for DNA analysis should present two primary features: specificity, in order decodify the sequence as precisely as possible, and sensibility, to go deeply in genome and transcriptome quantification. Related to this, *Real-Time PCR (Polymerase Chain Reaction)* is the gold standard biotechnology for DNA analysis.

*PCR* is a molecular reaction discovered by the American biochemist Kary B. Mullis in 1983 [2]. It is based on the cyclic amplification of a specific DNA target sequence by a couple of small complementary oligoribonucleotides (primers) and a thermostable Taq Polymerase enzyme acting as catalyst of the amplification reaction.

Real-Time PCR (qPCR) is an advanced version of this reaction, improved by the introduction of a fluorescent probe, able to label the target sequence during its amplification [3]. The fluorescent probe can bound DNA in a specific or non-specific way. The first one is referred to fluorescent probes such as TaqMan, Molecular Beacon and Scorpions. In this case, the fluorophore is linked to one of the two ends of the probe sequence and this is complementary to a specific region inside the target gene [4]. The non-specific labeling, instead, is related to probes such as SYBR® Green, which bound the target intercalating into its DNA minor grooves, thus, without any hybridization [5].

Fig.2 reports the Real-Time PCR mechanism using specific fluorescent probes for detection (*TaqMan*). Chapter 2 will describe the PCR mechanism in detail.

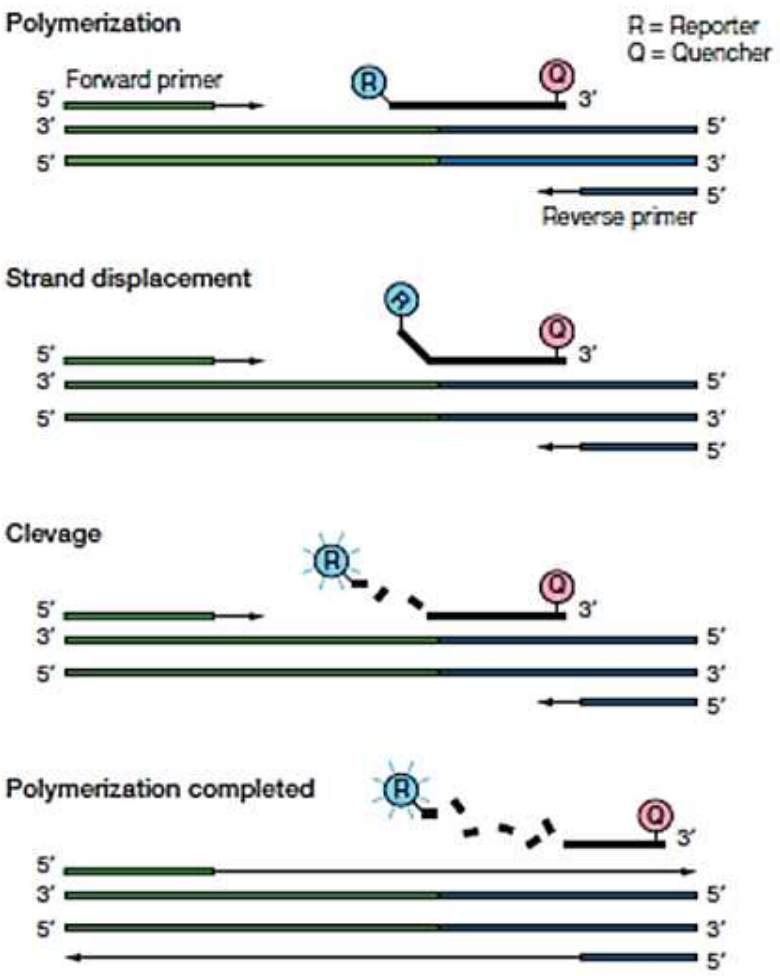


**Fig.2.** Real-Time PCR mechanism using specific fluorescent probes for detection (*TaqMan*).

Though technologies such as Real-Time PCR are rapidly diffusing in biomedical field, their massive use is strongly limited due to their experimental procedures requiring:

- *Specialized staff*
- *Complex protocols addressing not only the detection of DNA via RT-PCR but also the extraction from cells.*
- *Expensive instruments*

In order to overpass these limitations, my Ph.D. project has been focused on the development of fast, multiplex, innovative and easy-to-use technological platforms for DNA analysis (from extraction to detection), implemented into portable and miniaturized devices. These types of

technologies are called Point-of-Care (PoC) and could create the conditions for a more efficient clinical analysis, introducing a series of advantages:

- *Fast and cheap procedures for biological samples preparation and analysis*
- *Fast diagnosis*
- *Identification and analysis of different DNA mutations (complex phenotypes and drug-resistance related)*
- *Disease-specific and therapy-specific pattern definition*

My research activity has been divided into three main parts, which will be described in the subsequent chapters:

1. **Development and characterization of a miniaturized platform for DNA extraction.**
2. **Development and characterization of miniaturized systems for DNA detection with both optical transduction methods (via RT-PCR) and electrical methods (electrochemical detection).**
3. **Development of molecular methods for the detection of environmental analytes.**

## *References*


1. Schena M., Microarray Analysis, - Wiley, ISBN: 978-0-471-41443-8.
2. Mullis K., Faloona F., Scharf S., Saiki R., Horn G. and Erlich H. (1986), Specific Enzymatic Amplification of DNA In Vitro: The Polymerase Chain Reaction, Cold Spring Harbor Symposium on Quantitative Biology 51 : 263.
3. Valasek M.A., Repa J.J. (2005), The power of real-time PCR, Advances in Physiology Education Published 1 September, 67.
4. Filion M. (2012), Quantitative Real-time PCR in Applied Microbiology, Caster Academic Press, Norfolk.
5. Zipper H. et al. (2004), Investigations on DNA intercalation and surface binding by SYBR Green I, its structure determination and methodological implications, Nucleic Acids Res. 32(12) : e103.

# 2. CURRENT METHODOLOGIES IN DNA ANALYSIS

DNA analysis is a crucial point for a wide range of applications, including environmental monitoring of bacterial and viral contamination, food control, homeland security and, above all, clinical diagnostics. For these applications, in fact, traditional approaches commonly used in the laboratory involved phenotypic techniques such as detection via antibody recognition and plate counting. However, these methods were affected by a series of limitations, in terms of complexity of experimental procedure adopted, costs and time consuming (48 hours to have a result in the case of plate counting) and low sensitivity (antibody methods).

In this sense, genotypic methods, based on nucleic acids detection, made a real revolution in the biological diagnosis, thanks to their ability to combine high specificity and sensitivity with precise quantification and fast response.

To execute the DNA molecular analysis, several analytical steps need to be accomplished. First of all, (a) the NA extraction from biological samples, *i.e.* blood, urine, saliva, swab (sample prep); then, (b) the target sequence amplification (PCR) and finally, (c) the detection of the amplified product (Fig.1).

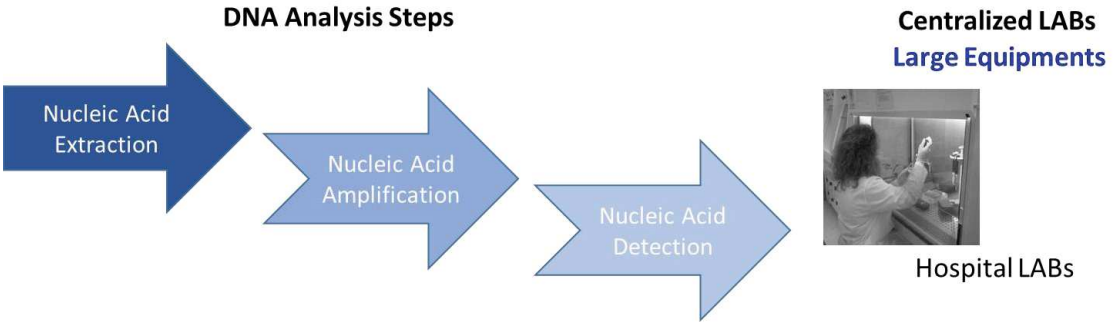


**Fig.1.** Schematic illustration of DNA analysis

In this chapter, we will describe the *state of art* of methods and protocols for DNA analysis, from extraction to amplification and detection.

## 2.1 – DNA Extraction Methods

DNA purification is a preliminary step for all genetic diagnostic technologies.

The isolation and collection of genetic material from a biological sample of any species (virus, bacterial, yeast, animal cell or plant cell) and origin (blood, urine, saliva fluid or tissue biopsy) basically comprises four main phases:

1. Lysis of cells structure from sample
2. RNA and protein degradation
3. DNA separation from cell debris (binding and washing steps)
4. DNA isolation and collection (elution step)

The lysis of cells structure is focused on the denaturation of cell membrane and other intracellular compartmentalisations, so that all genetic material can be purified and released. Cell lysis, and production of debris, is usually performed by using physical manipulations such as sonication, boiling, freeze–thaw cycles [1,2] and chemical agents such as Sodium dodecyl sulphate or Triton X-100 detergents, which alter the lipid-lipid associations inside membrane causing its “dissolution”. Once released the intracellular material (DNA, RNA, proteins, polysaccharides, metals, salts, organic compounds, and dyes), RNA and proteins are degraded by enzymatic reaction by means of RNAase and protease added to the purification system.

After all degradation phases, DNA must be separated and isolated from the cell debris. For this purpose, different approaches have been developed to increase the yield of genetic material after purification. This because is important to keep as much DNA as possible, during all isolation steps, avoiding loss of material before the final elution.

The literature reports different examples of DNA purification methods and many of these are developed using plastic materials and include a complex fluidic network that manages fluid

movement such us mixing, splitting etc. etc. Strategies for DNA separation evolved from liquid–liquid purification method, such as isolation by precipitation with phenol-chloroform, to most advanced liquid–solid purification systems, mostly, based on silica in the form of micro-filter mounted in a plastic column or layers covering magnetic beads.

DNA *phenol-chloroform based purification* is a conventional method in which proteins, lipids, carbohydrates, and all others cell debris are removed through extraction of the aqueous phase with the organic mixture of phenol and chloroform [3,4]. Phenol denatures proteins, which stay in the organic downer phase, whereas the DNA is in the aqueous upper phase (Fig.2A). Thus, a biphasic emulsion forms when phenol and chloroform are added. The upper phase, then, is collected and DNA can be precipitated from the supernatant by adding ethanol or isopropanol and high concentration of salt. DNA precipitate is, then, collected by centrifugation and dissolved with TE buffer or sterile distilled water (Fig.2B).

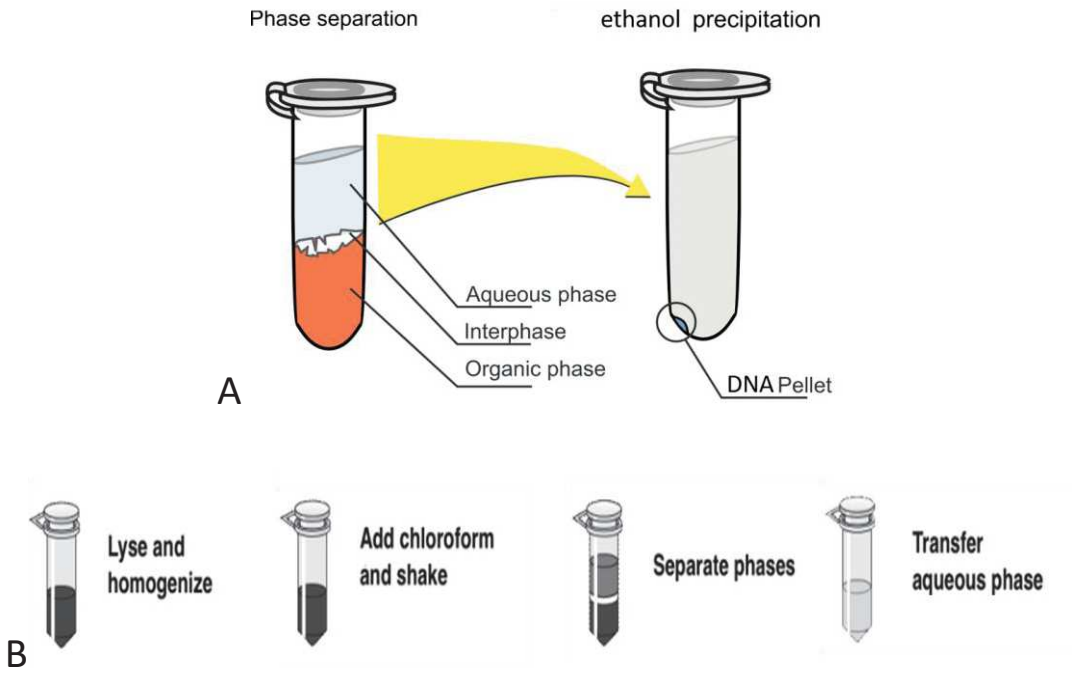


**Fig.2.** A) Phase distribution and ethanol precipitation in phenol-chloroform DNA extraction; B) Phenol-chloroform based purification protocol.

However, a common drawback for this type of DNA purification method is related to the procedure itself, which is basically time and cost-consuming, labor intensive, dangerous (because of the use of hazardous chemicals) and low yields. Moreover, since is totally manual, there is also a strong risk of cross-contamination, thus, affecting the purity of the final product.

For these reasons, more automated solid phase extraction became the most common methods for DNA purification, since they include minimal hazardous chemicals, easier manipulations and increased efficiency. Any of the solid phase system, based on affinity chromatography by reversible surface adsorption, can be incorporated into a spin filter or column, or can imply the use of other surfaces such as beads.

*Separation of DNA by plastic filtered spin columns* (i.e. Qiagen kits) is obtained by a series of centrifugations of sample in plastic tubes [5]. Theses tubes contain a silica filter on which surface, step-by-step, is collected and adsorbed the DNA to be purified (Fig.3A). Cells from biological sample, previously degraded using lysis buffers, are applied to the columns and centrifuged, and the DNA binds to the column using the appropriate pH and salt concentration conditions, provided by binding solutions. Some proteins and other debris may also bind the column, but they are later removed using washing buffers containing competitive agents during a series of washing steps. In this way, DNA molecules, adsorbed on the silica filter, are separated from cell debris. DNA is eluted, finally, in sterile distilled water or TE buffer. (Fig.3B). Kits with silica spin filters are fast to perform and do not require hazardous chemicals.

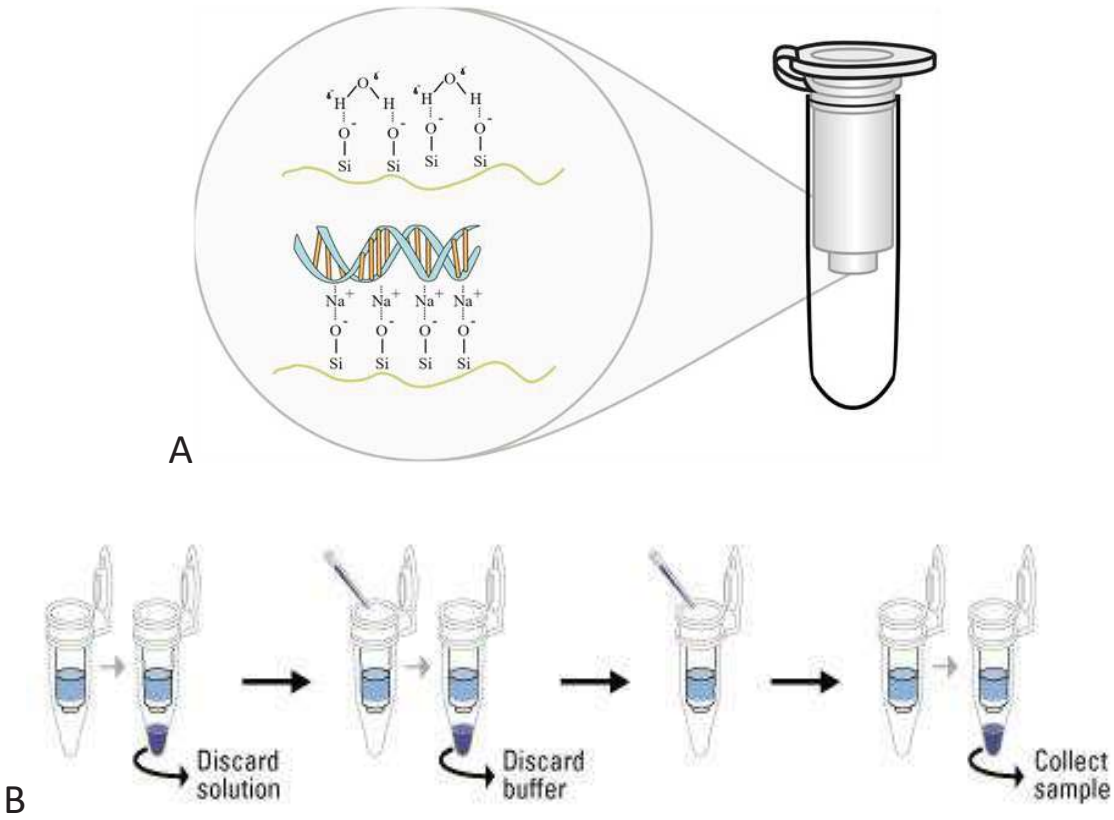


**Fig.3**. (A) Scheme of DNA-silica filter adsorption mechanism; B) DNA spin-column purification protocol.

A drawback, however, is that filters can be saturated with thick samples and many steps are required to load the binding, washing, and elution solutions.

*Separation by paramagnetic beads* (i.e. Magazorb kit). It is based on the electrostatic interaction between the DNA molecules and magnetic beads covered by silica surface [6]. Inside the tubes containing DNA and cell debris in solution after the lysis step, magnetic nanoparticles are added to this mixture, followed by the addition of binding buffer (1.25 M sodium chloride and 10% polyethylene glycol), which composition creates cation bridges for DNA-silica interaction with beads surface (Fig.4A). The solution is mixed by inversion and incubated for 3 minutes at room temperature. Then, the tubes are located in a magnetic rack and thanks to the attraction of beads by the magnet, the washing and discarding of debris can be performed avoiding the risk of DNA

loss. The magnetic pellet is, finally, resuspended in TE buffer and DNA is eluted (Fig.4B). Surface binding capacity is determined by the area available for binding.

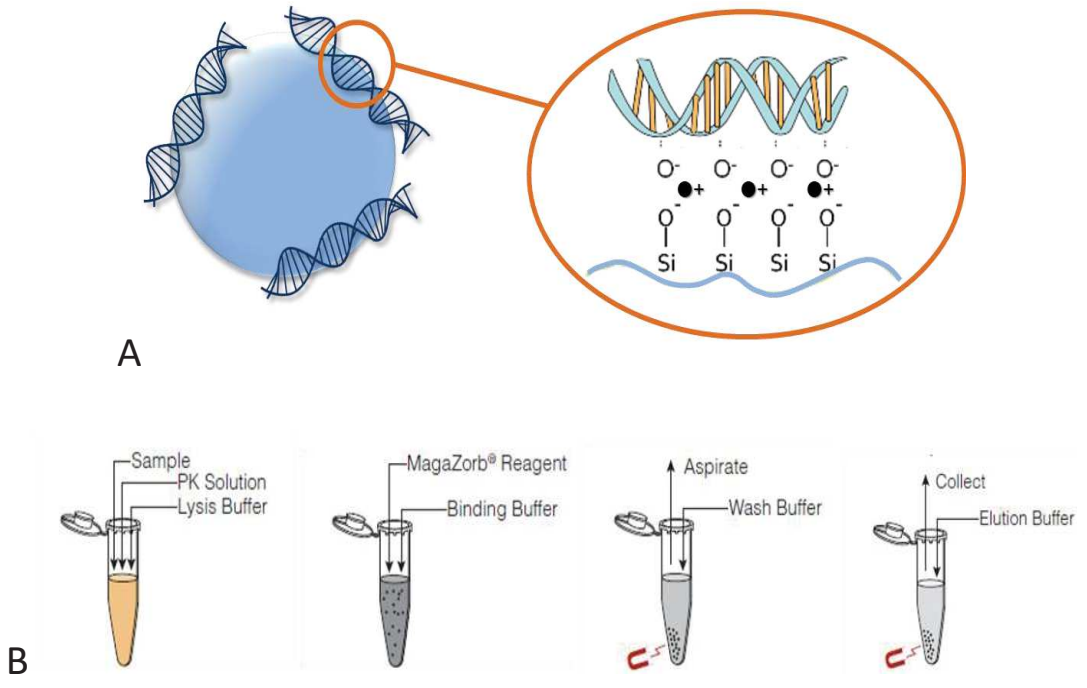


**Fig.4.** A) Scheme of DNA-bead adsorption mechanism; B) Protocol of DNA purification by paramagnetic beads.

Sometimes silica is derivatized with positive amino-groups to bind the negatively charged DNA more effectively than naked silica. A drawback of the current extraction protocol, however, is that the use of ethanol and chaotropic salts can inhibit the PCR reaction or other molecular techniques downstream the DNA purification.

Despite the improvement in terms of yield quality and protocol safety, solid phase extraction methods still have many widespread limitations.

One of those is the volume and the amount of biological sample required to trigger all procedure for purification. From liquid-liquid to solid-phase extraction, in fact, hundreds of microliters to millilitres volumes are used; this implies invasive biological samplings from patients for diagnosis.

Another common drawback is the miniaturization and integration of the purification technology in a single portable device. A lot of stuff is required to perform the whole experiment of genetic material isolation, frequently with a complex architecture to manage the fluidic steps, which implies an increase of the design complexity, high costs and a laboratory with dedicated and specialized staff.

Finally, there is also a problem related to the material used for DNA purification. Plastic is the mostly used for tubes and other standard equipment of commercial kits. However, plastic material is not the best choice in terms of miniaturization, integration and thermal properties, thus remaining a huge limitation.

A solution to all the drawbacks above reported is offered by the microfluidic technology [7]. Microfluidic platforms are extremely attractive thanks to the number of advantages, they present, compared to macroscopic equivalents. The small volumes, required for the experimental setup, reduce sample and reagent consumption. Reduced size of device implies the possibility of miniaturization and integration together with a higher surface-to-volume ratio; this means that the exchange areas for DNA molecules transport are larger, allowing an excellent quality separation and purification of genetic material from cell debris.

Moreover, most of the microfluidic technologies developed so far can be combined with silicon material. Silicon is a very appealing material for DNA purification, thanks to various physical aspects such as low heat capacity, good thermal conductivity and possible patterned structures to increase the surface–area ratio, with consolidated production technologies and industrialization processes at high volume. Additionally, it allows the integration of electrodes and microelectronics circuitry that imprint the so-called “intelligence on board”.

In this sense, in the DNA extraction module of my Ph.D. project, I worked on the interesting approach involving the microfabricated silicon pillars. It merges the advantages to increase the

surface within the capture area with the possibility to be monolithically integrated into a miniaturized device. As described in detail in the chapter 3, the studies reported in this thesis involving pre-analytical samples (pre-purified DNA) on cells, proved this approach having a great potential towards the development of a genetic point-of-care device.

## 2.2 – DNA Detection Methods

As described in the chapter 1 of this thesis, the discovering of the PCR method by Kary Mullis made a revolution in the DNA analysis.

In the last years, the quality of the DNA analysis evolved following the innovation of PCR method. This because, so far, DNA amplification was the best choice for genetic detection able to guarantee high sensitivity and specificity starting from samples where the DNA target is in a very low concentration (LoD < 100 copies per ml of biological sample).

*PCR* is based on the cyclic amplification of a specific DNA target sequence by a couple of small complementary oligoribonucleotides (primers) and a thermostable Taq Polymerase enzyme acting as catalyst of the amplification reaction. The primer pair (Foward and Reverse) is used to increase, by various amplification cycles, the number of copies of the target gene in an exponential way, starting from a small amount of DNA template; then, the final product (amplicon) can be studied by a both qualitative and quantitative analysis. More in details, each amplification cycle is divided into three phases (Fig.5):

1) *denaturation* of the DNA strand, so that the two strands of the target gene can be amplified separately.
2) *annealing* of the primer pair, according to complementarity between primers and target gene sequence.

3) primer *extension* by synthesizing a complementary strand from each one of the target template, forming the final amplicon.

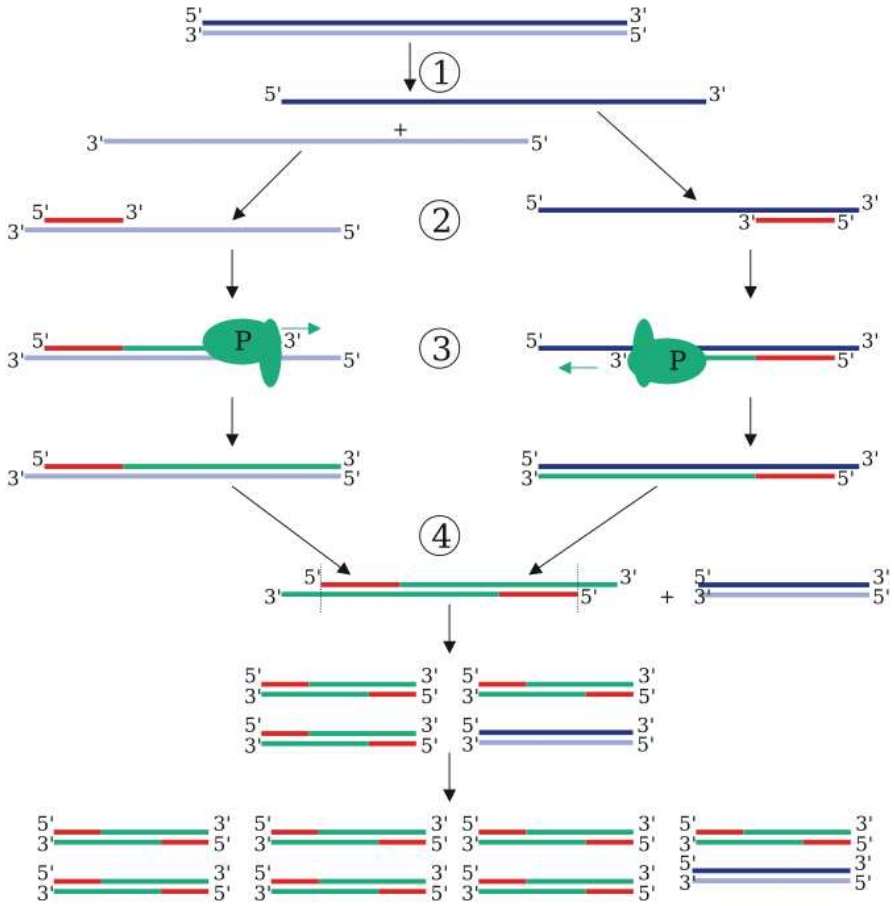


**Fig.5.** PCR scheme: (1) denaturation; (2) annealing; (3) extension; (4) final product.

In the DNA analysis, PCR was firstly used to amplify the starting genetic material before detection. On that, several methods have been developed.

*Southern blotting* is one of the earliest techniques based on DNA amplification for genotypic analysis; it is from Edwin Mellor Southern [8] and is a technique for DNA detection in a complex biological matrix. After an electrophoretic running, a gel containing amplified genetic targets, to be detected, is immersed in an alkaline solution and, then, covered by a nitrocellulose or nylon membrane, with a pile of adsorbent paper above. Thanks to the capillarity effect, alkaline solution

together with genetic material (from electrophoresis) starts going up from the gel towards the paper, causing the deposition of DNA samples on the nitrocellulose membrane. Once completed the migration of DNA, the membrane is immersed in another solution containing PCR oligonucleotides probes (labelled by fluorescent or radioactive dyes) specific for the genetic targets on membrane. In this way, probes can hybridize with the complementary DNA target and, after a washing step, allowing its identification by the optical detection of dye from probes (Fig.6).

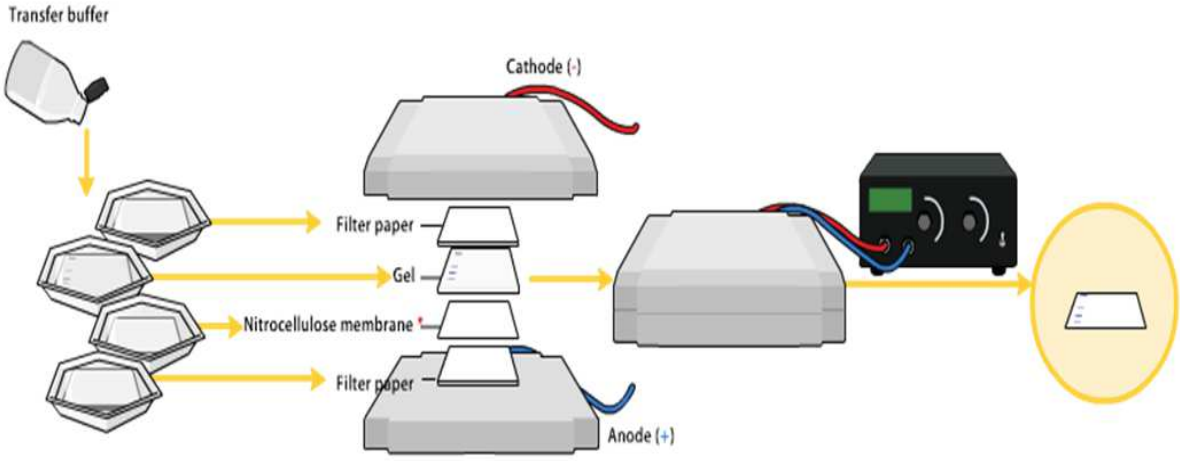


**Fig. 6**. Southern blotting method.

DNA molecular analysis, however, spreads with the introduction of multiplex and fast DNA detection platforms, such as *DNA-microarray*. It can be considered the first biochip and consists in a miniaturized system for fast, sensitive and high throughput genetic analysis of biologically relevant samples. The method is based on the reverse probes-target hybridization, which means an interaction between fixed probes and floating genetic targets from samples (Fig. 7).

Oligonucleotide probes (ssDNA) are spotted on the surface of a plastic, glass or silicon slide, in order to create an array in which each spot is specific for one of the DNA targets to be identified. In parallel, genetic targets, once amplified from biological samples by PCR, are labelled with different fluorescent dyes (such as Cyanine, Fluorescein, Rodhamine), one for type of target, and

released on the array for the hybridization with complementary probes. The intensity of the signal is used to determine the number of bound molecules.

The main feature and advantage related to this technique is the possibility to test hundreds of targets in a single reaction, thanks to the simultaneous detection of fluorescent signals, from spots containing specific labelling for specific targets hybridized in the microarray (Fig. 7). The multiplex detection is obtained exciting dyes of targets with two or more laser sources (at different wavelength) and collecting the signals by a unique CCD detector.

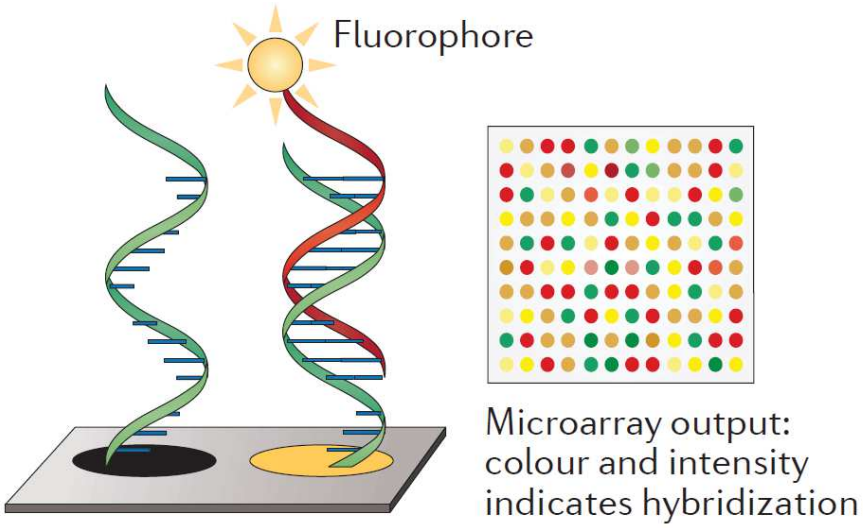


**Fig. 7.** DNA-microarray scheme.

Microarrays are used in many applications. Single-nucleotide polymorphism (SNP) arrays identify common polymorphisms associated with disease and phenotype, DNA–protein interactions and gene expression levels (by measuring the amount of gene-specific cDNA). Microarrays remain widely used in genomic research. However, variations in hybridizations are problematic, leading some people to recommend sequencing over gene expression microarrays.

*Sequencing* is a DNA amplification based method that overpass the limitations in genotypic analysis related to sensitivity and specificity.

The first sequencing approach was introduced by Fred Sanger in 1970s. This technique was based on the reconstruction of a DNA target sequence by the detection of a specific dideoxynucleoside

triphosphate (ddNTP) insertion into the DNA target amplification system. The detection is performed radiographically on the polyacrylamide gel electrophoresis (PAGE) [9,10].

First, DNA target template is amplified by using 4 different mixes containing one of the 4 specific ddNTPs (ddATP, ddGTP, ddCTP, ddTTP) and the amplification reagents (polymerase, primers, dNTPs).

Then, amplification products are loaded separately in 4 wells of the electrophoretic gel. After the run, different bands on the same lane appear; in this case, the varied sizes of bands are related to the position of the ddNTP insertion (that stopped the amplification process and broke up the target sequence). Since each lane of the gel contains a specific ddNTP amplification mix, reading bands (so amplification fragments) from the smallest to the biggest, allows the reconstruction of the total DNA target sequence (Fig.8).

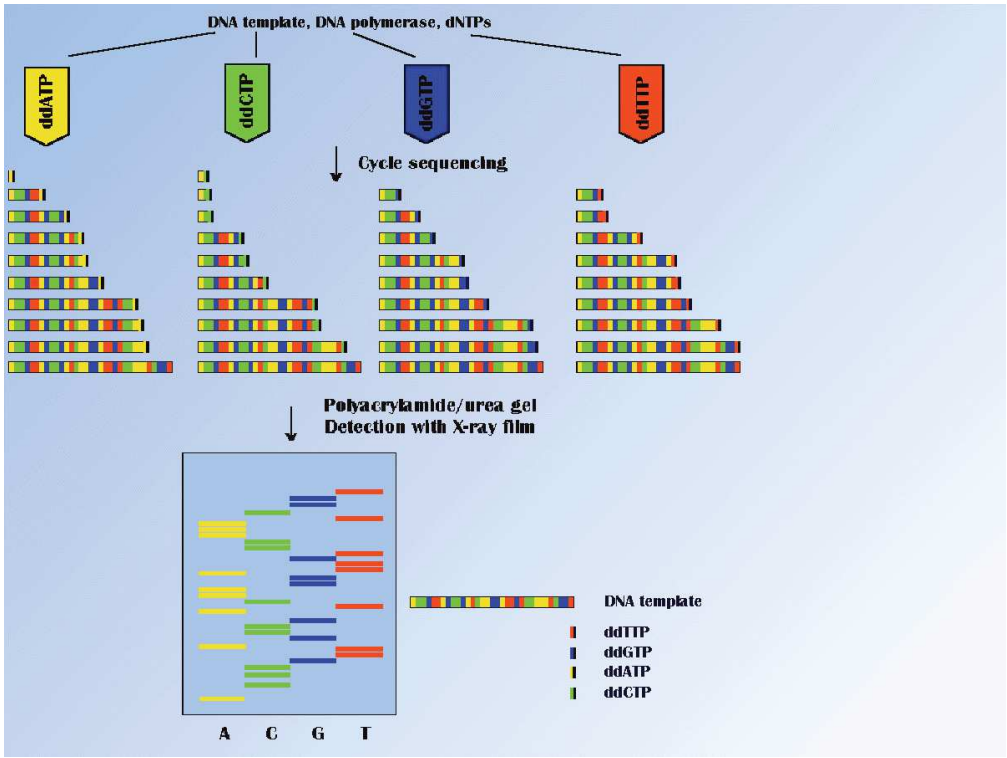


**Fig.8.** Sanger sequencing method.

Sanger sequencing has been improved, getting automated and faster, thanks to the replacement of the radiographic detection with the fluorescent one (using separate fluorescent markers for each nucleotide) and the replacement of PAGE running with capillary electrophoresis (Fig.9) [11].

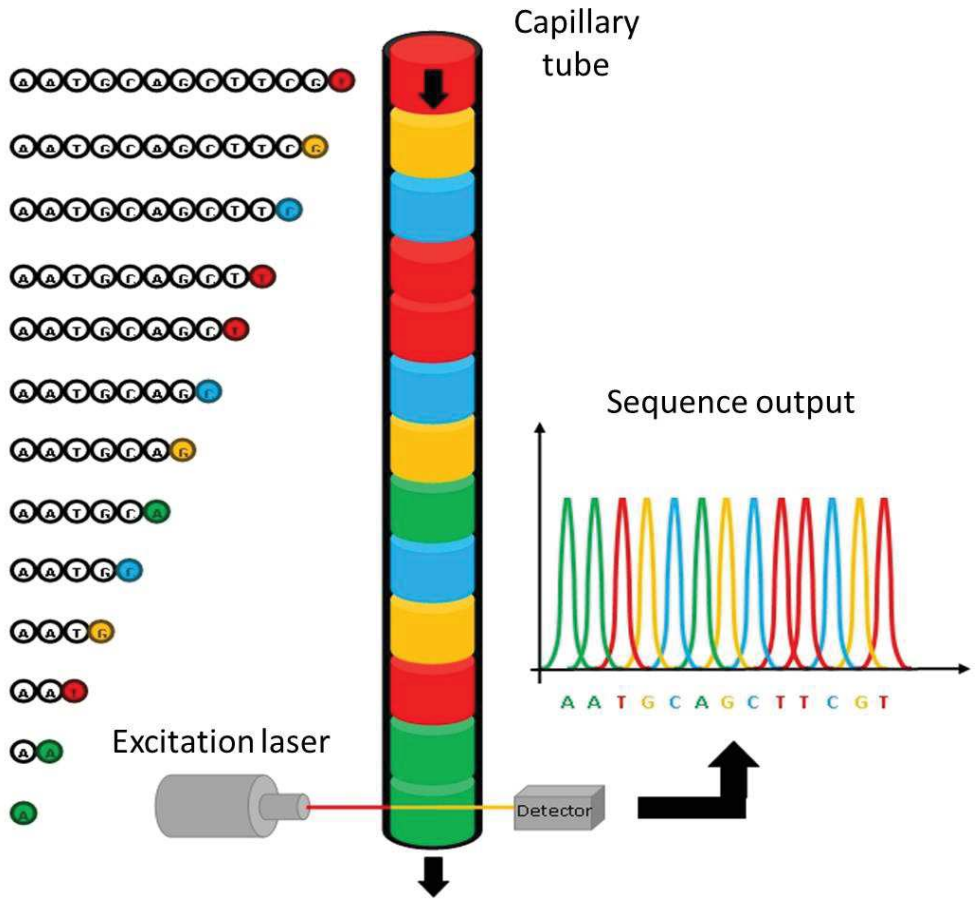


**Fig.9.** Sanger automated sequencing method; as each band of colour (caused by collections of dye terminated fragments, on the left in figure) pass in front the detector, through the capillary tube, it creates a fluorescent signal which is reported on the final graph.

This technique, however, suffered from few inherent limitations like decreased sensitivity for low level mutant alleles, complexities in analysing highly polymorphic regions, high amount of DNA template required, and low number of DNA sequences reconstructed per time.

Thus, Roche, Illumina and other commercial manufacturers introduced several Next Generation Sequencing (NGS) technologies in order to overcome Sanger sequencing limitations.

The Roche innovation is based on the pyrosequencing method, in which the target DNA sequence is reconstructed thanks to a luminescent reaction triggered by the incorporation of a dNTP during the DNA amplification; in this case, in fact, the dNTP releases a pyrophosphate group (PPi) each time is incorporated in the polymerization process. The PPi is, then, used by the ATP sulfurylase to produce ATP in presence of adenosine 5´ phosphosulfate. ATP triggers the reaction of luciferin oxidation by luciferase, releasing oxyluciferin and photons. The light produced in the luciferase-catalyzed reaction is detected by a camera and analyzed in a pyrogram. The excess or not incorporated bases are removed by the apyrase enzyme. This process is repeated with each of the four bases until the DNA sequence of the single strand template is determined (Fig.10).

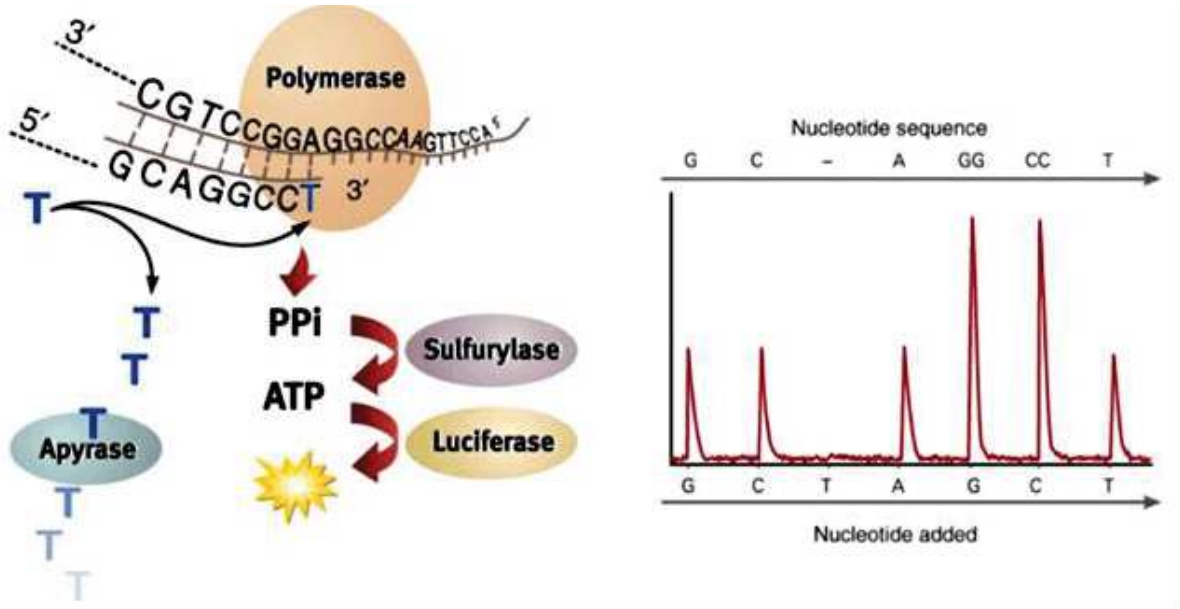


**Fig.10.** Pyrosequencing scheme.

The template DNA is fixed, and solutions of A, C, G, and T nucleotides are sequentially added and removed from the reaction. Light is produced only when the nucleotide solution complements the first unpaired base of the template. The sequence of amplification mixes which produce

chemiluminescent signals (thus forming the final pyrogram) allows the determination of the sequence of the target DNA [12].

Illumina method is based on the massive sequencing of a target DNA by solid-phase PCR. In this case, the DNA is first nebulized and 200 bp fragments are obtained. The fragments are, then, ligated to specific oligonucleotides adapters, at both ends, in order to be immobilized on the surface of a glass flow cell, which contains arrays of alternate primers for the solid-phase bridge PCR amplification step. DNA fragments, in fact, binds the primers thanks to the adapters, and, once anchored, create bridges by which are massively amplified [13,14]. The amplification generates clusters of copies from a specific DNA fragment (Fig. 11A).

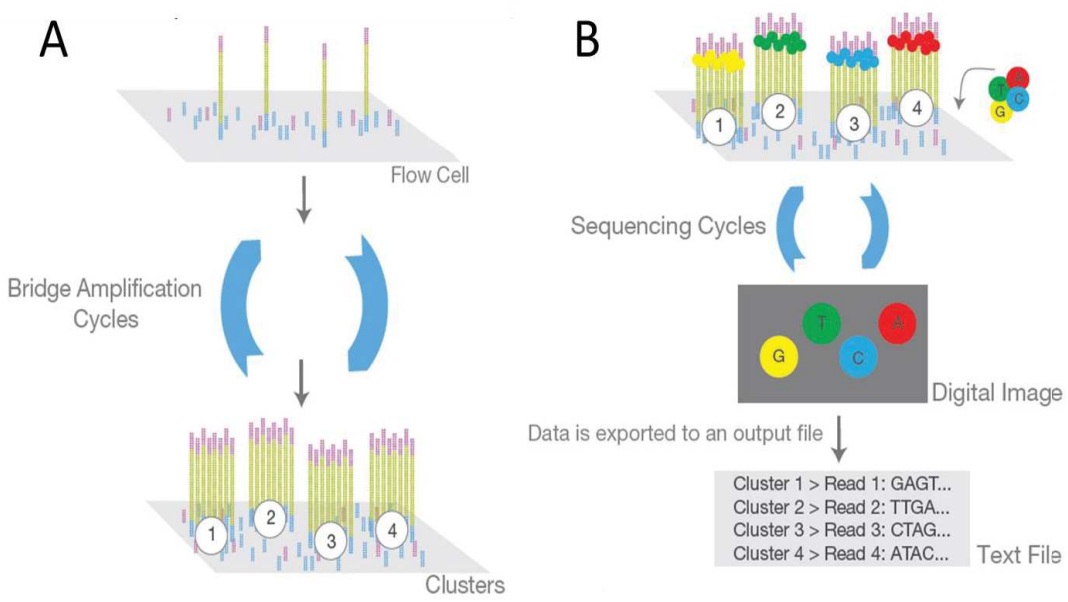


**Fig.11.** Illumina sequencing method: A) clustering of 200 bp DNA fragments by solid-phase bridge PCR; B) sequencing of clusters and fluorescent imaging.

These clusters are, then, used for the last step of sequencing, performed by adding primers on one of the ends of the molecules and by introducing specific dNTPs to the flow cell; these are modified to terminate the polymerization of the growing sequence and are labelled with specific fluorescent dyes, one for each type of bases (similarly to the Sanger automated sequencing method).

Depending on the type of dNTP incorporated, for each cycle of sequencing the system gives a specific fluorescent signal that is collected by a CCD camera and digitalized in order to obtain a fluorescent mapping of DNA fragments clusters (Fig. 11B). The Illumina read length is approximately 35 bases, but over billion reads are generated at a time.

NGS techniques in clinical research and medical diagnostics were applied for the study of cancer variants, detection of minimal residual disease, exome sequencing, detection of Single Nucleotide Polymorphisms (SNPs) and their disease association, epigenetic regulation of gene expression and sequencing of microorganism genome.

All techniques described, however, are still quite complex to perform, needing specialized laboratories and staff and are rather expensive to be used for large-scale screening.

To allow the extensive use of these molecular methods in diagnostics, scientific research is nowadays strongly focusing on the development of new technologies and devices allowing fast and low-cost DNA analysis. Therefore, there is a huge demand for methods and systems able to perform analysis of DNA in the sample-in-answer-out format, with a sensitivity comparable to that one of conventional PCR technologies and an implementation of portability, in order to move the diagnostics to decentralized environments (Fig.12).

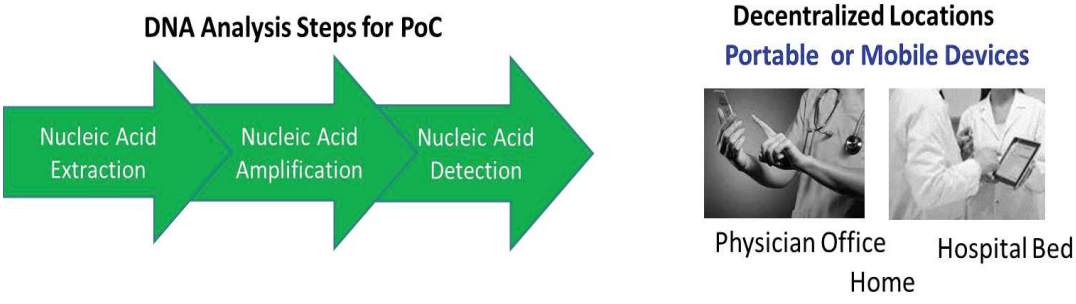


**Fig.12.** Schematic illustration of NA analysis in PoC format

These technologies are the so-called “genetic Point-of-Care” (PoC), identified by the National Institute of Health (NIH) as one of the major priorities for molecular diagnostics [15]. These systems must integrate and automate all steps necessary for molecular analysis such as DNA sample preparation (extraction and purification) and detection.

In the developed world, PoC technologies could help in the decentralization of diagnostics from the hospital’s core laboratory to the physician’s office. This allow massive diagnostic screening and better facing the threat of genetic and infectious diseases. Its clinical utility could be much more relevant, for example, in developing countries where infectious disease diagnosis is still a challenge due to poor clinical laboratory infrastructures and cost constraints [16]. Based on the above considerations, multidisciplinary research teams have spent great efforts over the world to develop miniaturized biosensors based on innovative technologies and new chemical strategies for DNA analysis.

So far, the detection of DNA in PoC is based on the PCR technology for in vitro genetic analysis, directly near the patient (in hospital, in the physician office, clinic, or home).

In literature, for example, various PCR based PoC have been reported for DNA detection of different pathogen microorganisms. Fernandez-Carballo et al. in 2016 presented a portable and low-cost point-of-care (PoC) system based on continuous flow PCR for quantitative detection of Chlamydia trachomatis and Escherichia coli [17]. Hsien et al. described a sequence-specific electrochemical DNA technology (E-DNA) able to detect up to 100 copies per ml of S. typhimurium by loop-mediated isothermal amplification, 10 TCID50 for H1N1 influenza virus, and 300 copies (in 50 µl) of Salmonella *enterica* [18]. Other research teams reported miniaturized devices based on PCR using innovative transduction methods for the detection of pathogen species such as: Escherichia coli (by using piezoelectric-excited cantilever sensors) [19]; Neisseria meningitidis (using electrochemical transduction) [20]; Staphylococcus aureus (by means of graphene oxide

based fluorescent probes) [21]; Mycobacterium tuberculosis (using surface plasmon resonance) [22]. Example of genetic SNP (Single Nucleotide Polymorphisms) application are, also, reported [23].

Following the reported examples, in my Ph.D. project I focused on the introduction of innovative genetic PoC technologies for the detection of pathogen bacterial DNA in infectious diseases.

Actually, I have been working on the development and characterization of PCR-based device for sensitive and high throughput detection of specific target DNA in miniaturized boards, integrating all stuff required for the Real-Time PCR analysis.

Among all PoC platforms reported in literature, however, there is still an unsolved issue related to the experimental procedure required for detection; PCR reaction, in fact, implies high time and costs for samples analysis.

For this reason, I have been working, in parallel, on the introduction of unconventional miniaturized devices for the PCR-free detection of DNA. These methods are more advantageous thanks to the possibility, they gave, to detect molecules of a target DNA without any amplification process, that means avoiding the necessity of specialized staff, long working period and expensive kits for the DNA detection, in addition to all advantages related to the miniaturization [24, 25].

## References


1. Steiner J.J., Poklemba C.J., Fjellstrom R.G. and Elliott L.F. (1995), A rapid one-tube genomic DNA extraction process for PCR and RAPD analyses, Nucleic Acids Res, 23:2569 –70.
2. Johnson D.W., Pieniazek N.J., Griffin D.W., Misener L. and Rose J.B. (1995), Development of a PCR protocol for sensitive detection of Cryptosporidium oocycsts in water samples. Appl Environ Microbiol, 61:3849 –55.
3. Sambrook J. and Russel D. (2001), Molecular Cloning: A Laboratory Manual, vol. 3, Cold Spring Harbor Laboratory Press, New York, NY, USA, 3rd edition.
4. Chomczynski P. and Sacchi N. (2006), The single-step method of RNA isolation by acid guanidinium thiocyanate-phenolchloroform extraction: twenty-something years on, Nature Protocols, vol. 1, no. 2, pp. 581–585.
5. Padhye V.V., York C. and Burkiewiez A. (1997), Nucleic acid purification on silica gel and glass mixture, United States patent US 5658548, Promega Corporation.
6. Berensmeier S. (2006), Magnetic particles for the separation and purification of nucleic acids, Applied Microbiology and Biotechnology, vol. 73, no. 3, pp. 495–504.
7. Kim J., Johnson M., Hill P. and Gale B.K. (2009), Microfluidic sample preparation: cell lysis and nucleic acid purification, Integr Biol, 1:574 – 86.
8. Southern E.M. (1975), Detection of specific sequences among DNA fragments separated by gel electrophoresis, Journal of Molecular Biology. 98 (3): 503–517. ISSN 0022-2836. PMID 1195397. doi:10.1016/S0022-2836(75)80083-0.
9. Sanger F., Coulson A.R. (1975), A rapid method for determining sequences in DNA by primed synthesis with DNA polymerase, J. Mol. Biol. 94 (3): 441–8. PMID 1100841. doi:10.1016/0022-2836(75)90213-2.
10. Sanger F., Nicklen S., Coulson A.R. (1977), DNA sequencing with chain-terminating inhibitors, Proc. Natl. Acad. Sci. U.S.A. 74 (12): 5463–7.

11. Maxam A.M., Gilbert W. (1977), A new method for sequencing DNA, Proc. Natl. Acad. Sci. U.S.A. 74, 560–564.

12. Ronaghi M., Uhlen M., Nyrén P. (1998), A sequencing method based on real-time pyrophosphate, Science 281, 363–365.

13. Luo C., Tsementzi D., Kyrpides N., Read T., Konstantinidis K.T. (2012), Direct comparisons of Illumina vs. Roche 454 sequencing technologies on the same microbial community DNA sample, PLoS One 7.

14. Quail M. A. *et al*. (2012), A tale of three next generation sequencing platforms: comparison of Ion Torrent, Pacific Biosciences and Illumina MiSeq sequencers, BMC Genomics 13, 341.

15. Mabey D., Peeling R.W., Ustianowski A. and Perkins M.D. (2004), Nat. Rev. Microbiol., 2, 231–240.

16. Yager P., Domingo G. J. and Gerdes J. (2008), Annu. Rev. Biomed. Eng., 10, 107–144.

17. Fernández-Carballo B.L. *et al.* (2016), Biomed. Microdevices, 18, 34–40.

18. Hsieh K. *et al.* (2015), Acc. Chem. Res., 48, 911–920 and references therein.

19. Rijal K. and Mutharasan R. (2013), Analyst, 138, 2943– 2950.

20. Patel M.K., Solanki P.R., Kumar A., Khare S. and Gupta S. (2010), Biosens. Bioelectron., 2010, 25, 2586–2591.

21. Pang S., Gao Y., Li Y., Liu S. and Su X. (2013), Analyst, 138, 2749–2754.

22. Hsu S.H., Lin Y.Y., Lu S.H., Tsai I.F., Lu Y.T. and Ho H.S. (2013), Sensors, 14, 458–467.

23. Foglieni B., Brisci A., San Biagio F., Di Pietro P., Petralia S., Conoci S., Ferrari M. and Cremonesi L. (2010), Clin. Chem. Lab. Med., 48, 329–336.

24. Sébastien D. *et al.* (2006) PCR-free DNA detection using a magnetic bead-supported polymeric transducer and microelectromagnetic traps. Anal. Chem., 78(13):4457-64.

25. Mahadhy A., Mamo G., Ståhl-Wernersson E., Mattiasson B. and Hedström M. (2014), PCR-Free Ultrasensitive Capacitive Biosensor for Selective Detection and Quantification of Enterobacteriacea DNA, Mahadhy et al., J Anal Bioanal Tech, 5:5.

# 3. INTEGRATED MODULES FOR DNA EXTRACTION

The development of miniaturized devices able to perform DNA analysis is still one of the fascinating fields in biomedical research. This marries the vision of future home-made molecular diagnosis by simply using a microchip integrated into smart portable devices.

In this field, the issue of DNA preparation from biological samples is still challenging since several starting materials can be employed (blood, urine, saliva etc.) and, consequently, complex architectures and protocols are needed. Therefore, the literature reports few examples of miniaturized sample preparation devices when compared with those for DNA detection. Many of these are developed using plastic materials and include a complex microfluidic network that manages fluid movement, mixing, splitting etc [1-8] (see chapter 2). Plastic materials for integrated microfluidics have the advantage of low cost but the miniaturization, integration and the thermal properties required by some of the extraction steps (i.e. lysis) remain the main limitations.

In this chapter the technologies developed for DNA extraction and purification during my Ph.D. are described.

## 3.1 – Prep Disk Technology

### *3.1.1 – Platform Description.*

In my Ph.D. project I worked, in a first step, in the characterization of the advanced Prepdisk platform (from Qiagen) for DNA purification based on magnetic beads biotechnology (Fig.1).

This technology developed in cooperation with HSG IMIT (Germany) consists of a plastic disk (Fig. 1A) integrating all steps and modules for DNA isolation from a biological sample (blood, urine, saliva, etc.). The plastic chambers in the disk, contain all buffers normally used in the conventional DNA purification kits (lysis, binding, washing and elution buffer); two more chambers are specific for the loading of starting sample (red ring in figure) and collection of final DNA sample (green ring); one chamber contains the magnetic beads.

All chambers are connected by a microfluidic system actuated by centrifuge force so that, depending on the number and speed of rotations of Prepdisk, the mixing of sample with purification buffers and the interaction between DNA and beads (*adsorption mechanism*, see section 2.1) can occur. The instrument used to hold and play rotations of Prepdisk is reported in Fig.1B. The main advantage related to this technique is the gain in manual skill and time required for the experimental procedure.

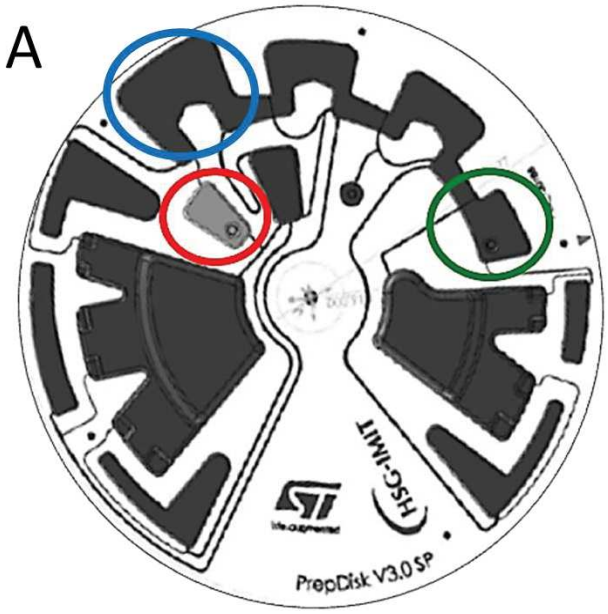

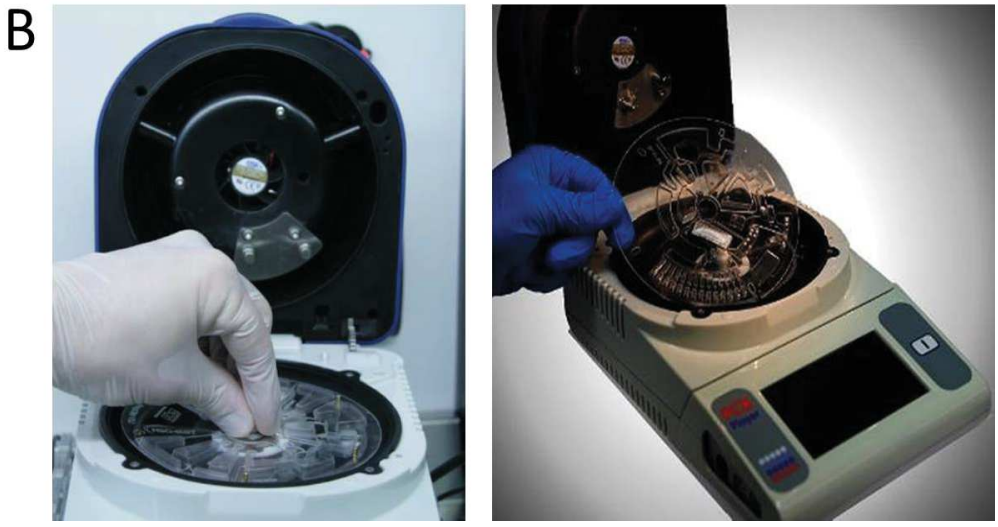


**Fig.1.** A) Prepdisk: sample loading (red circle) and elution (green circle) chamber. B) Prepdisk player.

Once loaded the sample, the Prepdisk is introduced in the player and, through a specific software (Fig.2), the protocol for DNA purification is set, defining time and speed of a series of rotation steps; each rotation step is, then, specific for each extraction step, from lysis to elution of DNA.

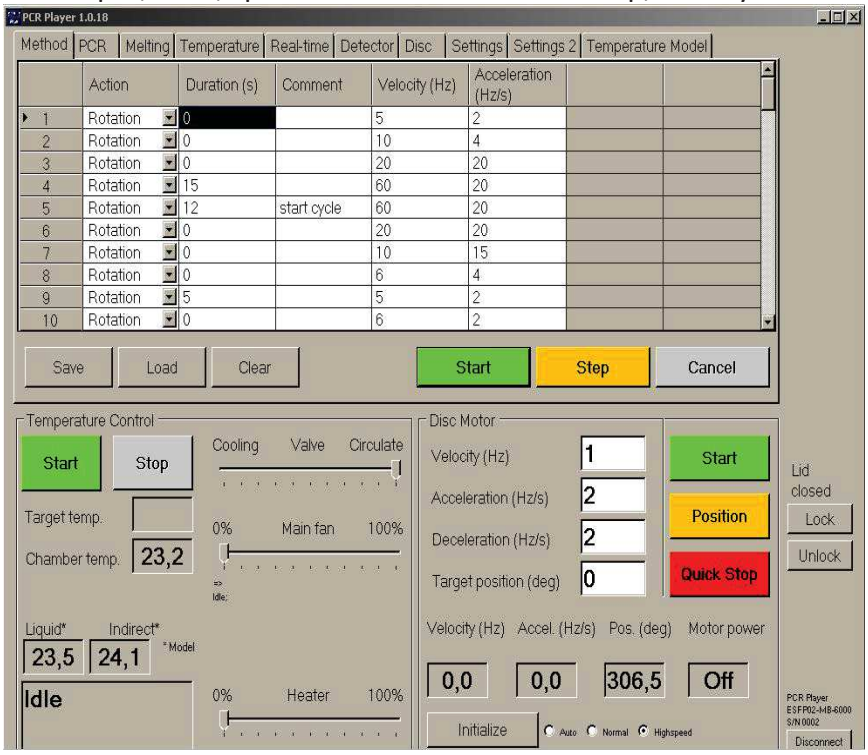


**Fig.2.** Example rotation protocol for DNA purification in Qiagen Prepdisk.

Once the protocol is completed, DNA eluate is, then, collected from the elution chamber ready for any subsequent amplification and diagnostic experiments.

To test the extraction efficiency of this technology, I analyzed the Prepdisk DNA purification yield by using a water sample contaminated with Hepatitis B virus genome (HBV) $10^5$ copies/µl concentrated. In this case, the final DNA eluted sample has been amplified and quantified by Real Time PCR, performed by the Q3 platform, developed by STMicroelectronics [6,7,8], and cycles threshold (Ct) obtained after the amplification have been compared.

Results, reported in Fig.3, show that DNA is not totally collected in the elution chamber. There is, in fact, a Ct value of 30 for the eluted DNA which is indicative of a concentration of $10^3$ copies/µl, as reported in Fig.3 (red curve), that is lower than the expected one of the positive control (blue curve in figure) which is 23.7, indicative for $10^5$ copies/µl (starting concentration of HBV genome in Prepdisk).

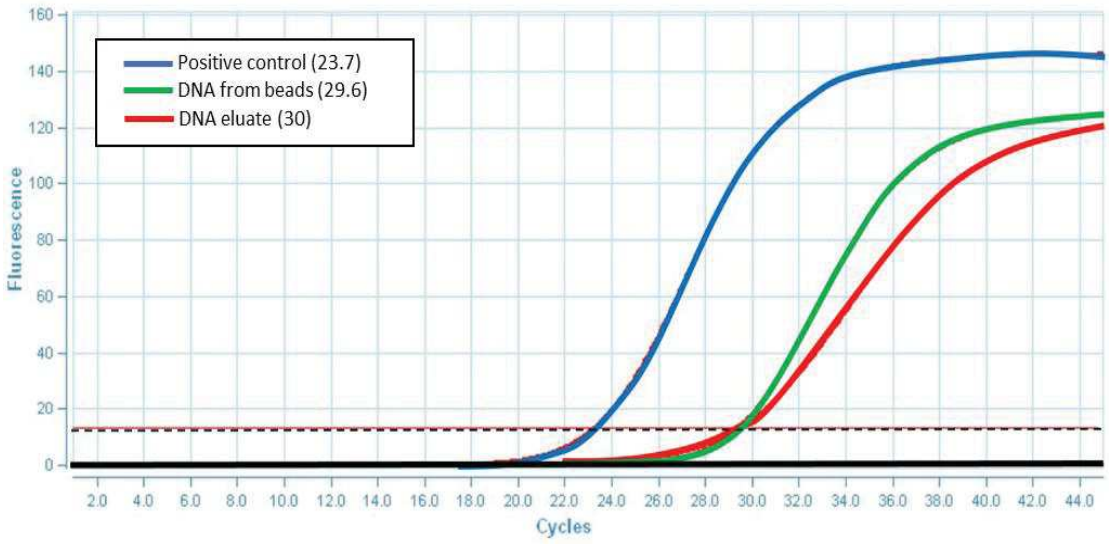


**Fig.3 -** Amplification curves and cycles threshold: positive control, $10^5$ copies/µl (blue); DNA collected by beads sonication, $10^3$ copies/µl (green); DNA eluate, $10^3$ copies/µl (red).

In order to better understand this decrease of the elution yield, I collected, in parallel, the magnetic beads from the Prepdisk (after DNA elution) and sonicated them for 5 minutes, to remove DNA eventually anchored on their surface. Then, I purified, manually, the DNA from the magnetic beads, and quantified the eluate by PCR. The Ct for this DNA sample extracted by

sonication of beads was 29.6 (residual $10^3$ copies/µl of DNA) indicating that part of the starting sample is not totally eluted with the rotations in Prepdisk.

In parallel, I compared, also, the DNA yield of Prepdisk with that one from the commercial kits, using the same type and amount of sample. Results are reported in Table 1.

**Table 1.** Extraction efficiencies comparison.

| KIT | Copies of DNA | Sample volume | Elution buffer volume | Eluate volume | RT-PCR volume | RT-PCR Ct |
|---|---|---|---|---|---|---|
| Prep Disk | $10^6$ | 200 µl | 200 µl | 200 ± 5 µl | 20 µl | 29.92 |
| Magazorb | $10^6$ | 200 µl | 200 µl | 200 ± 5 µl | 20 µl | 27.98 |
| Qiagen (high volumes) | $10^6$ | 200 µl | 200 µl | 200 ± 5 µl | 20 µl | 27.91 |
| Qiagen (small volumes) | $10^6$ | 10 µl | 50 µl | 50 ± 5 µl | 20 µl | 28.96 |

Data, shown above, led us to suppose that notwithstanding time and automation of DNA purification have been achieved, material and chemistry adopted by Prepdisk for purification is still not, totally, efficient because of the high loss of starting DNA.

For this reason, in a second phase, I worked on the implementation of this DNA purification technology by the development of a new platform that reproduced all features from Prepdisk, but improved by the integration of new and more performant modules for DNA isolation.

### *3.1.2 – Functional test of hybrid disk P1B.*

In a second phase of the study, we developed and characterized a second generation of the disk-platform disk consisting in a hybrid disk and its specific player P1B (Fig.4). This platform has been

assembled considering the integration of the fluidic system and chambers, typical of Prepdisk, and the chip for the amplification and quantification of DNA eluate at the end of the purification procedure.

In this sense, the functionality of the fluidic system on disk and player for rotation have been tested using the Prepdisk player as reference (Fig.1B).

Purification protocol by rotation has been set and split by the P1B player software, passing through the lysis, binding, washing, beads transfer and elution of DNA; in this way was possible to analyse step by step:

- Alignment of beads with magnets.
- Movements of beads among the disk chambers.
- Fluidics of sample and DNA to be extracted (Fig. 4-1)
- Fluidics of purifications buffers, from sticky packs breaking up to the filling of the chambers (Fig. 4-2, 4-3, 4-4, 4-5)

A

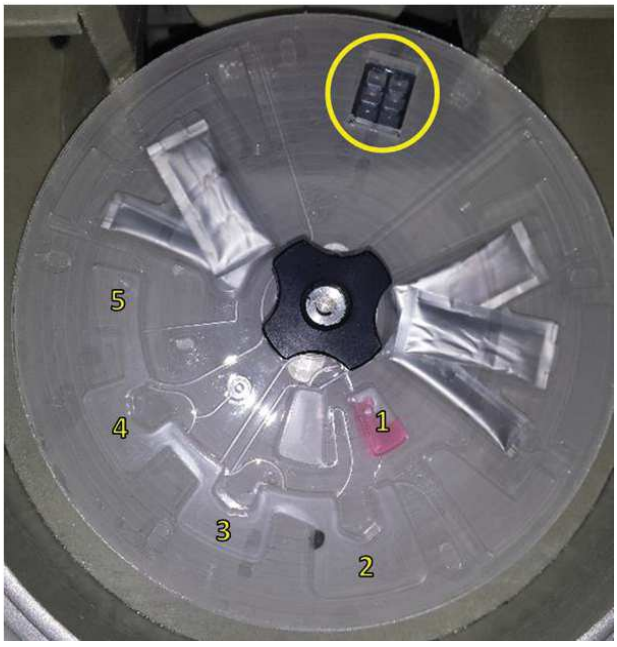


**Fig.4.** DNA-disk platform (A) Hybrid disk: sample prep + polycarbonate disk + Real Time PCR chip (yellow ring). (1) Sample loading chamber; (2) lysis chamber; (3) washing chamber I; (4) washing chamber II; (5) DNA elution and collection chamber; (B) P1B player and software.

For the functional test, in order to visualize the sample position inside the disk, 0.2 ml of an eosin sample diluted in water has been used. Alignment of beads has been verified comparing the magnets position in the lid of P1B with that one in the lid of Qiagen disk player.

In the above instrument, the exact distance between the two magnets and between the magnets and the crankshaft was measured by the centre of the disk holder (Fig. 5A). The detected positions have been meticulously reproduced on P1B magnets, optimizing the position of one magnet along the x/y axes and both along the z axis (Fig. 5B).

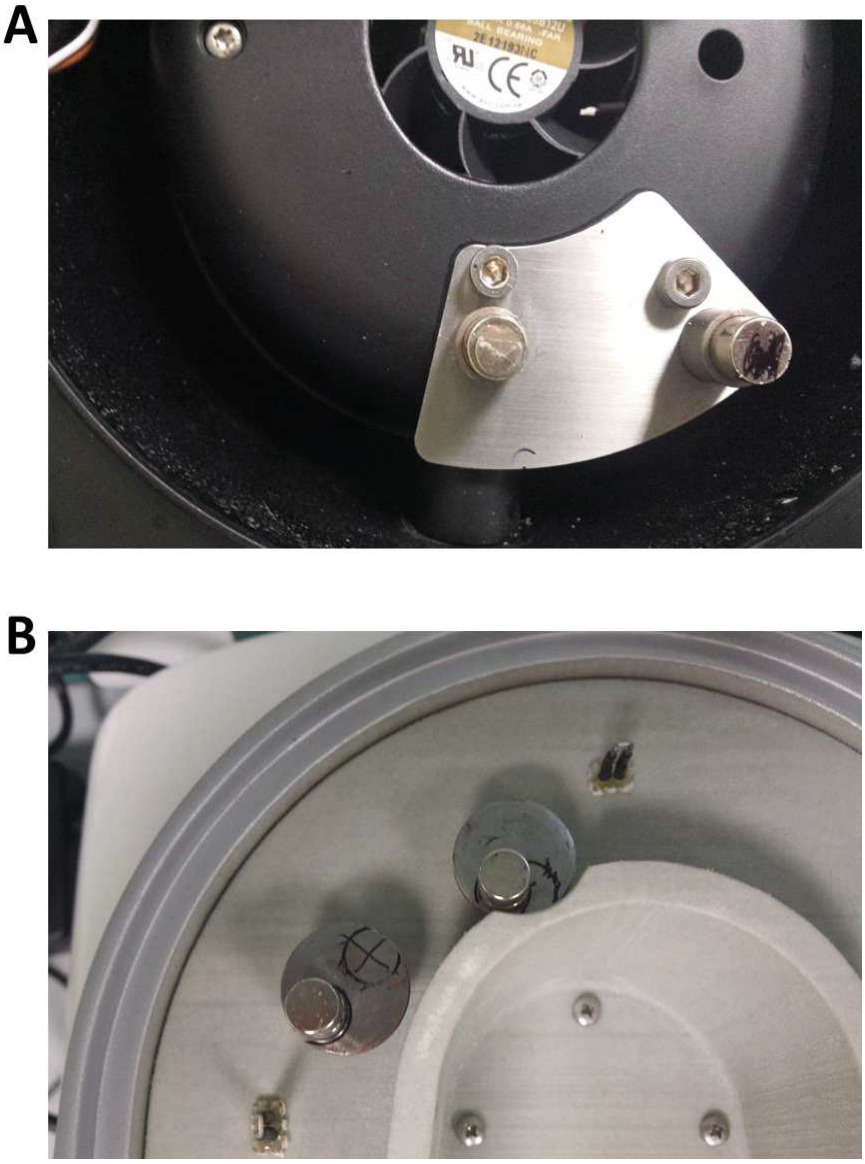


**Fig.5.** Magnets position: A) Qiagen disk player; B) P1B disk player.

In parallel, in the prep disk player the positions of the magnets have been recorded step by step through a normal extraction protocol, interrupting it in several steps to observe the disk (Fig.6).

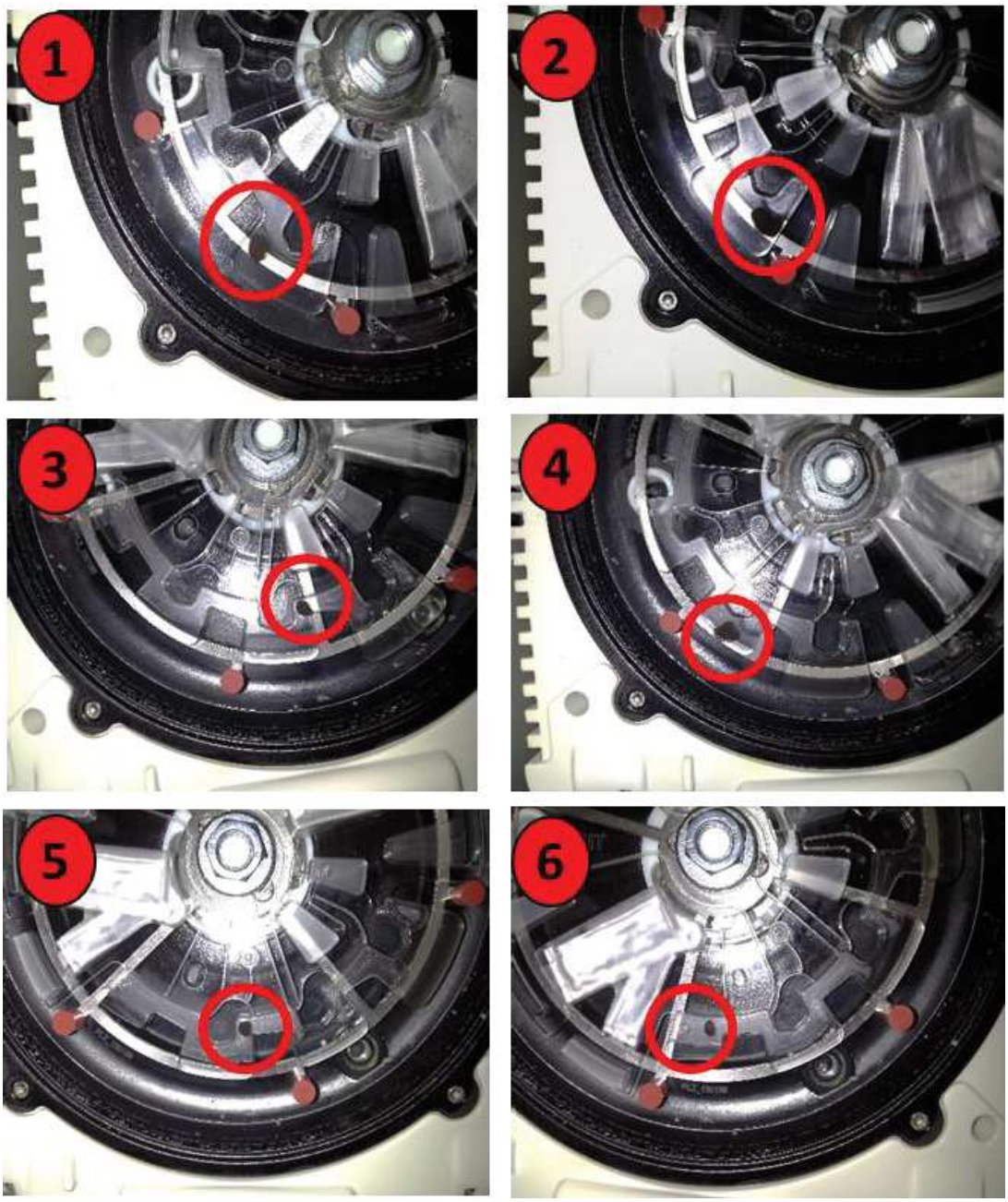


**Fig.6.** Movements of magnetic beads in sample prep (Qiagen disk player); the red ring shows the position of the beads during the various steps of the extraction protocol.

A first magnet displacement test was performed on the P1B hybrid disk. Results showed that the alignment problem persist despite the applied changes; the beads were in the chamber 2 during the entire extraction protocol as they were not properly aligned with the magnets (Fig.7).

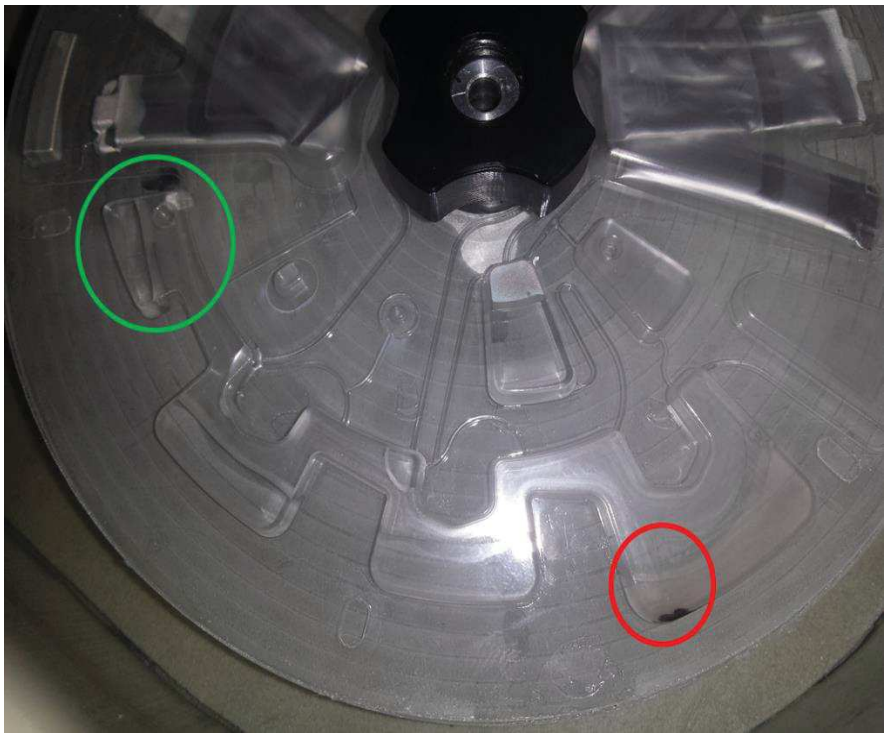

**Fig.7.** Movements of magnetic beads in hybrid disk (disc player P1B): the red ring highlights the actual position of beads at the end of the protocol; the green ring indicates the expected position.

This was related to a problem of rotation angles offset between sample prep in Prep Disk and hybrid disk in P1B, with a deviation of 19°. Fixed the scrap, the problem of beads-magnets alignment, in a subsequent rotation test, was solved; the displacement of the beads among the disk chambers perfectly reproduced the Qiagen player reference (Fig. 8).

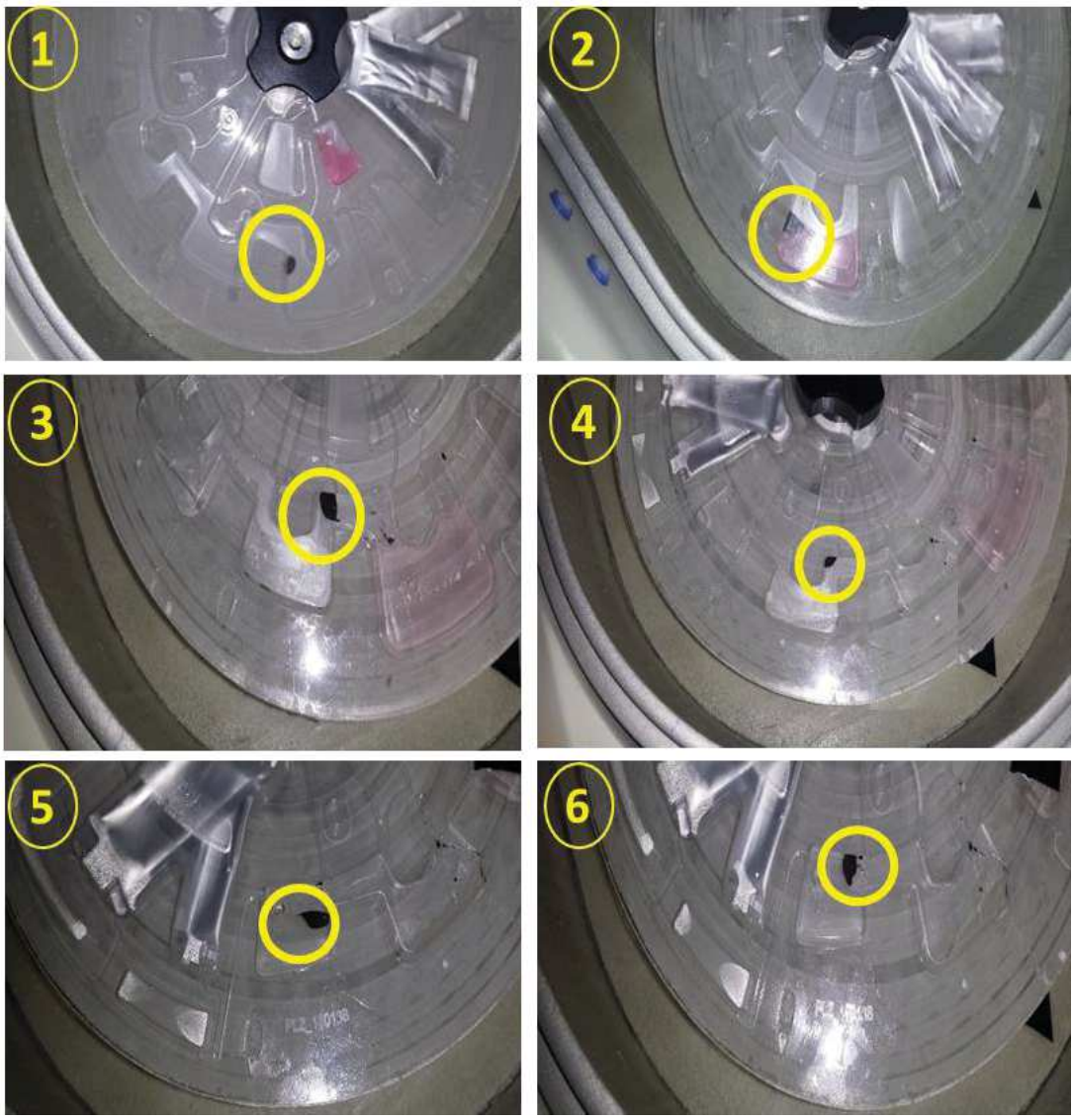


**Fig.8.** Movements of magnetic beads in hybrid disk (P1B disk player); yellow ring highlights the position of beads during all protocol steps.

Correction of angular offset was made considering also the orientation by which the sample prep disk was assembled to the polycarbonate disk. On other hybrid disks produced later, in fact, any slight variation in this sense affected the angular offset and, consequently, the alignment of the beads with the magnets and their movements inside the disk.

The extraction buffers, during rotations, were distributed irregularly leaving the 3 collection chambers (already described in Figures 4-3, 4-4, 4-5) almost empty.

Initially it seemed that the problem was related to the duration of the 40 Hz rotation step during the warming process at 56 °C (lysis phase). The temperature ramp of the P1B was, in fact, slower

than that of Qiagen due to higher thermal dispersion; this caused the prolongation of the lysis step from 1 to 6 minutes. We then repeat step 14 of the extraction protocol by removing the heating phase (thus bringing it back to 1 min effective); but also in this case the buffers didn't distribute correctly (Fig.9).

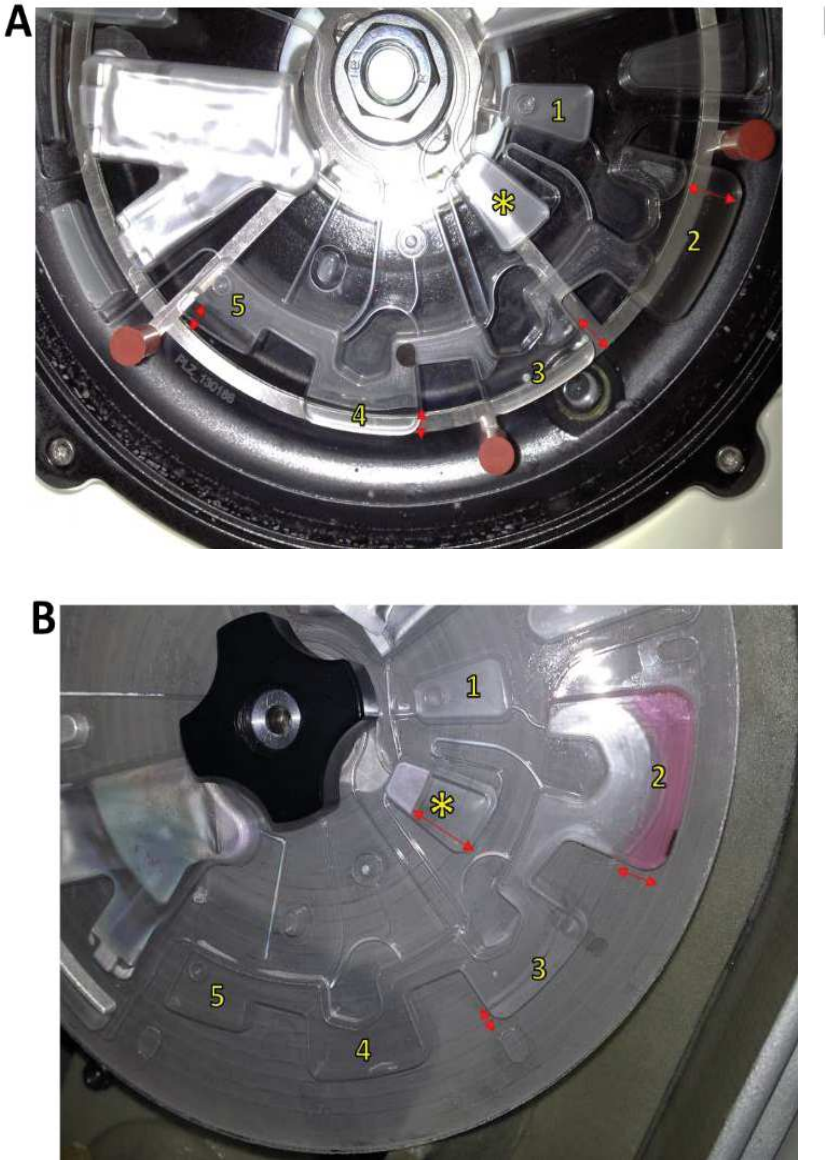


**Fig. 9.** Irregular fluidics of extraction buffers: A) Qiagen; B) P1B. Red arrows indicate the level of fluids inside the extraction chambers (2-3-4-5) and inside a pre-chamber (*).

As shown in figure, despite the sample flowed correctly from room 1 to 2 (lysis), extraction buffers irregularly distributed and accumulates in an intermediate pre-chamber (Fig.9B*) leaving the

chambers 3-4-5 (respectively washing 1-2 and elution) still partially empty, as indicated by the red arrows in Fig.9B.

Subsequently, we focused on the difference in weight between the sample prep (6.18 g) and prep assembled on polycarbonate (44.7 g). We have assumed that this difference could affect the acceleration of rotations and, consequently, the fluids dynamics. Therefore, we modified step 4 of the protocol, relating to sticky pack breaking and fluids pumping inside the chambers, increasing the speed from 60 to 70 Hz; applying this modification we, then, repeated the test.

In this case, the buffers have been distributed correctly, filling the extraction chambers in the right way and with the right volumes (Fig.10B).

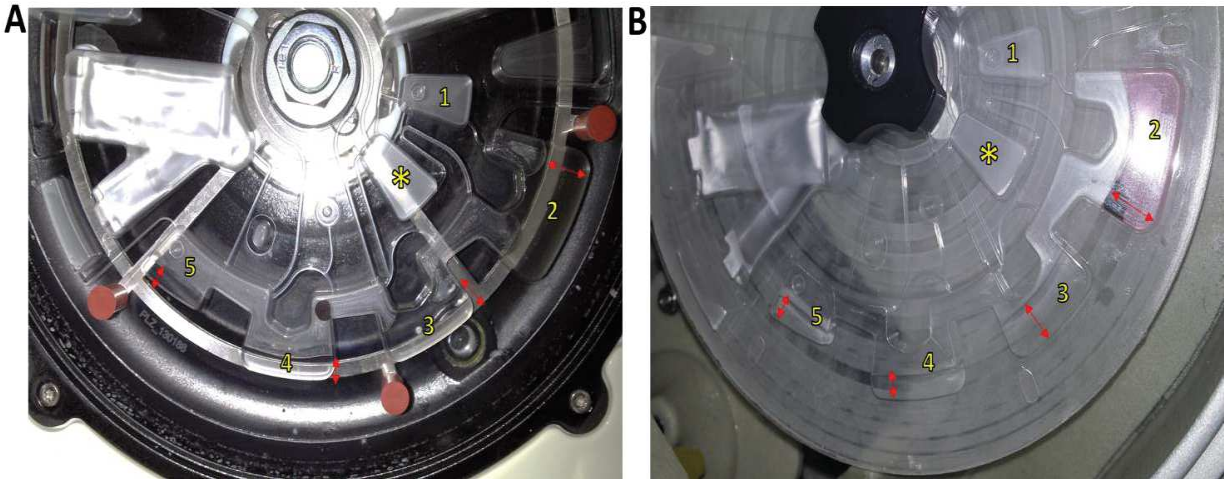


**Fig.10.** Correction of extraction buffers fluidics: A) Qiagen; B) P1B after the modification of the step 4 of protocol. Red arrows indicate level of fluids inside the extraction chambers (2-3-4-5) and inside a pre-chamber (*)

## 3.2 – Silicon pillars Technology.

Silicon is a very appealing material in terms of DNA purification. It combines good physical aspects for sensing, such as low heat capacity, good thermal conductivity, and possible patterned structures to increase the surface–area ratio, with consolidated production technologies and industrialization processes at high volumes. Additionally, it allows the integration of electrodes and microelectronics circuitry that imprint the so-called “intelligence on board”.

When the DNA to be extracted is viral or bacterial, these genomes are present in very low concentration in the starting sample compared to the co-present human DNA. In this case, therefore, the purity of the extracted material must be high and, operatively speaking, after the lysis, two additional steps of purification and concentration are mandatory. Viral and bacterial DNA extractions are usually achieved by Solid Phase Extraction (SPE) based on capturing the DNA present in the lysed solution on solid surfaces (purification step) and then eluted with appropriate buffers (concentration step) [9].

$SiO_2$ is the most used solid surface since it is well-known to bind DNA in the presence of chaotropic salts and ethanol [10]. Most of the current commercial extraction kits use silica in the form of micro-filter mounted in a plastic column or beads that are moved by external magnets. Sometimes silica is derivatized with positive amino-groups to bind the negatively charged DNA more effectively than naked silica. However, the technical features (i.e. porosity, surface-to-volume ratio, etc.) of these systems are not explicitly disclosed since they are covered by trademarks.

From the prospect of achieving a chip for DNA extraction based on SPE on the silica surface, in this project, I worked on the development and characterization of a new miniaturised microfluidic module, that is a biofilter (BF) device based on microfabricated silicon micropillars, that merges the advantages to increase the surface within the capture area with the possibility to be monolithically integrated into a miniaturized device.

The characterization was focused on the analysis of efficiency to catch and release DNA. Also for this experiment, I used HBV (Hepatitis B Virus) clone water solution at a concentration typical of real samples for infectious diseases ($10^5$ copies) as analytical samples. The device has been developed in three different geometrical structures, so that the effect of the Surface-to-Volume Ratio (SVR) on the extraction efficiency can be investigated. The total extraction performance was also evaluated and compared with those of commercial kits.

Finally, the device exhibiting the best extraction efficiency was tested in combination with a silicon integrated real time PCR amplification chip as a preliminary step towards the development of genetic point-of-care devices.

### *3.2.1 – Geometrical features of the microstructures*

The whole biofilter system is reported in Fig.11. One of the key parameters for effectively capturing the DNA in SPE using the pillar approach is the surface-to-volume ratio (SVR): the higher the value, the larger the surface available for capture under the same chemical conditions (ionic force, pH, etc.) of the employed solutions. In order to gain more insight into the aspects related to our BF device, we developed three pillar microstructures generating three types of extraction chips (BF-1, BF-2 and BF-3) featured by different SVR characteristics. Fig. 12 illustrates a typical image of the fabricated BF microdevice (Fig.12a) and the structural features of the pillars areas in the three device typologies (Fig.12b and c). In particular,

Fig.12b clearly highlights the three kinds of packing pillar arrangements differing from each other in pillar diameter (12 μm in the case of BF-1 and 15 μm for both BF-2 and BF-3) and inter-pillar distance (8 μm in the case of BF-1, 10 μm for both BF-2 and 15 μm for BF-3).

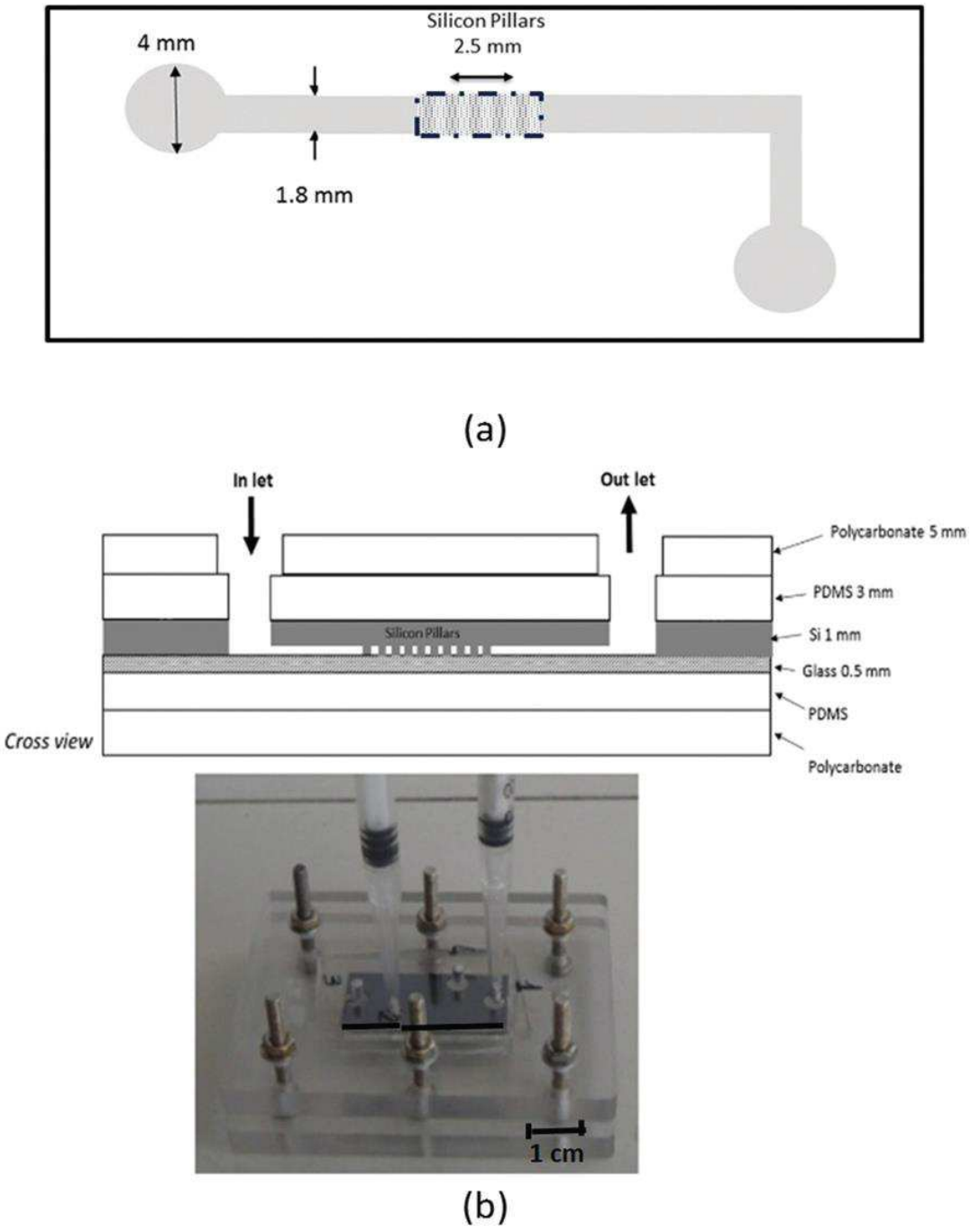


**Fig.11**. a) Scheme of the silicon pillars based biofilter; b) scheme of the "sandwich" model of biofilter system.

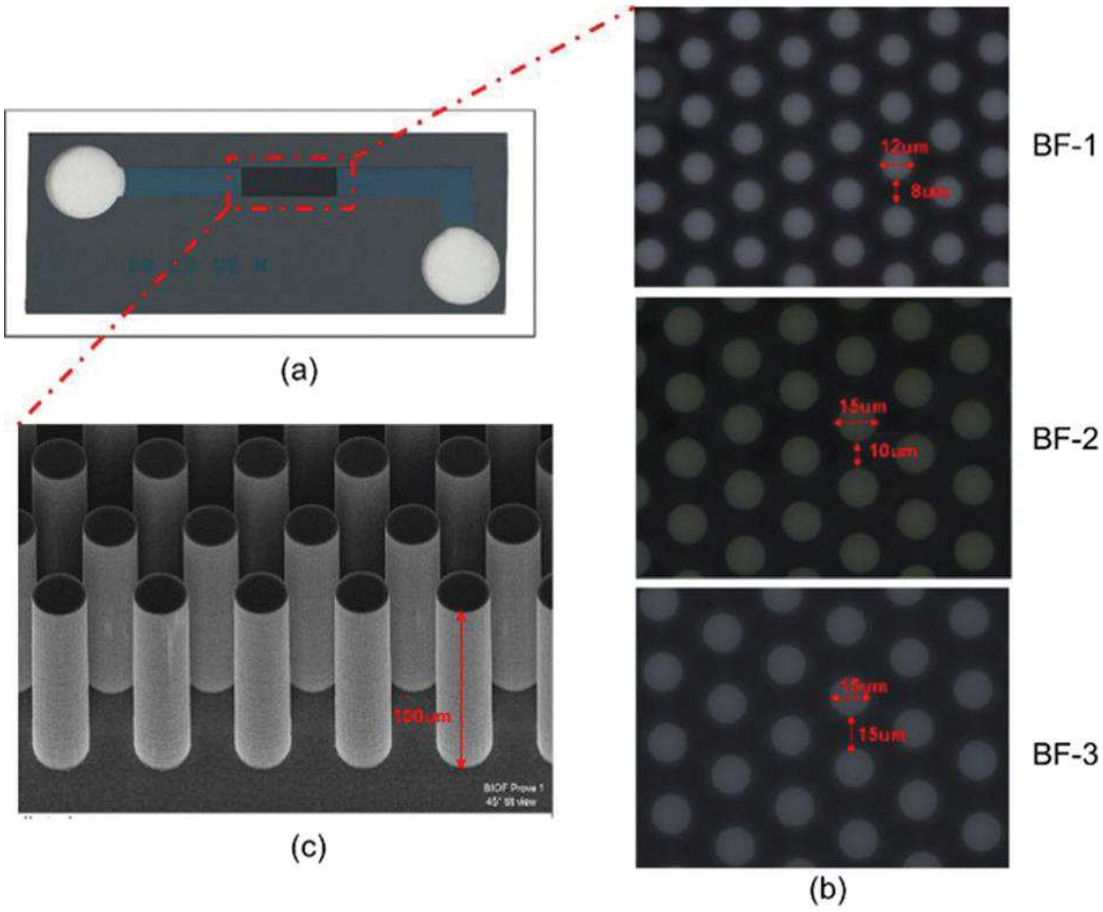


**Fig.12.** (a) Image of a microfabricated BF device (pillar active area is highlighted); (b) optical image (50×) of BF-1, BF-2 and BF-3 pillar areas (top view); (c) SEM images of typical pillars (BF-3 device).

It can be also noticed that the pillars are arrayed in a close-packed arrangement in order to maximise the packing feature and to increase the surface area as much as possible. In light of this, each microstructure contained a different number of pillars from about 23 000 in the case of BF-1, to 12 000 for BF-2 and to 7300 for BF-3. The pillars are cylindrically shaped as shown in the SEM image reported in Fig.12c.

A system of breakwater, located before and after the pillars array, regulates the input (Fig.13A) and output (Fig.13B) of sample flow.

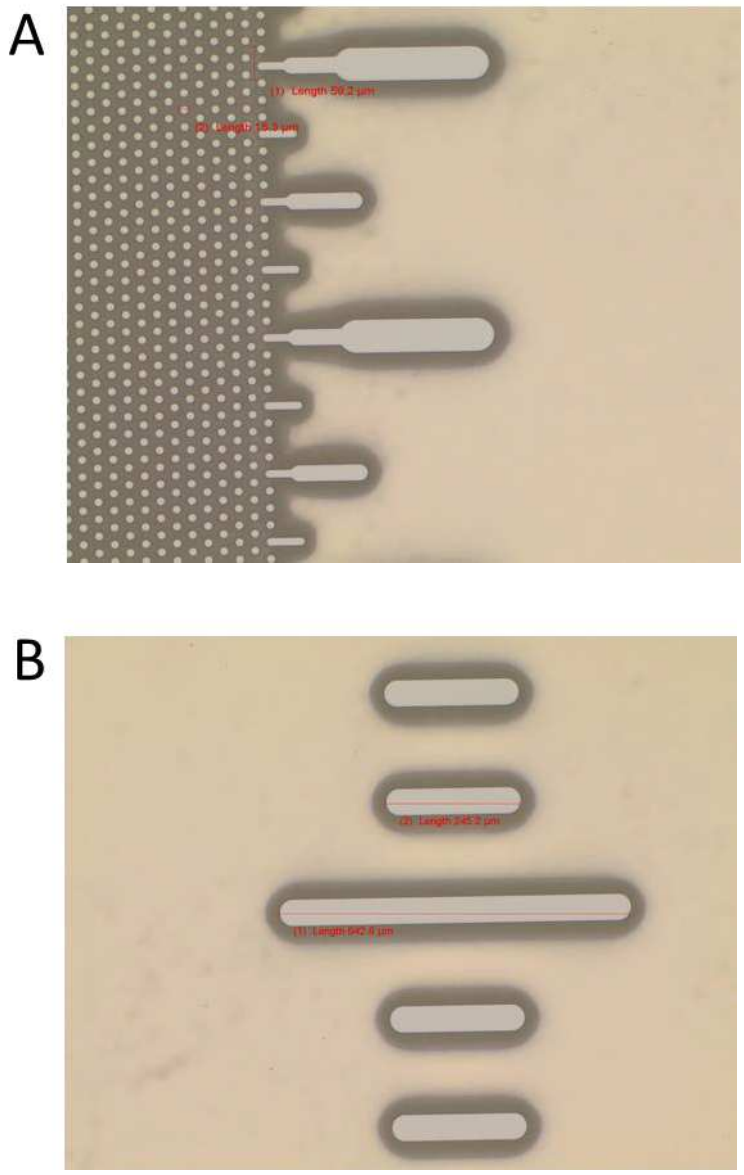


**Fig.13.** Breakwater system upstream (A) and downstream (B) the pillars array.

The above discussed geometrical features yield different surface-to-volume ratios (SVR). As summarised in Table 1, the device exhibiting the highest SVR value is BF-1 (39.90 $mm^{-1}$) while BF-2 and BF-3 exhibit lower values equal to 30.11 $mm^{-1}$ (BF-2) and 22.50 $mm^{-1}$ (BF-3), respectively. It can be noticed that the major contribution to the total S/V comes from the active pillar area. Such an area contributes to the total surface of the BF chip, about 78% in the case of BF-1, 71% in the case of BF-2 and 61% in the case of BF-3. On the basis of this finding, we can reasonably attribute the major impact in the DNA capture to that area.

### *3.2.2 – Effect of Surface-to-Volume Ratio and ionic force on extraction performance*

The extraction performance of the BF devices was measured using synthetic DNA clone of the HBV genome at a concentration close to that found in real samples ($10^5$ copies/µl). This clone was selected as an analytical model to assess the extraction performance before testing real samples (such us blood, urine, and saliva etc.) that include the so-called "bias" interference [11].

Experimental detail on reagents and protocol adopted for the tests are reported in the *Experimental Part* section at the end of this chapter.

We firstly evaluated both the binding and elution capability of the above-described microstructures. After sample loading, the unbound, washed and eluted DNA was measured by real time PCR on the tube.

Fig.14 illustrates the comparison of the obtained data in terms of DNA amount (total cps) for the three typologies of BF devices. It can be clearly noticed that the DNA binding capacity increases with the SVR of the device. The BF device exhibiting the highest SVR (BF-1) also shows the highest values of captured DNA. This latter is defined as the difference between the total starting DNA (blue bar) and the sum of total unbound (orange bar) and total washed DNA (grey bar). In agreement with this, the calculated binding efficiency (Eq 1) corresponds to 54% for BF1 (SVR 39.9 $mm^{-1}$) versus 26% for BF-2 (SVR 30.5 $mm^{-1}$) and 22% for BF-3 (SVR 22.50 $mm^{-1}$). This is expected on the basis of the increasing number of potential binding surface sites upon SVR increasing.

$$\text{Binding efficiency} = \frac{C_{\text{starting}} - C_{\text{not bound}}}{C_{\text{starting}}} \times 100 \qquad \text{(Eq 1)}$$

$C_{starting}$ = starting total amount of HBV clone; $C_{not\text{-}bound}$ = not-bound amount of HBV clone after flowing into the BF devices.

Even if the trials were performed on the uncoated SiO2 surface, a remarkable amount of DNA was captured: about $1.8 \times 10^5$ cps for BF1, $1.1 \times 10^5$ cps for BF2 and $8.0 \times 10^4$ cps for BF3 in the case of EB1 (yellow bars of Fig.14) and about $1.1 \times 10^5$ cps for BF1, $7.5 \times 10^4$ cps for BF2 and $5.5 \times 10^4$ cps

for BF3 in the case of EB2 (blue bars of Fig.14). This is due to the presence of silanol groups on the surface formed during the chemical treatment with $NH_4OH$ : $H_2O_2$ : $H_2O$. These groups probably induce the formation of hydrogen bonds between the surface and the skeleton of the DNA molecule in the presence of high ionic strength solutions. Further mechanistic investigations are currently under way in our laboratories in this concern.

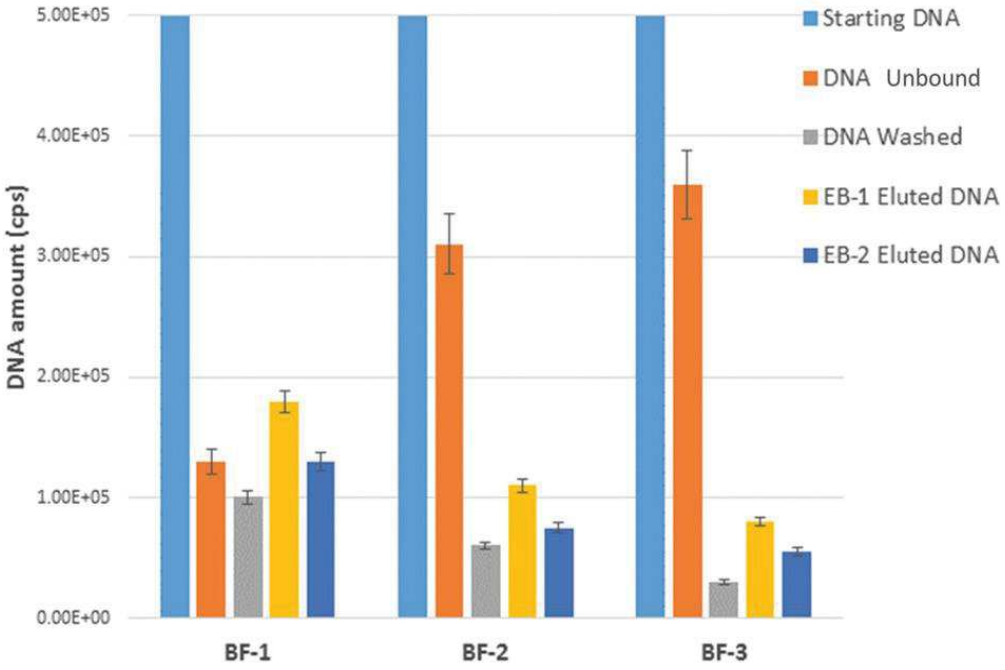


**Fig. 14.** - Binding and elution profiles of BF devices.

It should be emphasized that the binding capacity occurs without the employment of chaotropic salts or ethanol that are well-known inhibitors of the PCR or other molecular techniques and make the design of miniaturized systems more complex (vide supra).

In terms of elution capability, we observe that water (EB-1) works better than the low-ionic strength buffer EB-2. In fact, the calculated elution efficiency percentage (Eq 2) in the case of water was about 50% higher than EB-2 buffer (75% water versus 50% EB-2). This can be tentatively attributed to the better ability of water to make the electrostatic interaction between DNA and surface hydrating DNA molecules thermodynamically unstable.

Finally, we calculated the total extraction efficiency of the three types of BF devices by means of Eq 3 and compared them with those related to two commercial state-of-the-art kits, Magazorb and Qiagen based on magnetic beads and silica filter, respectively.

$$\text{Elution efficiency} = \frac{C_{\text{eluted}}}{C_{\text{bound}}} \times 100 \qquad \text{(Eq 2)}$$

$C_{eluted}$ = eluted amount of HBV clone; $C_{bound}$ = amount of HBV clone bound into the BF [$C_{starting}$ − ($C_{not\text{-}bound}$ + $C_{washed}$)];

$$\text{Extraction efficiency} = \frac{C_{\text{eluted}}}{C_{\text{starting}}} \times 100 \qquad \text{(Eq 3)}$$

$C_{eluted}$ = eluted amount of HBV clone; $C_{starting}$ = starting total amount of HBV clone;

Fig.15 illustrates the obtained results. It is noteworthy that BF-1 shows the best extraction performance achieving about 36% efficiency using water as elution buffer versus 22% for BF-2, 16% for BF-3 (blue bars) and 20% for both Magazorb and Qiagen (green bars). Using EB-2 as elution buffer (orange bars), the final extraction efficiency of BF-1 is comparable with those of the commercial kits, while those of BF-2 and Bf-3 were slightly lower. The latter finding is in line with the previous results discussed above for elution efficiency. As far as the better result displayed by BF1 is concerned, we believe that a probable synergy between the filter structure and the experimental protocol adopted may play a key role.

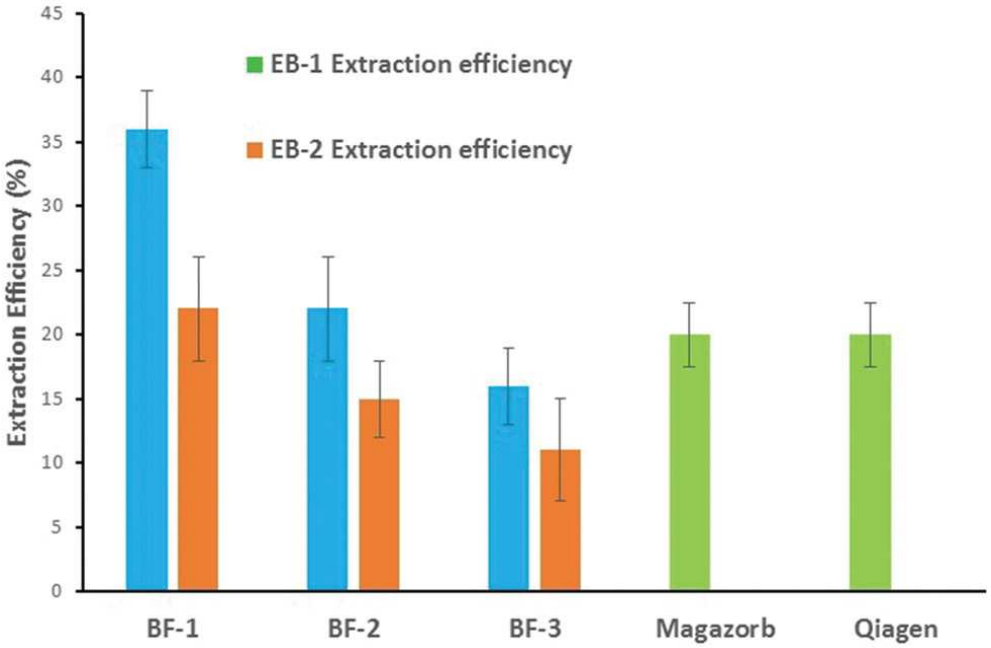


**Fig.15.** Comparison of extraction efficiencies of BF devices and commercial kits.

### *3.2.3 – Extraction and Real-Time amplification on the chip*

As a preliminary step towards the development of a genetic point-of-care device, we evaluated, in a semi-integrated configuration, the real genetic testing using the biofilter exhibiting the best extraction efficiency (BF1) in combination with a silicon integrated real time PCR amplification chip. In order to be compliant with the analytical procedure for quantitative analysis, the microchip has been designed to feature six reaction chambers to host both positive (Ctr+) and negative (Neg) controls and the sample. Furthermore, the microchip contains integrated temperature sensors and heaters to perform a one-step Real Time PCR process quickly [12–14].

Fig.16a illustrates the scheme of the system configuration (the BF-1 extraction chip combined with the real time PCR chip) employed for this study. The on-chip amplification results on the extracted sample by BF1 are shown in Fig.16b.

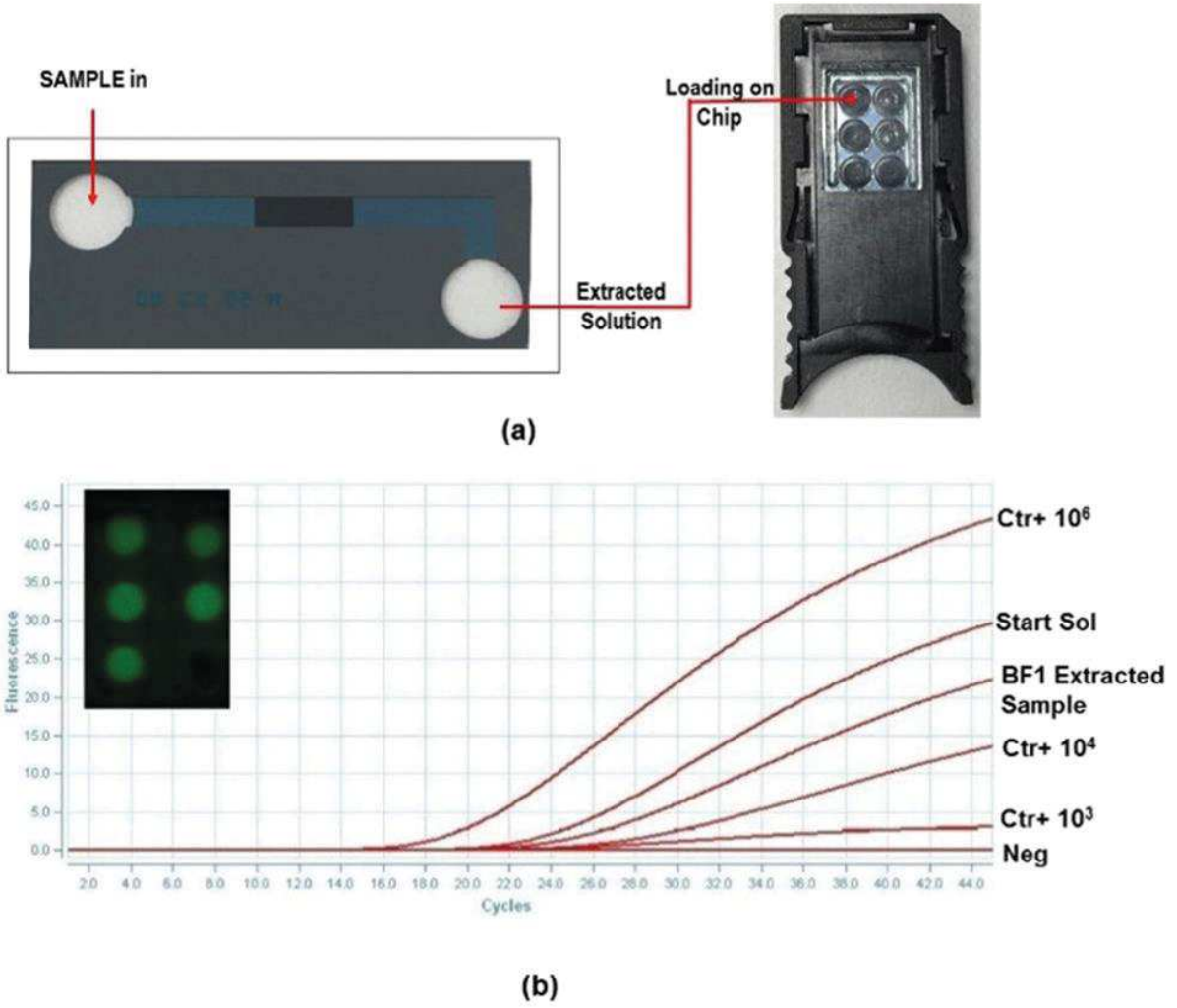


**Fig.16** (a) System configuration for semi-integrated genetic PoC test: extraction step with BF1 filter and real time PCR with a microchip; (b) semi-integrated experiment results (the inset reports a fluorescence image captured during the PCR).

The Ct values for both the starting ($5 \times 10^5$ cps) and the BF1-extracted solutions were 22.4 and 26.3, respectively. The final concentrations of these solutions were calculated by the calibration curves embedded into the chip. Specifically, it was obtained by means of the Ct values exhibited by the three positive controls ($1 \times 10^6$, $1 \times 10^4$ and $1 \times 10^3$ cps) equal to 19.4, 23.9 and 31.0, respectively (the negative control gave no results as expected). The calculation led to values of about $1.9 \times 10^5$ for the starting solution and 7.8 × 104 for the extracted solution. Based on these results, the extraction efficiencies calculated by Eq 3 correspond to about 40%. This is fully in

agreement with the results obtained previously in the analytical characterization of BF1, and confirms the best extraction performance with respect to the commercial kits. Furthermore, our results indicate that technology that uses micropillars in combination with an integrated real time PCR microchip can be very appealing for future developments of a fully-integrated genetic PoC device able to perform molecular genetic analysis close to the patient.

# Experimental Part

## *3.2 – Silicon pillars Technology.*

*Materials.*

Stock solutions of a HBV clone complete genome (ref product 05960116), consisting of the HBV genome 3.2 kbps and a plasmid PBR322 vector 3.8 kbps in TE (Tris 10 mM, EDTA 1 mM, pH = 8) and the HBV real time PCR kit (ref product FO2 HBV MMIX KIT 48) were purchased from Clonit and used according to the Instructions for Use. Tris-HCl, EDTA, TE buffer and sterile deionized water were purchased from Sigma and used as received.

*Silicon biofilter fabrication.*

The BF devices (30 mm × 13 mm in size) consist of a microfabricated corner-shaped silicon channel (linear length 20 mm, large 1.8 mm) in which silica coated pillar arrays were etched in an area (5 mm long, 1.8 mm large) located in the middle of the channel. Three series of pillars arrays with a size of 5 × 1.8 mm2 (BF-1, BF-2 and BF-3) were fabricated varying the pillar diameter (from 12 to 15 µm) and the pillar-to-pillar distance (from 8 to 15 µm). The height of the pillar in all three arrays was 100 µm. The inlet and outlet ports of the channel are circular holes, 4 mm in diameter. Table 2 summarizes the geometrical details of all BF types.

**Table 2.** Pillars geometries in BF devices.

| Filter type | Pillar diameter (mm) | Pillar pitch (mm) | Pillar height (mm) | Total number of pillars | Total SVR ($mm^{-1}$) |
|---|---|---|---|---|---|
| BF-1 | 0.012 | 0.008 | 0.1 | 23 040 | 39.9 |
| BF-2 | 0.015 | 0.01 | 0.1 | 12 190 | 30.5 |
| BF-3 | 0.015 | 0.015 | 0.1 | 7380 | 22.5 |

The microfabrication of these devices was carried out by a standard VLSI (Very Large Scale Integration) technology based on multi-step processes. The first step was the cleaning of the wafer with a solution of $H_2O_2$ : $H_2SO_4$ (1 : 1) followed by washing with deionized water and drying at 90 °C. After that, the silicon wafer was coated with a positive photoresist layer (KrF (248 nm) purchased from FujiFilm) of 4.7 µm by a spin coating process (1000 rpm, for 1 min). UV light irradiation was performed through a photomask, and the development process with TMAH (tetramethylammonium hydroxide)-based solution (OPD4262 purchased from FujiFilm) was carried out. After that, the microstructures were fabricated by silicon etching using a standard Bosch process (United States Patent 5501893) forming silicon channels (18 mm long × 1.8 mm large), the active pillar areas (2.5 mm long × 1.8 mm large) and the inlet and outlet holes (4 mm diameter), respectively. A next stripping step by oxygen plasma was carried out to remove the residual photoresist. A subsequent final dry oxidation process at 1000 °C with $O_2$, and $H_2O$ gas (rate 1 cm $s^{-1}$) was carried out, leading to a surface silicon oxide layer of 320 nm in thickness. This was measured by Scanning Electron Microscopy (SEM) analysis obtained using a high-performance Schottky field emission, LEO 1550 SEM. The instrument was operated at 5 kV in a secondary electron imaging mode. The silicon part was then sealed with a glass slide (0.5 mm thickness) by a standard anodic bonding process producing the final microchip. The internal volume of the device was 5 µL. The microstructures of the microfabricated devices were imaged by both optical microscopy (OLYMPUS SZX16) and SEM.

*Fluidics.*

To test the BF devices an appropriate fluidic connection was fabricated. A PDMS layer (3 mm thickness) was employed to cover the device from both sides. A final polycarbonate rigid holder (5 mm thickness) was mounted on to guarantee the structural rigidity and the ease of handling the

device. Both PDMS layers and the polycarbonate holder contained holes that are aligned with the inlet and outlet ports of the silicon device. The fluid was actuated into/out of the devices by applying/removing pressure through syringes mounted on top of the inlet and outlet ports (Fig.11).

*BF chemical treatment.*

Before using, the BF devices were chemically treated by flowing through their channel a solution of NH4OH : $H_2O_2$ : H20 (5:1:1) preheated at 60 °C for 5 min. Then channel rinsing was carried out 3 times with deionized water. Finally, the devices were dried under nitrogen flowed through the inlet port.

*Extraction experiments and BF functional characterization.*

DNA binding/elution experiments were performed by using a starting solution containing $10^5$ copies/µL of HBV complete genome dissolved TE buffer. A 5 µl volume of this solution (starting solution) was loaded into the BF channel through the inlet port and incubated for 10 min at room temperature. The solution was then recovered by aspiration from the outlet port (not-bound solution). A washing step with 10 µL of TE buffer was then carried out. The final elution step was executed by flowing 5 µL of elution buffer.

Two types of elution buffers were tested: (EB-1) water (EB1-elution solution); (EB-2) Tris-HCl 10 mM, EDTA 1 mM at pH = 8.0 (EB-2-elution solution). All experiments were performed at room temperature. The recovered samples (not-bound solution, EB1-elution solution and EB2-elution solution) together with the starting solution were quantified in terms of HBV clone concentration by using real time PCR. The experiments were performed on an AB7500 Thermo-Cycler. 5 µL of the above-mentioned solutions were added to 20 µL of a HBV kit master mix. The PCR thermal cycling

was as follows: 10 min at 95 °C, followed by 45 cycles of 95 °C for 15 s and 60 °C for 60 s. The quantitative measurements of HBV clone concentration were performed by a calibration curve calculated with the standard HBV concentrations of $1 \times 10^5$, $1 \times 10^4$, $1 \times 10^3$ and $1 \times 10^2$ cps. For comparison, the same starting analytical sample (solution of the HBV clone containing a total amount of $5 \times 10^5$ copies) was extracted using two commercial kits: (a) a Magazorb DNA Mini-Prep Kit (Promega) and (b) a Qiagen QIAamp DNA Mini Kit (Ref. 51306), according their Instructions for Use. All experimental steps are reported in Fig.17.

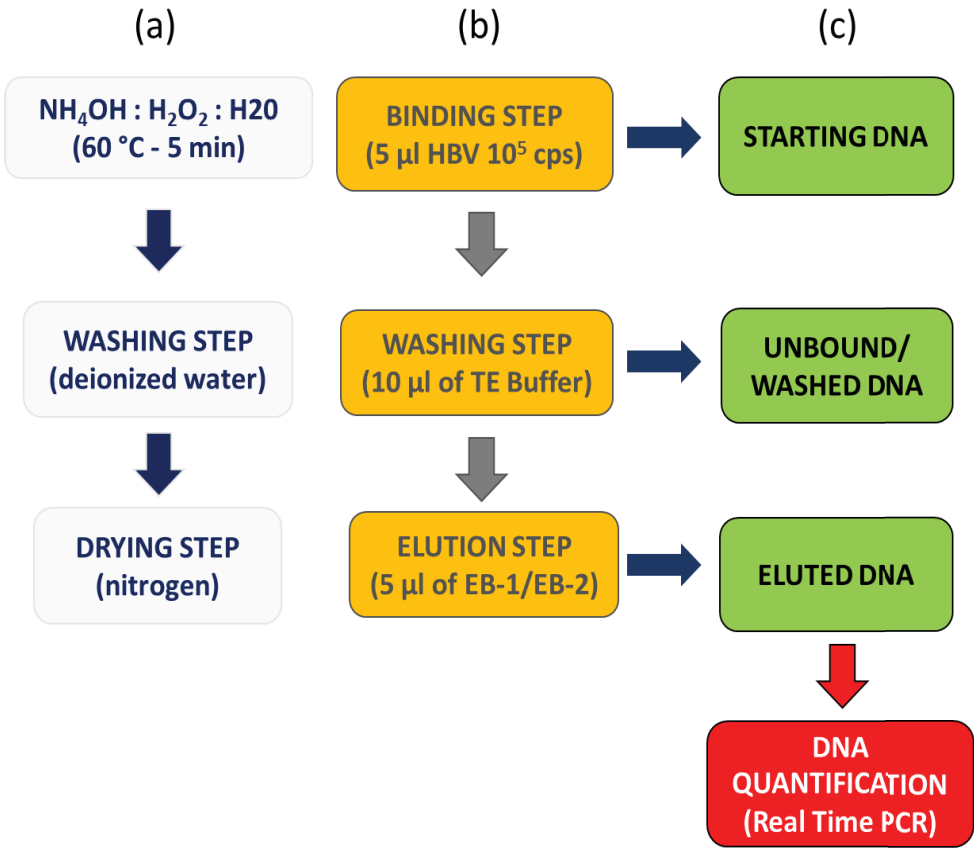


**Fig.17.** Experimental procedure in BF functional characterization: (a) chemical treatment; (b) DNA purification; (c) sample collection.

*DNA Extraction and amplification on chip.*

A complete extraction experiment was performed on a BF1- type biofilter device starting from a solution containing $10^5$ copies/µL of the HBV clone in TE buffer (starting solution). The eluted

solution (5 µL) was analyzed via real time PCR on the chip using a disposable miniaturized silicon device integrating temperature sensors and heaters (RT-PCR chip) containing six PCR reaction chambers (15 µL each in volume).

The chip is thermally and optically driven by using a Q3 instrument and the collected fluorescence signals versus PCR cycles are analyzed by Q3 software. The platform has been custom-developed by STMicroelectronics and the details related to the manufacturing process and features are described in ref. [15-18]. 5 µL of both starting and eluted solutions were pipetted into two out of the 6 chambers of the RT-PCR chip, and preloaded with 10 µL of the HBV kit master mix. The others 4 chambers were loaded with 1 negative sample (1 µL of water + 14 µL of HBV master mix) and three positive controls (1 µL of $1 \times 10^6$, $1 \times 10^4$ and $1 \times 10^3$ copies/µL + 14 µL of HBV master mix) for the calibration curve.

## *References*


1. J. J. Benitez *et al.* (2012), Lab Chip, 12, 4848–4854.
2. M. C. Breadmore *et al.* (2003), Anal. Chem., 75, 1880–1886.
3. X. Chen, D. Cui, C. Liu, H. Li and J. Chen (2007), Anal. Chim. Acta, 584, 237–243.
4. N. C. Cady, S. Stelick and C. A. Batt (2003), Biosens. Bioelectron., 19, 59–66.
5. K.-H. Hwang, H.-K. Lim, S.-Y. Jung, K. Namkoong, J-H Kim, N. Huh, C. Ko and J-C Park (2008), Anal. Chem., 80, 7786–7791.
6. H. M. Hegab, M. Soliman, S. Ebrahim and M. Op de Beeck (2013), J. Bionsens. Bioelectron., 4, 1–6.
7. L. Chen, A. Manz and P. J. R. Day (2007), Lab Chip, 7, 1413–1423.
8. S. Petralia and G. Ventimiglia (2014), BioNanoScience, 4, 226–231.
9. J. M. Buller (2001), Forensic DNA Typing: Biology and technology behind STR Markers, Academic Press, SanDiego, USA.
10. J. West, M. Boerlin, A. D. Jadhav and E. Clancy (2007), Sens. Actuators, B, 126(2), 664–671.
11. Martin F. Polz and Colleen M. Cavanaugh (1998), Appl. Environ. Microbiol., 3724–3730.
12. S. Petralia, M. E. Castagna, M. O. Spata, M. G. Amore and S. Conoci (2016), Biosens. J., 5, 136.
13. S. Petralia, M. E. Castagna and D. Motta (2016), BioNanoScience, 1, 1–7.
14. M. Spata, M. E. Castagna and S. Conoci (2015), Sens. Biosens. Res. J., 6, 79–84.
15. Hegab H. M., Soliman M., Ebrahim S. and Op de Beeck M. (2013), J. Bionsens. Bioelectron., 4, 1–6.
16. Chen L., Manz A. and Day P.J.R. (2007), Lab Chip, 7, 1413– 1423.
17. Park B.H., Kim Y.T., Yung G.H. and Seo T.S. (2014), Microchim. Acta, 181, 1655–1668.
18. S. Petralia and G. Ventimiglia (2014), BioNanoScience, 4, 226–231; N. Y. Lee, Int. Neurourol., 2013, 17, 2–10.

# 4. INTEGRATED MODULES FOR DNA DETECTION

## 4.1 – "CDC" Silicon Chip Technology for Real-Time PCR.

The miniaturization of Real-Time PCR amplification systems is a key point towards the development of the so called "genetic point-of-care" technologies able to offer a sample-in answer-out diagnostic analysis, enabling shorter analysis times, reducing reagent consumption, minimizing risk of sample contamination and enhancing the assay performance such as sensitivity, selectivity and limit of detection.

In this sense, in the second module of my Ph.D. project I have been working on the characterization of an innovative Real-Time PCR based silicon technology for the quantitative and qualitative identification of multiple analytes of specific DNA sequences in a PoC format.

### *4.1.1 – "CDC" Real-Time PCR device.*

The miniaturised device for DNA detection via RT-PCR is based on a silicon microchip that integrates both Real-Time PCR micro reactors (6-15 µl in volume) and silicon temperature sensors and heaters (Fig.1). Thanks to the integrated sensors and heaters, the chip allows a temperature control accuracy of ± 0.2 °C, heating rate of 15°C/s and cooling rate of 8°C/s. Additionally, a specific chip design architecture [1] enhances the optical fluorescent signal in combination with a smart detection software, so that an improvement of sensitivity is achieved respect to the commercial tools. The chip is thermally and optically driven by a miniaturized instrument specifically developed for it design. Details on the CDC device are reported in the Experimental Part section at the end of this chapter.

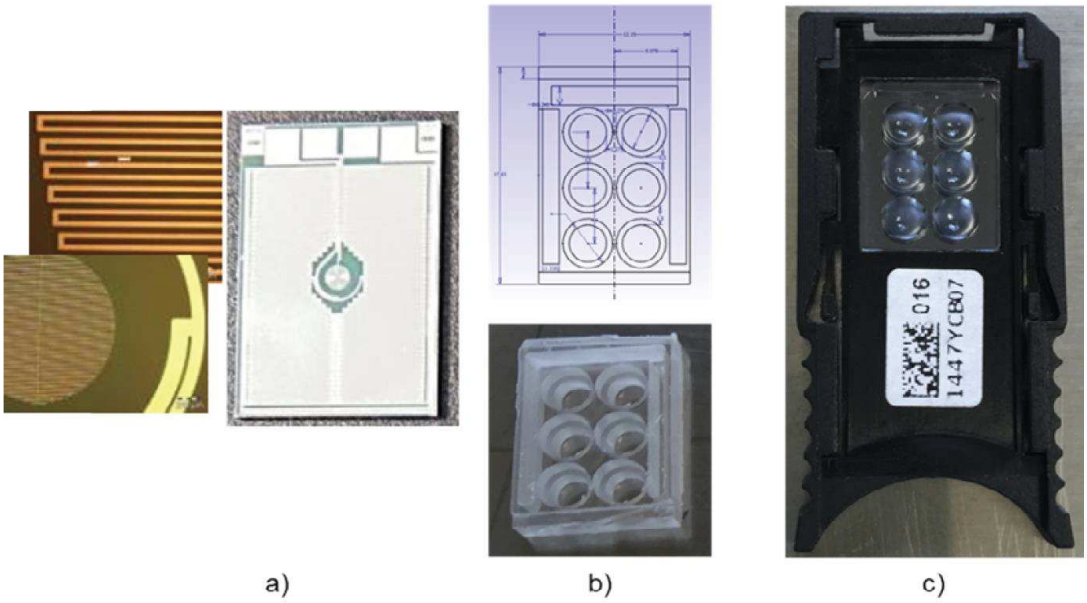


**Fig.1.** CDC chip: a) silicon part; b) polycarbonate ring and c) disposable microchip.

### *4.1.2 – "CDC" device characterization*

*a) Annealing temperature*

In order to validate the functioning of the system, Real-Time PCR experiments for pathogen Hepatitis B Virus (HBV) genome detection have been performed. The sample used is a synthetic plasmid containing all HBV genome (7.1 Kb) and, to optimize the device performance, we explored different annealing temperatures and probe concentrations. Fig.2 reports a typical Real-Time PCR curves and fluorescence images obtained during the above described experiments.

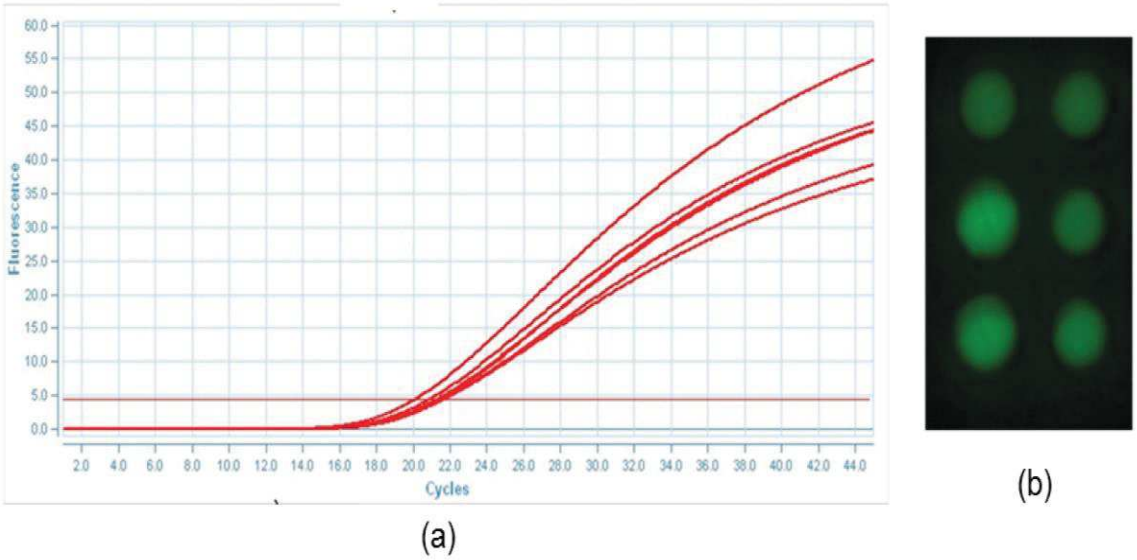


**Fig.2.** DNA detection via Real-Time PCR: a) amplification plot; b) fluorescence images of device.

More in details, an amount of 15 µl of PCR master mix (containing HBV-clone $10^5$ cps/µL) was loaded on each chamber (the loading process was performed at 70°C in order to melt the paraffin wax) and the amplification at three different annealing temperatures (60, 62 and 63°C) was conducted. The fluorescence images after each cycle was analyzed by the smart-software and the Ct values calculated.

The results are reported in Fig.3. The data indicate no relevant difference in terms of Ct for the three temperatures investigated with an average value for Ct of about 21.5. The reference samples processed on gold standard 96-well reaction plate in Applied Biosystems 7500 equipment report for the testing at different annealing temperature an average value of Ct 22.4 ± 0.5.

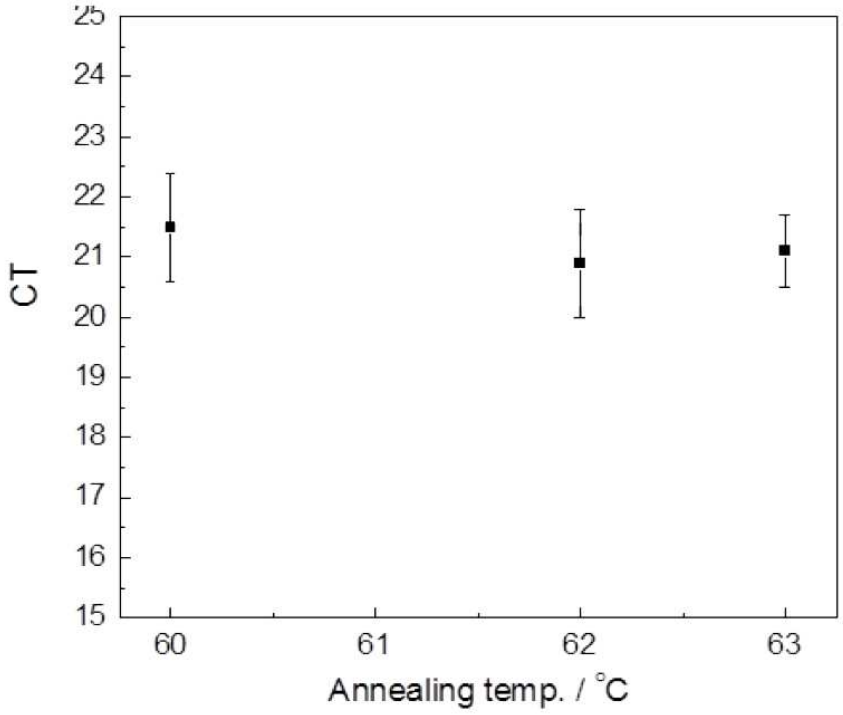


**Fig.3.** Ct values at different annealing temperature

These data indicate an improvement on PCR efficiency performed on microchip device of about 1 Ct respect to the commercial equipment. This advance was explained by the specific microchip design architecture that include a chamber designed to collect the paraffin wax (15 µL) on the upper cylindrical part (diameter 3.5 mm) while the biological mix (10 µL) is collected on the lower zone (diameter 3.2 mm): this shape in combination with a smart detection software improve the final signal enhances the optical fluorescent signal of platform.

*b) Probe characterization.*

To investigate the robustness of the assay at the annealing temperature of 60°C (since no difference in the annealing temperature was found-*vide supra*), additional experiments were performed with different probe amounts. With the same method above described, an amount of 15 µl of PCR of master mixes containing a concentration of $10^5$ cps/µL HBV-clone and different

probe amount (0.01, 0.05, 0.1 and 0.2 μM), were loaded into the microchip pre-heated chambers and Real-Time PCR amplifications carried out. Fig.4 reports the related experimental results.

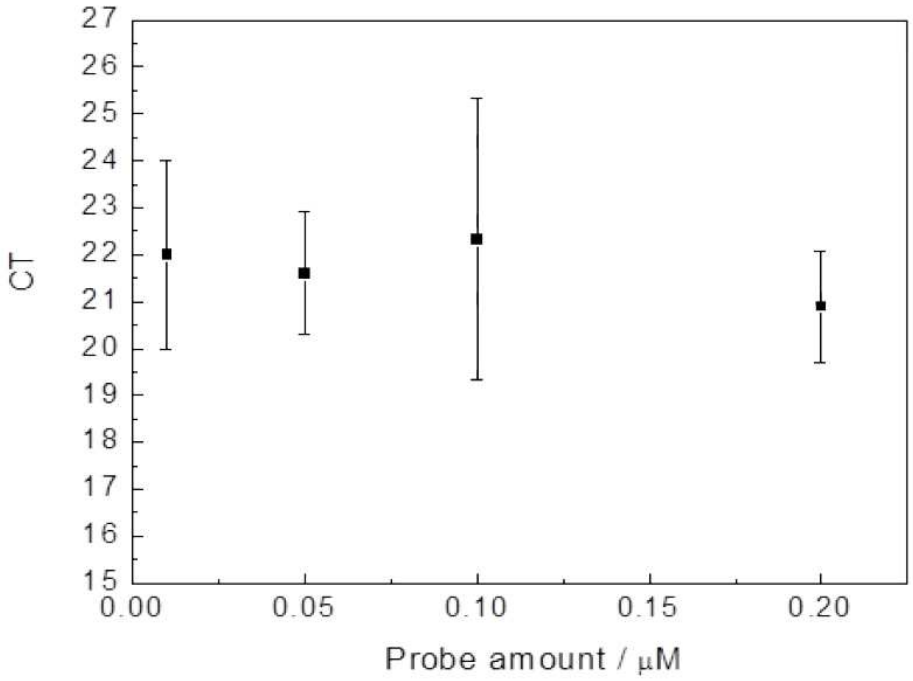


**Fig.4.** Ct values at different probe concentrations.

Also in this case no variation of Ct was found with an average value for Ct of about 21.3. No fluorescence signal was registered for the negative sample (data not showed). The reference samples processed on gold standard 96-well Applied Biosystem 7500 show an average value of Ct 22.7 ± 0.4.

These results prove the assay is robust in the experimental condition ranges confirming the improvement of sensitivity of about 1 Ct compared to the commercial equipment. Additionally, they indicate that the platform allows to use very low amount of probe (0.01 μM) without any efficiency variation.

## 4.2 – PCR free electrochemical detection of DNA.

Notwithstanding the important improvements introduced by the PCR-based technology described so far (section 4.1), the issue of costs and time for DNA analysis (i.e. the PCR reaction) remained a clear limitation for PoC DNA detection. For this reason, this module of my Ph.D. project was, subsequently, focused on the development of a silicon based miniaturized device for the PCR-free electrochemical detection of DNA.

Actually, the innovation consisted in a chemical strategy that integrates in a single miniaturized electrochemical device all elements required to, directly, detect pathogen genomes without any amplification step, but using the electrochemical transduction process.

### *4.2.1 – Miniaturized Electrochemical device.*

The electrochemical device was manufactured using the VLSI technology on an 8" silicon wafer substrate. The silicon chip is composed by 4 electrochemical cells each containing three planar microelectrodes, working electrode (WE) in Platinum, a counter (CE) and a reference (RE) electrode made in gold, produced with different shapes (both circular and rectangular) and arranged following different layouts (Fig 5). Each electrochemical cell is composed by three planar electrodes: a working electrode in platinum with size 1000 × 2000 µm, a counter and a reference electrode made in gold with size 800 × 500 and 800 × 1250 µm, respectively. The electrode-to-electrode distance are 100 µm. See Table 1.

Experimental details of the electrochemical devices are reported in the *Experimental Part* section at the end of this chapter.

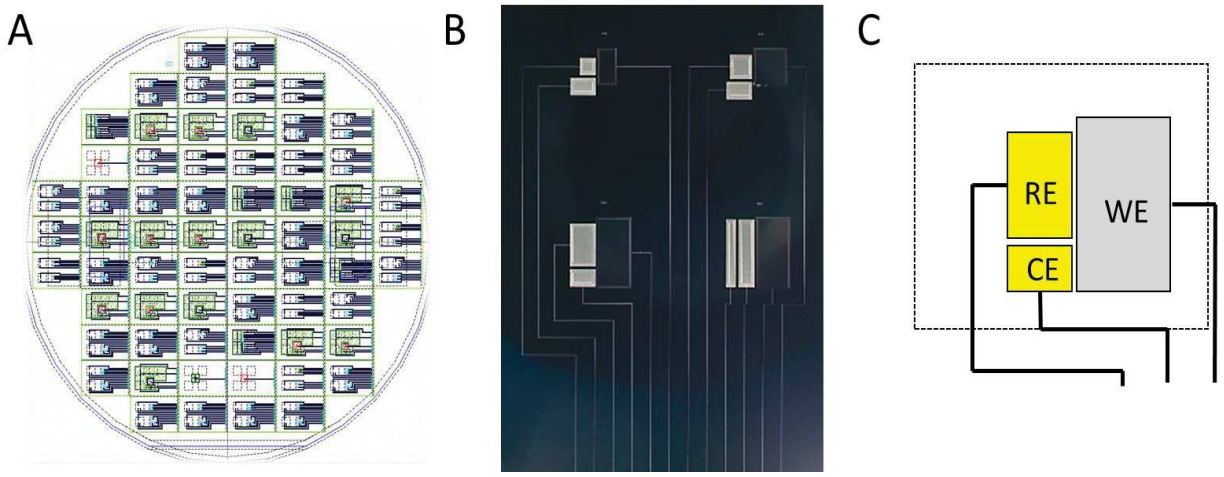


**Fig.5.** A) Silicon wafer. B) Electrochemical cells. C) Working (WE), reference (RE) and counter (CE) electrode.

**Table 1** Geometrical features for the four electrochemical tested cells.

| Elect. cells | WE area ($mm^2$) | CE area ($mm^2$) | RE area ($mm^2$) | Electrode Spacing (µm) |
|---|---|---|---|---|
| **1** | 2.4 | 0.4 | 1.0 | 100 |
| **2** | 2 | 0.4 | 1.0 | 100 |
| **3** | 1.6 | 0.4 | 1.0 | 100 |
| **4** | 1.2 | 0.4 | 1.0 | 100 |

This chip contains a resistor in the rear part (Fig.6A), important for the heating and temperature control during the denaturation and hybridization steps, and is assembled with a polycarbonate mask (Fig.6C), that defined the 4 reaction chambers for the 4 electrochemical cells. Each hybridization microchamber can be filled with 20 µl of sample solution, for test.

All elements, described, are assembled on a plastic holder to form the final device (Fig.6D).

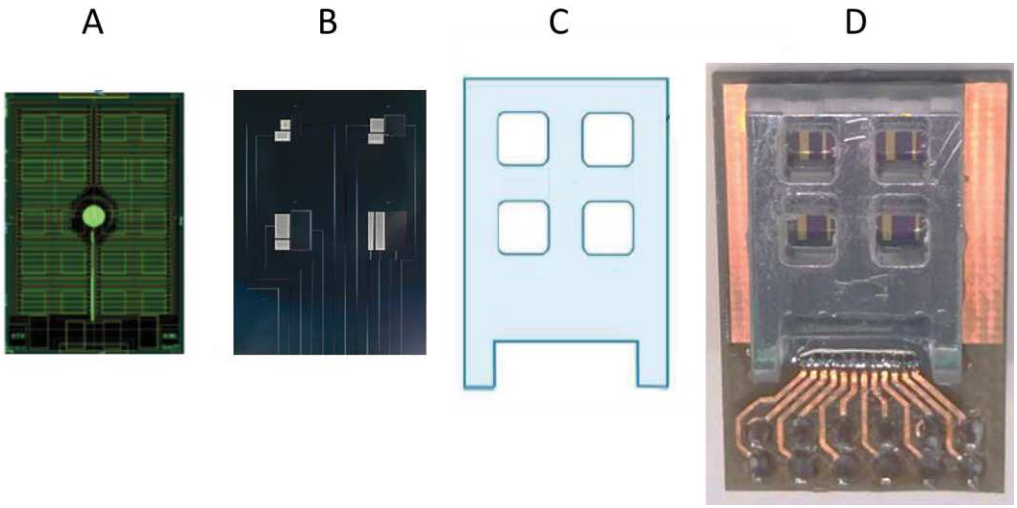


**Fig.6.** A) Resistor. B) Electrochemical cells. C) Polycarbonate mask. D) Whole device.

The working electrode, inside the electrochemical device, has been chemically modified to be used in the biological tests according to the procedure described in the *Experimental Part*. The chemical treatment scheme is summarised in Fig.7 together with the results of contact angle measurements confirming the goodness of each chemical treatment step.

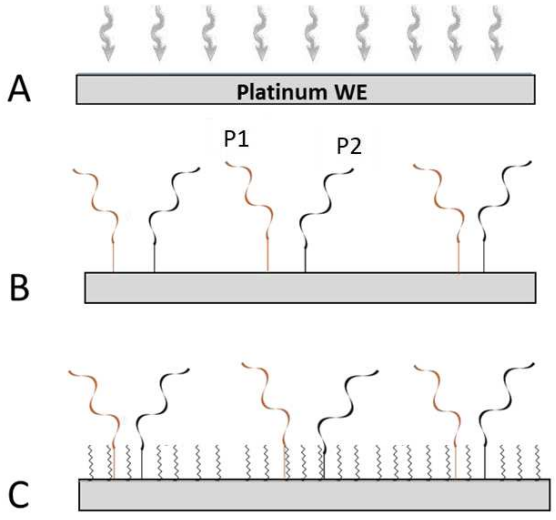


D

| Process step | Water Contact angle (°) |
|---|---|
| Untreated WE surface | 121.3 ± 5 |
| Cleaning | 83.3 ± 5 |
| P1 and P2 anchoring | 59.6 ± 3 |
| Alkyl passivation layer | 88.9 ± 2 |

**Fig.7.** Chemical treatment of WE surface: A) Oxygen plasma cleaning; B) probes anchoring; C) surface passivation; D) contact angle values.

### *4.2.2 – Electrochemical cells characterization.*

The first part of the study was focused on the electrochemical test of the cells, identifying the best electrodes layout in terms of sensitivity. To do this, I performed two series of SW measurements (experimental conditions are reported the *Experimental Part* section at the end of the chapter), using the complex $K_3Fe(CN)_6$ at different molar concentrations as analyte.

Results of the first series of measurements are reported below (Fig. 8-9-10-11). The dashed square delimitates the reaction chamber (Fig. 8A-9A-10A-11A); the tables reports all geometric values and combinations of electrodes.

(A)

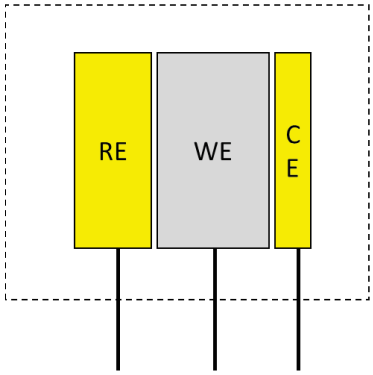


(B)

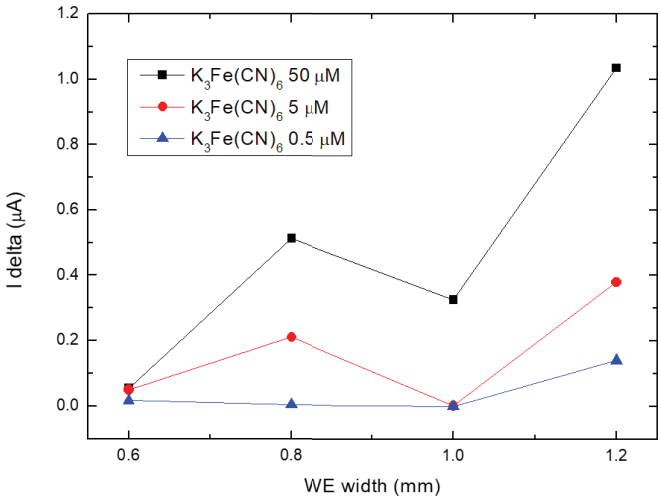


(C)

| Electrochem. Cells | RE area (mm) | WE area (mm) | CE area (mm) | Electrode Spacing (mm) |
|---|---|---|---|---|
| **1** | 0.5 x 2 | 0.6 x 2 | 2 x 2 | 0.1 |
| **2** | 0.5 x 2 | 0.8 x 2 | 2 x 2 | 0.1 |
| **3** | 0.5 x 2 | 1 x 2 | 2 x 2 | 0.1 |
| **4** | 0.5 x 2 | 1.2 x 2 | 2 x 2 | 0.1 |

**Fig.8.** Layout 1: (A) Electrodes layout. (B) $K_3Fe(CN)_6$ sensitivity graph. (C) Electrodes areas.

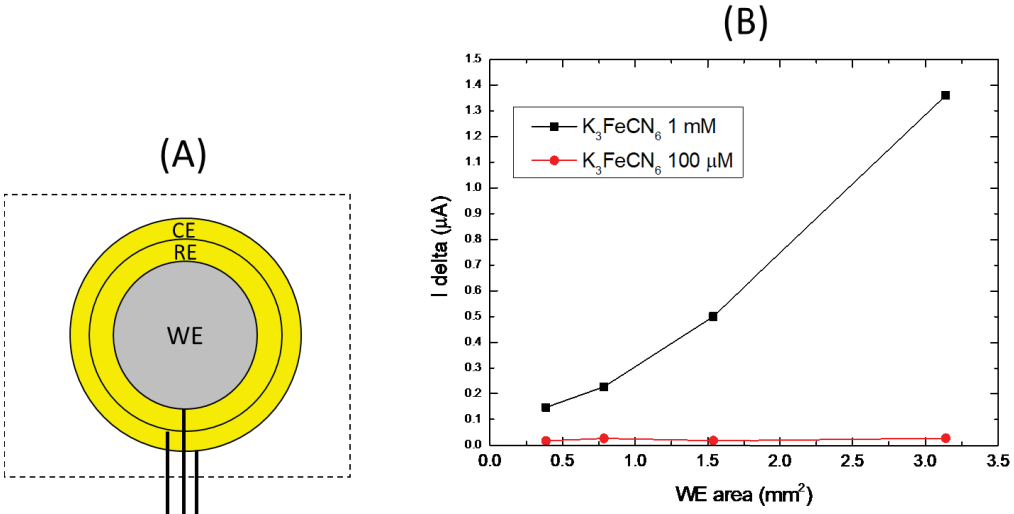


(C)

| Electrochem. Cells | WE | RE | | CE | | Electrode Spacing (mm) |
|---|---|---|---|---|---|---|
| | Diameter (mm) | Diameter (mm) | Ring thickness (mm) | Diameter (mm) | Ring thickness (mm) | |
| 1 | 0.7 | 0.9 | 0.2 | 1.5 | 0.2 | 0.1 |
| 2 | 1 | 1.2 | 0.2 | 1.8 | 0.2 | 0.1 |
| 3 | 1.4 | 1.6 | 0.2 | 2.2 | 0.2 | 0.1 |
| 4 | 2 | 2.2 | 0.2 | 2.8 | 0.2 | 0.1 |

**Fig.9.** Layout 2: (A) Electrodes layout. (B) $K_3Fe(CN)_6$ sensitivity graph. (C) Electrodes areas.

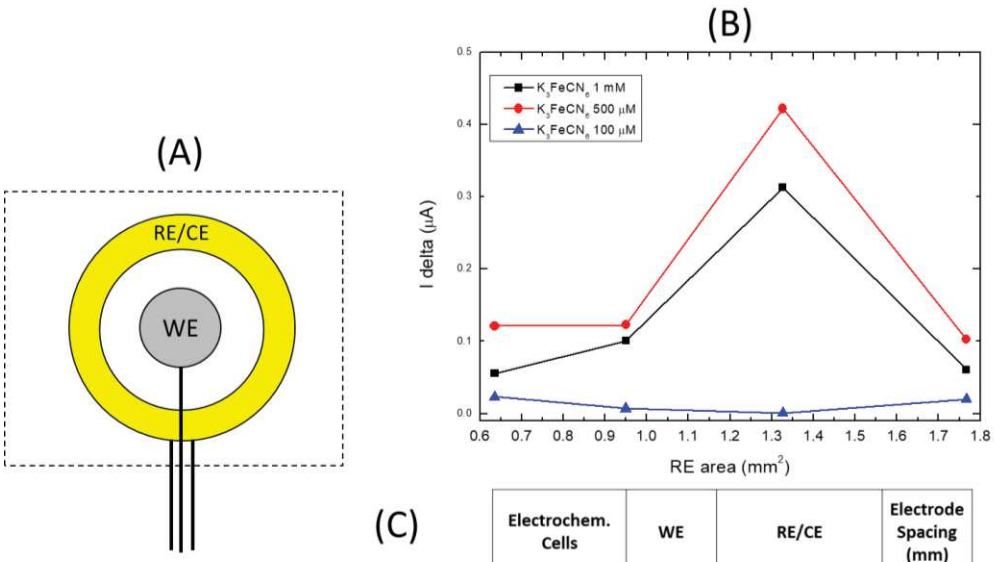


(C)

| Electrochem. Cells | WE | RE/CE | | Electrode Spacing (mm) |
|---|---|---|---|---|
| | Diameter (mm) | Diameter (mm) | Ring thickness (mm) | |
| 1 | 0.7 | 0.9 | 0.4 | 0.1 |
| 2 | 0.7 | 1.1 | 0.4 | 0.2 |
| 3 | 0.7 | 1.3 | 0.4 | 0.3 |
| 4 | 0.7 | 1.5 | 0.4 | 0.4 |

**Fig.10.** Layout 3: (A) Electrodes layout. (B) $K_3Fe(CN)_6$ sensitivity graph. (C) Electrodes areas.

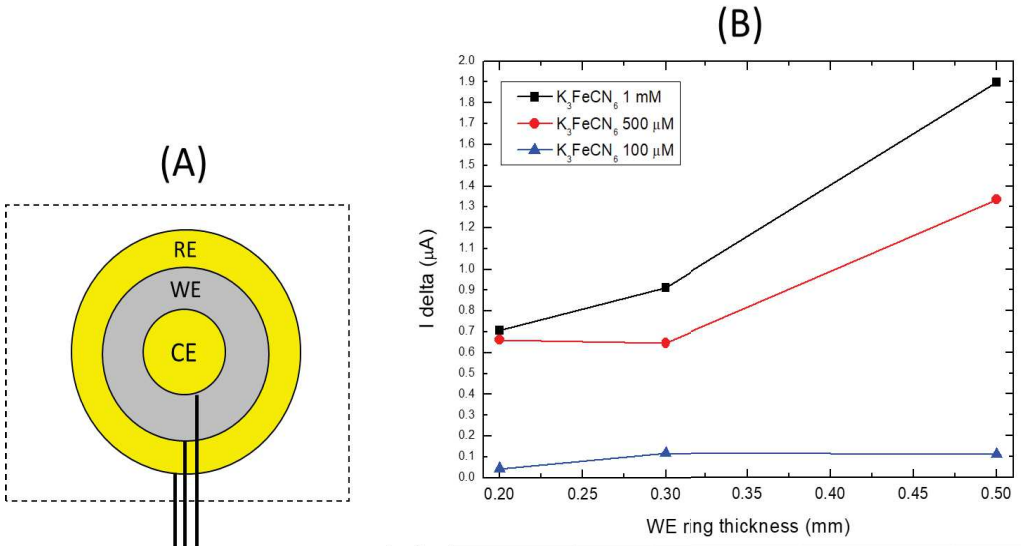


(C)

| Electrochem. Cells | CE | WE | | RE | | Electrode Spacing (mm) |
|---|---|---|---|---|---|---|
| | Diameter (mm) | Diameter (mm) | Ring thickness (mm) | Diameter (mm) | Ring thickness (mm) | |
| 1 | 1 | 1.2 | 0.2 | 1.8 | 0.2 | 0.1 |
| 2 | 1 | 1.2 | 0.3 | 2 | 0.2 | 0.1 |
| 3 | 1 | 1.2 | 0.4 | 2.2 | 0.2 | 0.1 |
| 4 | 1 | 1.2 | 0.5 | 2.4 | 0.2 | 0.1 |

**Fig.11.** Layout 4: (A) Electrodes layout. (B) $K_3Fe(CN)_6$ sensitivity graph. (C) Electrodes areas.

Considering the I delta values from the plots in figures, SW measurements for $K_3Fe(CN)_6$ electrochemical detection revealed that the best sensitivity was that one coming from the layout 1 (Fig.8B). This geometric combination, actually the cell with the biggest value of working electrode area, was able to detect up to 0.5 µM of $K_3Fe(CN)_6$, while all other circular layouts are sensitive only up to 100 µM of analyte (Fig. 9B-10B-11B).

Subsequently, I repeated the test changing the analyte with the Osmium complex $[Os(bpy)_2DPPZ]Cl_2$, i.e. the one that I used for the DNA detection (see section 4.2.3), in order to validate the layout 1 as the best electrode geometric combination for the DNA electrochemical PCR-free detection experiment. Also in this case, this layout showed a reliable performance, with a high sensitivity of the cell with the biggest WE area (Fig. 12B-C), so that this layout was chosen for the biological tests on the electrochemical device.

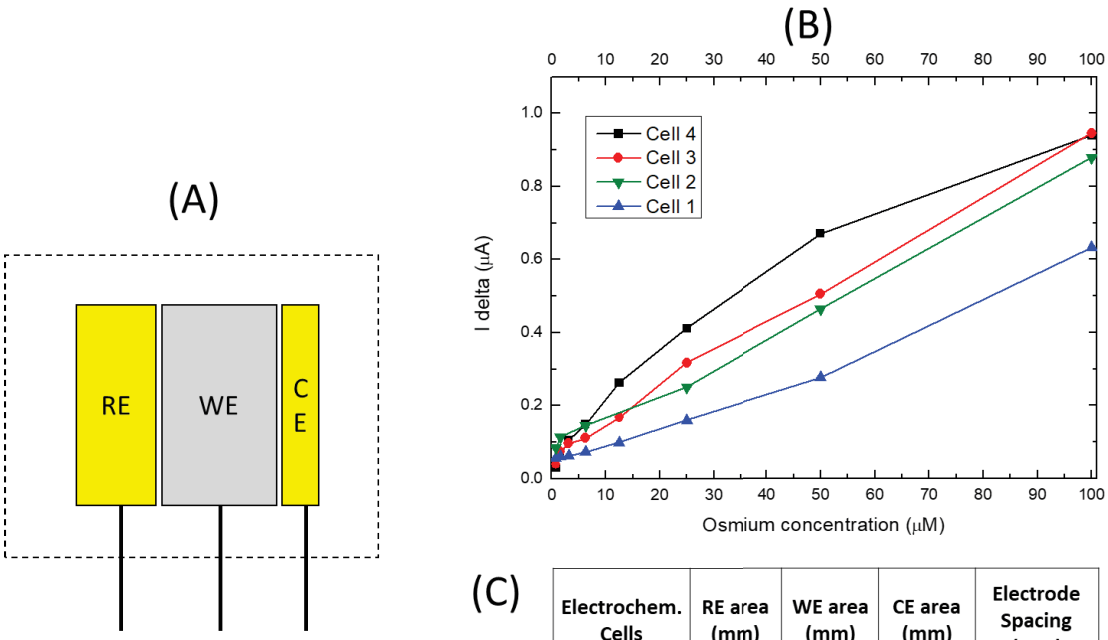


(C)

| Electrochem. Cells | RE area (mm) | WE area (mm) | CE area (mm) | Electrode Spacing (mm) |
|---|---|---|---|---|
| **1** | 0.5 x 2 | 0.6 x 2 | 2 x 2 | 0.1 |
| **2** | 0.5 x 2 | 0.8 x 2 | 2 x 2 | 0.1 |
| **3** | 0.5 x 2 | 1 x 2 | 2 x 2 | 0.1 |
| **4** | 0.5 x 2 | 1.2 x 2 | 2 x 2 | 0.1 |

**Fig.12.** Layout 1: (A) Electrodes layout. (B) [$Os(bpy)_2DPPZ]Cl_2$ sensitivity graph. (C) Electrodes areas.

### *4.2.3 – DNA electrochemical detection strategy setup*

For the biological validation of the electrochemical device Hepatitis B virus (HBV) clone has been used. This is a pathogen microorganism causing hepatitis and infection which can lead to cirrhosis and hepatocellular carcinoma and may increase the risk of pancreatic cancer; for the tests, I used both the analytical sample (7.1 Kb synthetic plasmid clone) and real sample (3.3 Kb genome, extracted from human blood).

The strategy has been conceived to employ a chemical approach combining a cooperative in situ hybridization with two specific probes (P1 and P2 in Fig.13) chemically anchored onto the Platinum working electrode surface and an electrochemical transduction by a redox intercalative Os-complex (Fig. 14).

The two thiol 5'-terminated hybridization HBV probes (Forward → HS-(CH2)6-GTGAGTGATTGGAGGTT and Reverse → HS-(CH2)6-CACATCAGGATTCCTAGG) were properly designed to recognize independently different sequences in both antiparallel strands of the HBV target genome (orange and blue bar in Fig.13). Moreover, to guarantee the simultaneous hybridization with the two strands of the genome target, a sequence gap of 138 bp between the two anchored probes (Fig. 13) was maintained to permit an efficient genome folding on the electrode surface, increasing the hybridization product stability.

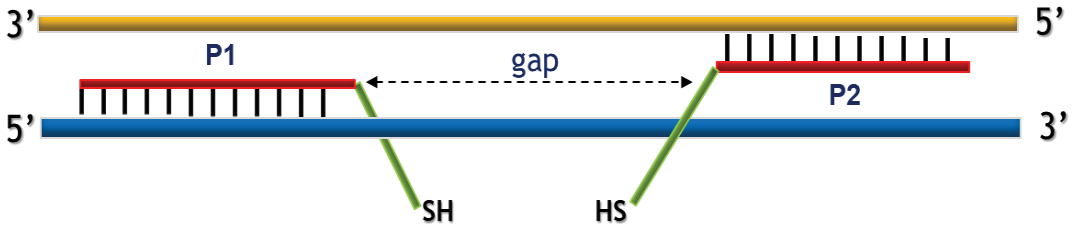


**Fig.13.** Hybridization strategy for the PCR-free detection of target genome.

The detection of the hybridization strategy, then, was based on the redox activity of the Os-complex [Os(2,20-bipyridine)(dipyrido[3,2-a:2',3'-c]phenazine)]$Cl_2$, ([$Os(bpy)_2DPPZ]Cl_2$) (Fig. 14A). This complex has been selected since it strongly and specifically intercalates to double stranded DNA with a Kb of $5 \times 10^6$ $M^{-1}$ [2,3] This complex gives a Square Wave (SW) electrochemical response at about 0.46 V (Fig.14B).

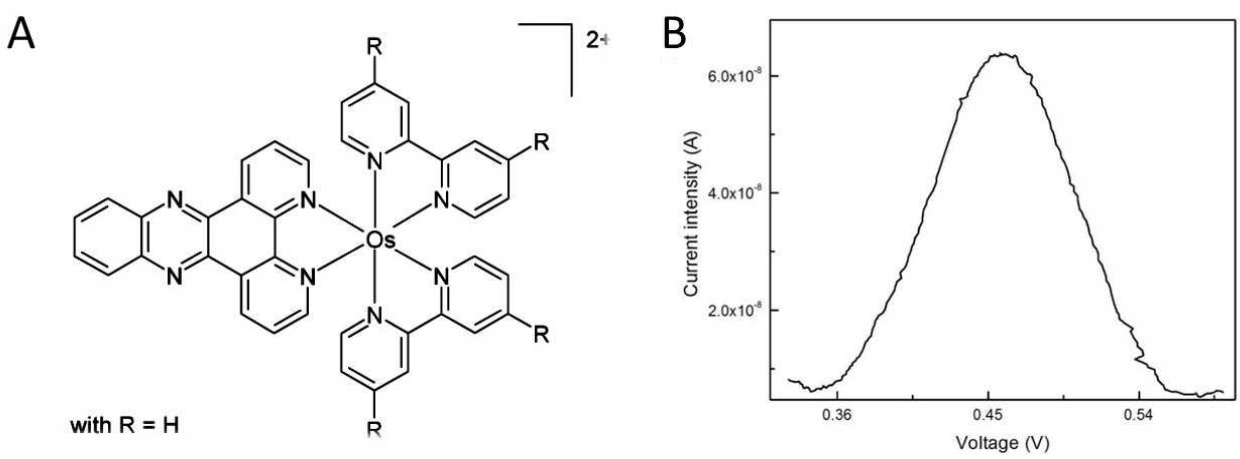


**Fig.14.** $[Os(bpy)_2DPPZ]Cl_2$ : A) chemical structure; B) SW response (oxidation at + 0.46 V)

The 11-mercaptodecane passivation layer (described in section 4.2.2) creates a barrier that avoids the interaction between the Os-complex and the WE surface; in this way, the Os-complex can't trigger the redox activity and the electrons exchange with the WE, thus reducing the intensity of the SW current signal coming from the electron release onto the WE surface (Fig.15).

However, if there is a dsDNA (i.e. the HBV target genome hybridized to the probes), this allows the Os molecules to intercalate and reach the right distance from the WE to trigger the redox process. This means that only if the target genome is present there is an increase of the current signal given by the electron release by the Os-complex oxidation (Fig.16A-B-C-D).

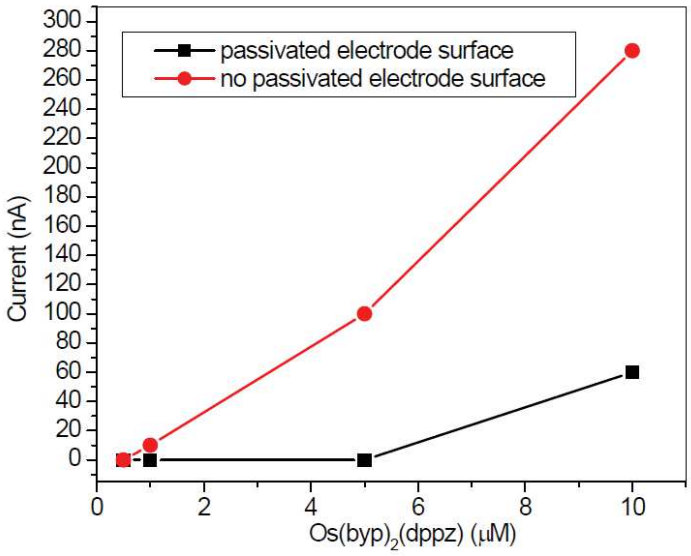


**Fig.15.** SW measurements on passivated (■) and not passivated (●) modified electrode surface (no HBV hybridization) at different $[Os(bpy)_2DPPZ]Cl_2$ probe concentrations. Not passivated electrode surface (●) exhibited a measurable redox currents over all explored range of the $[Os(bpy)_2DPPZ]Cl_2$ with signal increasing with the increasing of Os-complex concentrations. On the contrary, the passivated surface (■) shows a negligible redox currents up to $[Os(bpy)_2DPPZ]Cl_2$ concentration of 5 μM. This data demonstrates that alkyl-thiol layer guarantees an effectiveness surface passivation providing a diffusion barrier for unspecific redox signal.

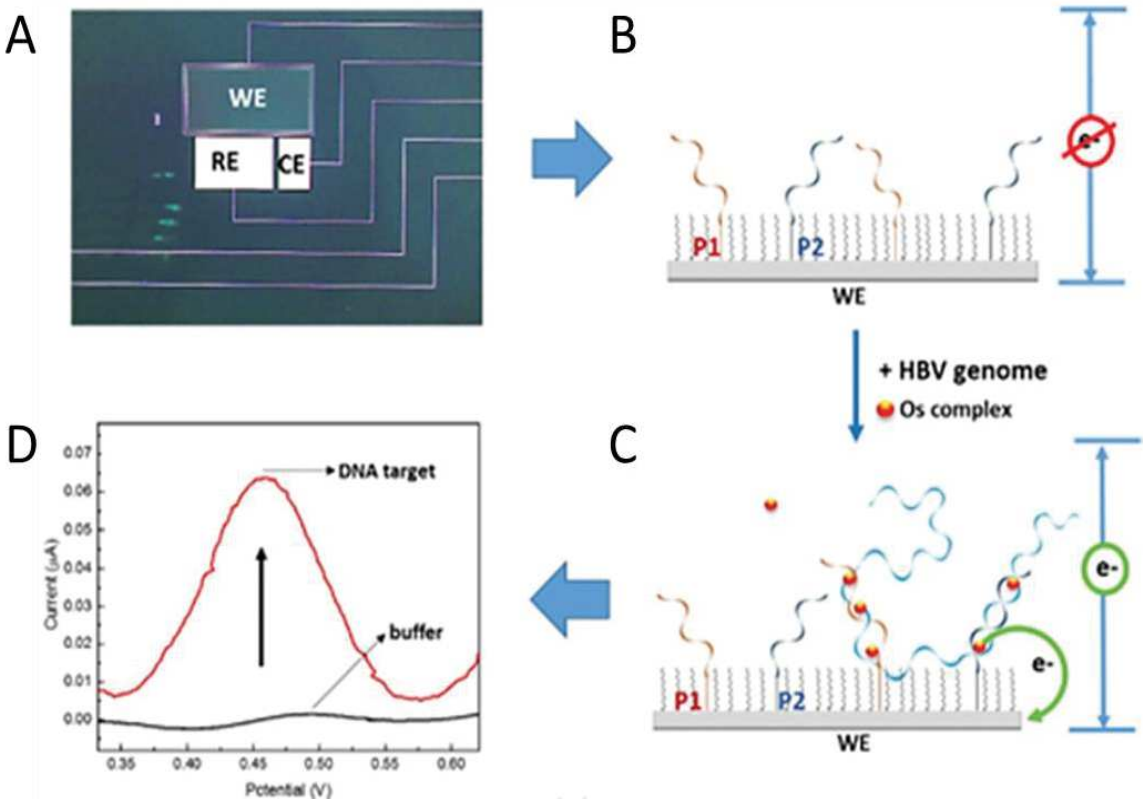


**Fig.16.** Operating principle of the PCR-free electrochemical pathogen system assay: A) planar biosensor microelectrodes; B) WE modified with P1 and P2 ssDNA probes; C) HBV target genome cooperative hybridization at the modified WE and intercalation of $[Os(bpy)_2DPPZ]Cl_2$; D) expected redox current trend in presence or absence of the hybridized HBV target genome.

### *4.2.4 – PCR free DNA detection*

Following the described strategy for the PCR-free HBV detection, the system was validated using various amounts of the synthetic HBV-clone target, as analytes, in a concentration range typical of Real-Time PCR calibrators before amplification (2, 20 200 and 2000 copies per reaction). We chose to start with 2000 copies being a value in the low concentration range of Real-Time PCR calibrators (typically from $1 \times 10^8 – 1 \times 10^2$ copies per reaction).

The HBV target hybridization on Pt-WE modified surface with P1 and P2 probe was carried following the protocol reported in the *Experimental Part* at the end of the chapter; the experiment has been performed at pH ~ 7.4, that is a pH value which optimally affects the hybridization [4,5].

An SW voltammogram was then recorded, from the electrochemical device, after the hybridization in presence of a solution containing $[Os(bpy)_2DPPZ]Cl_2$ at a concentration of 5 µM. In parallel, the same amounts of HBV-clone copies per reaction were amplified by Real-Time PCR, in order to estimate the cycles threshold for each template (2, 20, 200, 2000 copies) and use the LoD value as comparison.

The results from the PCR-free approach (Fig.17A, red curve) gave the current density values of 2.6 ± 0.3 µA $cm^{-2}$ for 2000 copies per reaction, 1.4 ± 0.2 µA $cm^{-2}$ for 200 copies per reaction and 0.8 ± 0.2 µA $cm^{-2}$ for 20 copies per reaction, whereas no significant signal was detected for the sample containing 2 copies per reaction (Fig.17A-B). These data prove a Limit of Detection (LoD) for the HBV synthetic genome of 20 copies per reaction, which is at a lower magnitude respect to the standard Real-Time PCR LoD (as illustrated in Fig.17A, green rings in red and black curve). Moreover, it has to be considered that Ct values from PCR based approach come from the exponential amplification of the starting amount of HBV-clone copies, while, in the proposed PCR-free approach the starting copies are directly detected (Fig.17B).

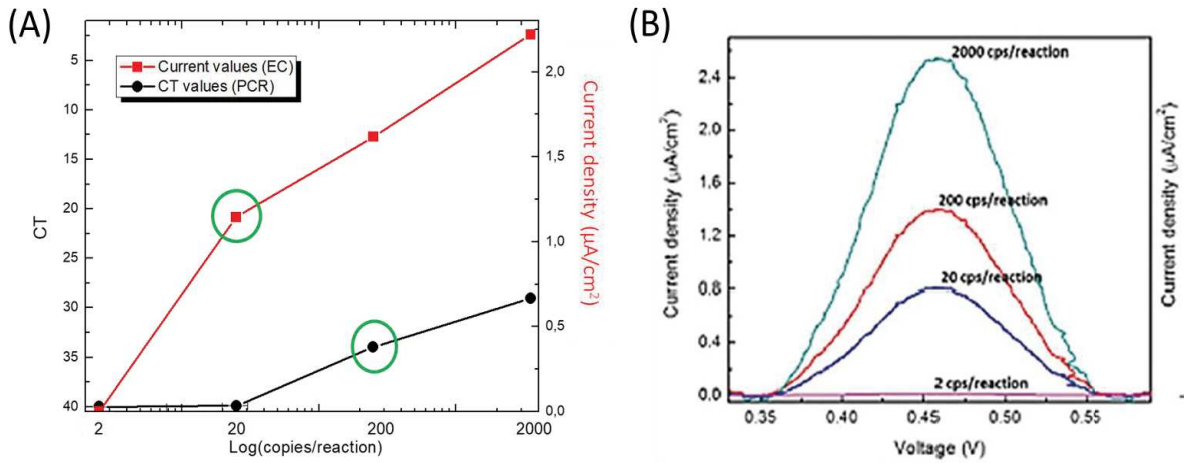


**Fig.17.** (A) Red curve: current density values from the PCR-free detection of the HBV-clone. Black curve: Ct values from standard Real-Time PCR detection. (B) SW analysis of HBV-clone copies.

To support the results above, the kinetics of hybridization has been verified by both Scanning Electron Microscopy (SEM) and Atomic Force Microscopy (AFM) analysis (section 4.2.5). Figure 18 reports the SEM and AFM images for the Pt-WE modified with P1 and P2 and, as comparison, the unmodified Pt-electrode surface, after HBV-clone 120 copies addition.

In the first case (Fig.18 A-i), the presence of P1 and P2 probes allows the clones to hybridized, stably, thanks to the cooperative effect described before; is possible, in fact, to see the clones regularly distributed on the WE surface (Fig.18 A-ii). In SEM image, all clones appear as single units well separated from each other (yellow ring in figure). This is well-supported by the AFM section profile (Fig.18 A-iii) showing a width average value of about 1.5 µm and a height average value ranging from 20 to 40 nm, according to the expected value for a single ds HBV-clone sized 7144 bps.

In the second case, instead, the absence of P1 and P2 probes causes the absorption of clones (Fig.18 B-i) on the WE surface and induces the formation of HBV-clone aggregates, irregularly distributed (Fig.18 B-ii and B-iii) and easily removable by washing step.

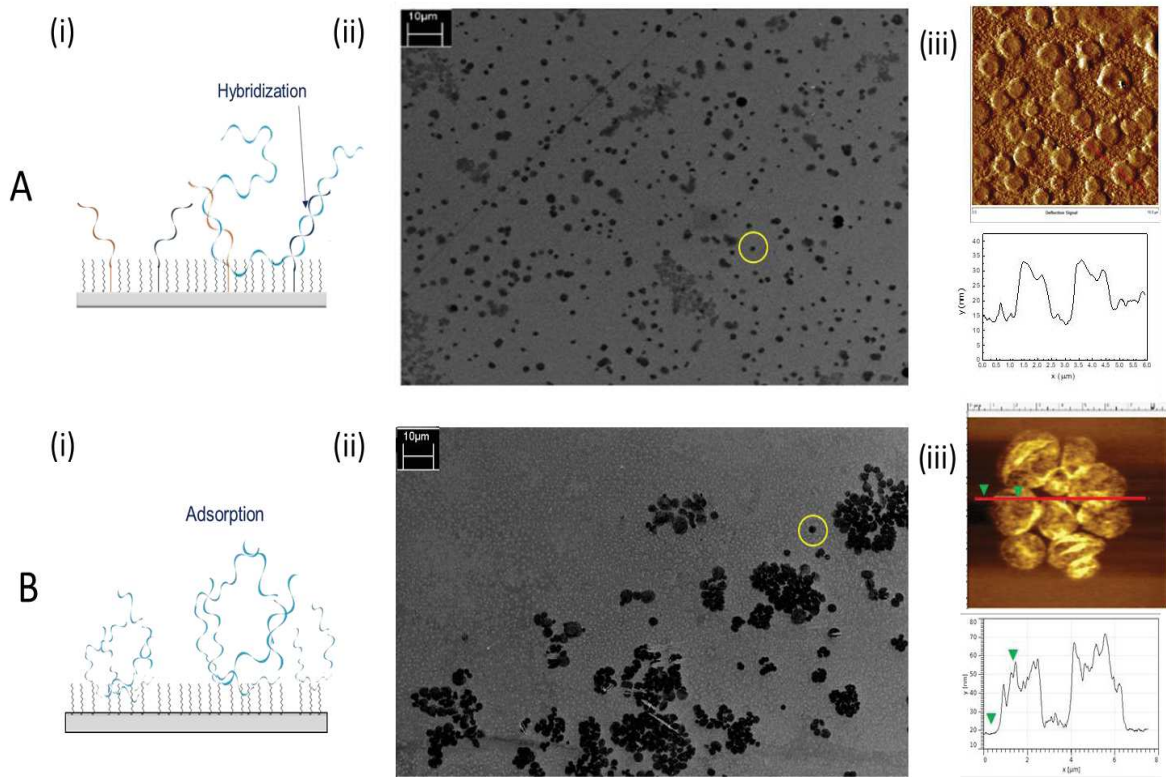


**Fig.18.** A) WE with anchored HBV probes: (i) hybridization scheme; (ii) SEM and (iii) AFM image of WE surface after HBV-clone addition. B) WE without anchored HBV probes: (i) adsorption scheme; (ii) SEM and (iii) AFM image of WE surface after HBV-clone addition. Yellow rings highlight the HBV-clone spotted onto the WE surface.

The cross-reactivity of the proposed biosensor system was, also, tested with an unspecific target, i.e. the Mycobacterium tuberculosis (MTB) synthetic clone at a concentration of 2000 copies per reaction.

SEM images and the SW plot, reported in Fig.19A, showed that there is no electrochemical signal when an unspecific target MTB is spotted on the WE modified with HBV probes, that means no interaction because of the missing probe-target specificity.

To demonstrate this, in parallel, I performed a second trial using 2000 copies per reaction of the specific HBV target in the same experimental conditions, as reported above (Fig. 19B). In this case, after washing step, both SEM image and the SW current voltammogram confirmed the presence of hybridized HBV clones on the WE surface.

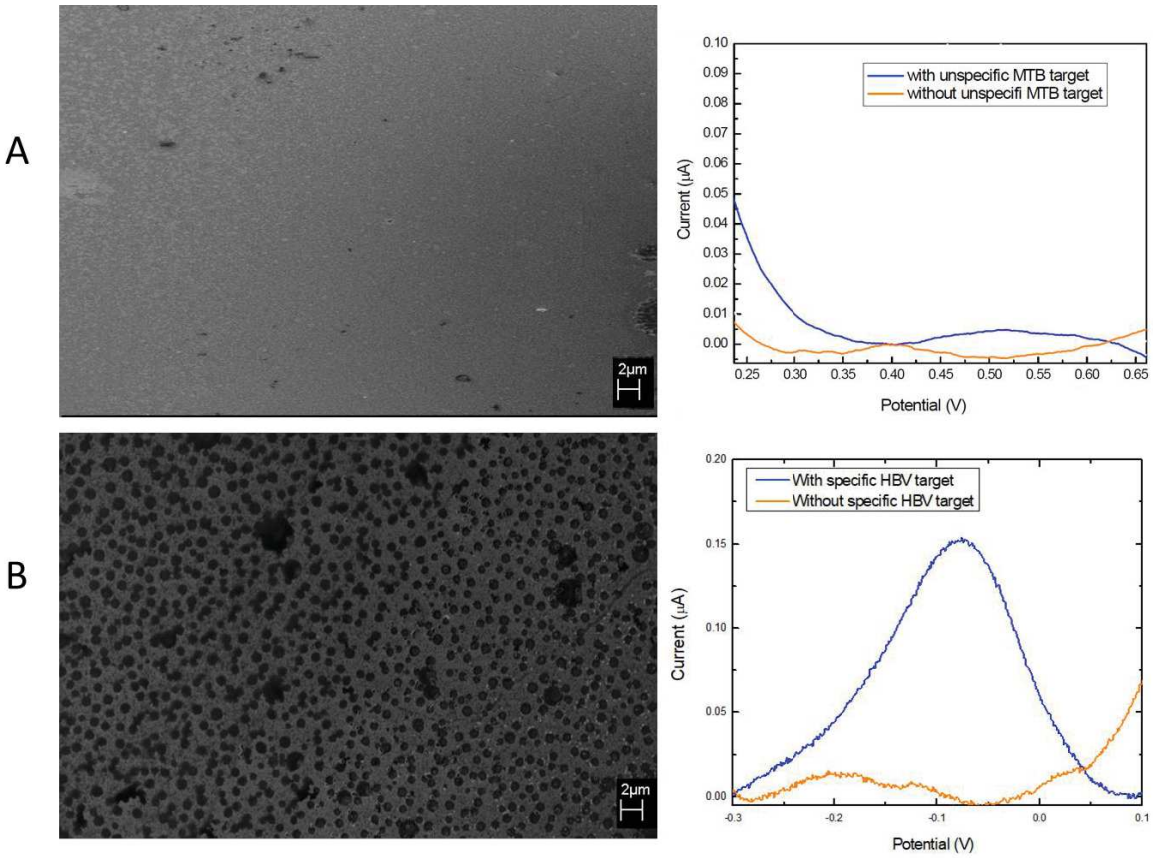


**Fig.19.** A) On the left: SEM image of WE surface section washed after hybridization step with 2000 copies of unspecific MTB target; on the right: SW voltammogram of device with (blue line) and without (orange line) the MTB target. B) On the left: SEM image of WE surface section washed after hybridization step with 2000 copies of the specific HBV target; on the right: SW voltammogram of device with (blue line) and without (orange line) the HBV target.

This proved that our chemical strategy not only fully reached the goal to achieve pathogen genetic detection without any amplification step, but also guaranteed the specificity of target quantification.

Encouraged by these results, we investigated our system assay with a real sample, testing an extracted HBV genome from human blood. This sample, bearing a starting concentration of $10^7$ cps per reaction (quantified by Real-Time PCR), was diluted to obtain testing solutions containing a total DNA amount of 2, 20 200 and 2000 copies per reaction, respectively. Electrochemical experiments were performed according to the previous test with synthetic clones (section 4.2.8) and the results are reported in Fig.20. In this case the positive response is observed up to 200 copies per reaction (LoD) with a current density value of 0.5 ± 0.1 µA $cm^{-2}$. This LoD value is one

order of magnitude lower than that of the analytical sample (synthetic HBV clone, section 4.2.8) and it should be probably attributed to the presence of interfering species in the extracted sample.

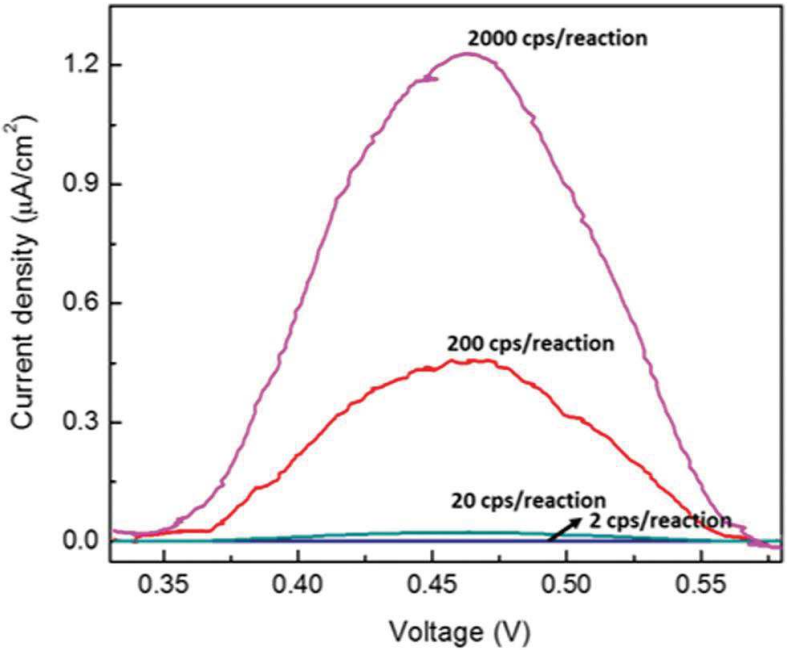


**Fig20.** Current density versus V for the testing of the HBV extracted sample (the hybridization was transduced by 5 μM of $[Os(byp)_2(dppz)]Cl_2$. All measurements were performed with a scan rate of 10 $mVs^{-1}$.

Interestingly, the current density values for analytical samples are always higher than those of the extracted ones at the same HBV genome concentrations (Fig.21). This difference is in excellent agreement with the different chain lengths of the two tested samples. In fact, the analytical sample HBV clone consists of the genome (3.3 Kb) cloned into a plasmid PBR322 vector (3.8 Kb) corresponding to a final circular structure of 7144 bps. On the other hand, the extracted sample does not include any vector, having then the size of the HBV genome, corresponding to 3300 bps. This difference results in a higher amount of $[Os(bpy)_2DPPZ]Cl_2$ intercalating into the ds HBV-clone, with a consequent higher redox signal.

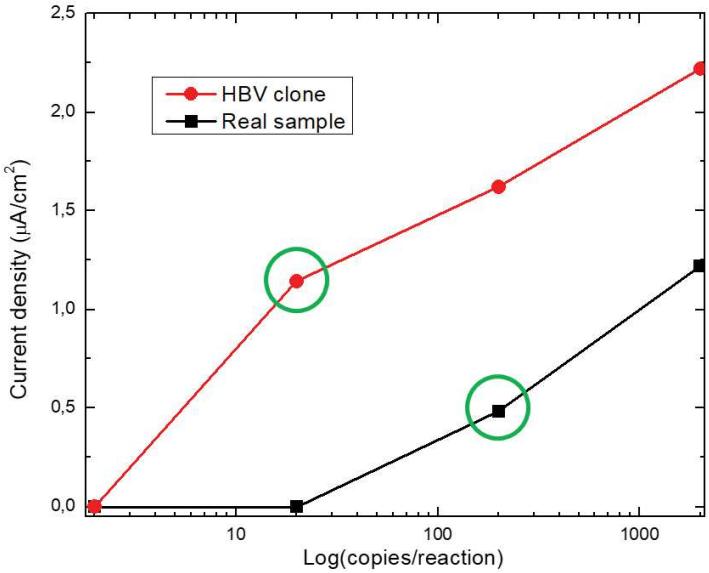


**Fig.21.** SW current signal trend comparison between the HBV-clone (red curve) and HBV real sample (black curve) hybridization. Green rings highlight the LoD for both measurements.

## 4.3 – Other applications of electrochemical detection technology.

Once verified the advanced performances of the proposed miniaturized detection technology, described above, other possible sensing applications have been tested. In this sense, the EC device has been used for the non-enzymatic detection and quantification of glucose in human plasma and saliva sample, and phenylalanine (Phe) in urine sample.

### *4.3.1 – Glucose sensing*

To perform the glucose (and aminoacids) sensing test, the EC device (Fig.22) was modified by substituting the Platinum coating of the WE with Nickel. This is, in fact, the most attractive nanomaterial for non-enzymatic detection of glucose, thanks to its peculiar properties [6].

In this third generation of glucose sensors, the catalytic activity of the glucose oxidase (GOx) enzyme has been substituted by Nickel, being more stable and versatile. This material exhibites

the advantages of good sensitivity, low production cost and extremely high stability and specificity if compared to GOx.

The sensing mechanism, investigated and proposed for the first time from Fleishman et al [7] and confirmed by recent works [8], establish that the catalytic sensing species $Ni(OH)_2$ and NiOOH are produced on the electrode surface by electrochemical oxidation on alkaline electrolyte of Ni0 layer [9]. As described in literature, glucose molecules are oxidized on the electrode surface by NiOOH species to radical intermediates that are rapidly converted to gluconolactone. The produced $Ni(OH)_2$ species are reconverted to NiOOH by applying a specific potential.

As for the PCR-free DNA detection experiments (section 4.2), the layout of EC device used for testing has been designed to host, on the same silicon device, four types of integrated electrochemical cells containing three planar microelectrodes with the function of working (Ni material), counter (Gold material) and reference (Gold material) electrodes, respectively. The four cells geometrically differ in the size of the Ni-WE that has been designed to expose a surface area from 1.2 $mm^2$ to 2.4 $mm^2$ (Fig.22)

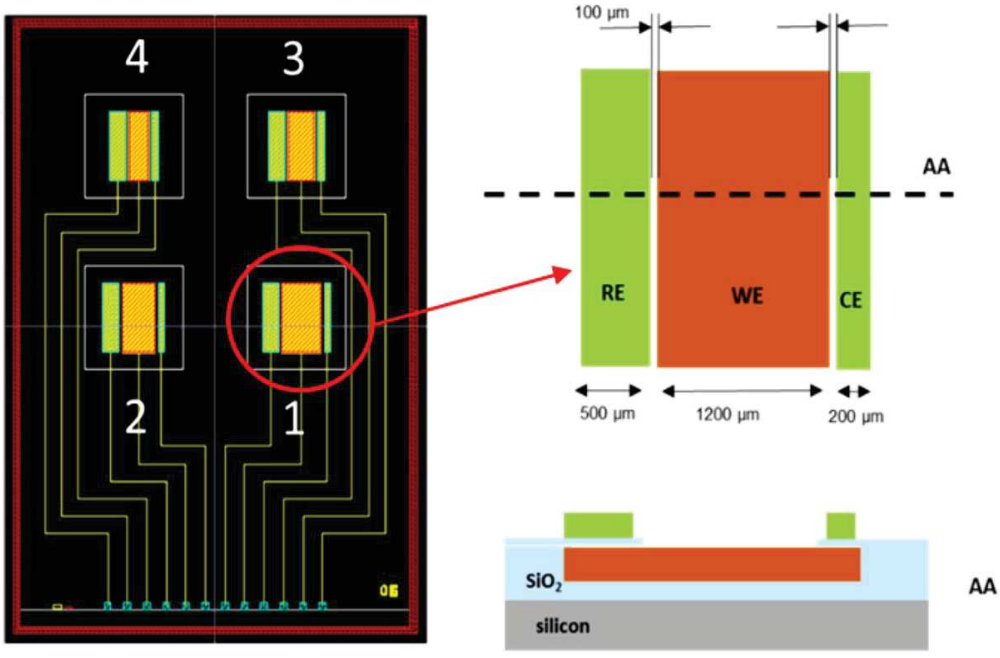


**Fig.22.** EC device layout (left); zoom and cross section of Cell 1 (right).

The first aim was to evaluate the analytical performances of the device as function of the WE area. Fig.23 illustrates the current intensities obtained by chronoamperometry experiments at a voltage potential of + 0.8 V for the four electrochemical cells, with a glucose concentration ranging from 0 to 60 µM (pH 11.2 in PBS). A linear detection ranges from 0.3 nM to 6 mM is observed for all four types of cell, with a LoD of about 10 µM. It can be noticed that cell 1 (WE area 2.4 $mm^2$) show the highest current intensities values over the entire explored range of glucose concentration, with a sensitivity (calculated as the slope of the linear part of the curve) of about 40.0 ± 0.2 µA $mM^{-1}cm^{-2}$.

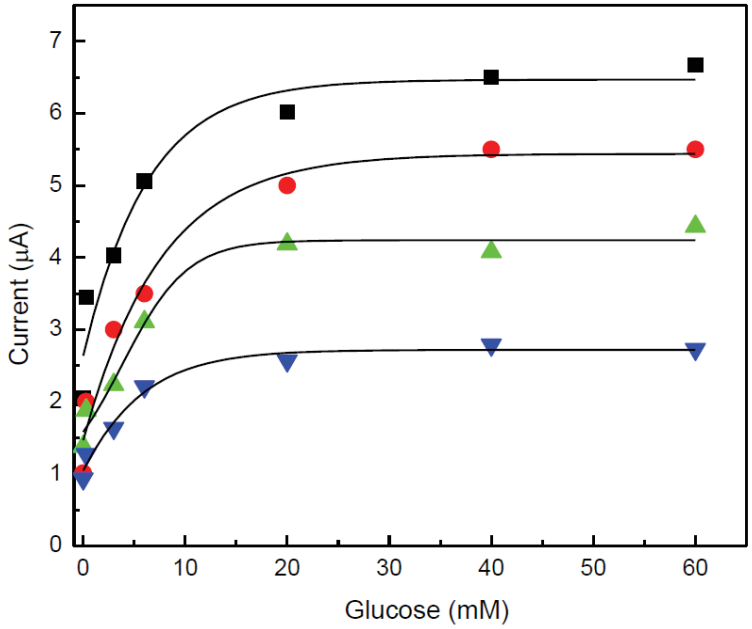


**Fig.23.** Ni EC device Glucose sensing (pH 11.2 in PBS): EC Cell 1 – WE area 2.4 $mm^2$ (■); EC Cell 2 – WE area 2.0 $mm^2$ (●), EC Cell 3 – WE area 1.6 $mm^2$ (▲); EC Cell 4 – WE area 1.2 $mm^2$ (▼).

On the basis of the above discussed data, cell 1 has been selected for the next analytical performances investigation. Moreover, since the non-enzymatic glucose sensing is largely influenced by the pH values, the Cell 1 was characterized at different pH values in PBS buffer of 7.4, 9.0, 11.2 and 13.0, using a concentration of glucose of 20 mM as analytical sample (Fig.24).

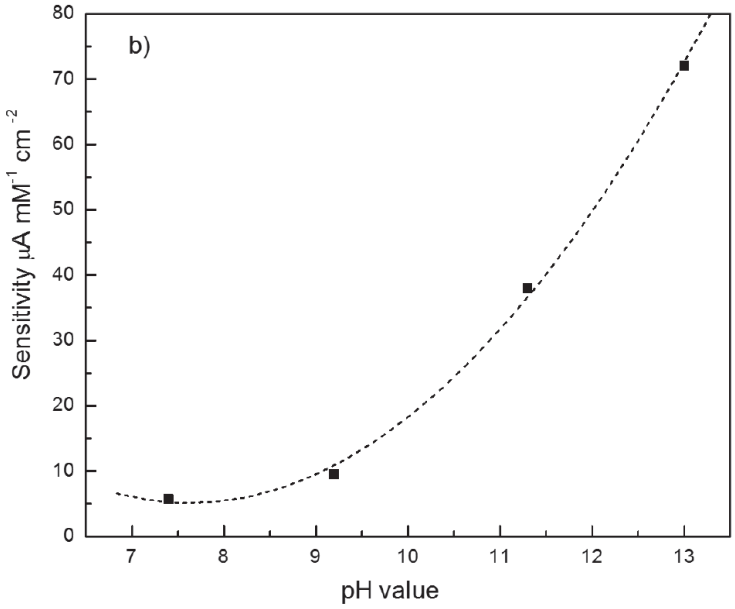


**Fig 24.** Cell1- Ni EC device glucose sensing vs pH values (PBS buffer).

Results clearly indicate an increasing of the sensitivity with the increasing of pH value, with a maximum of 70 µA $mM^{-1}$ $cm^{-2}$ at pH 13.0.

Once set the EC cell and the experimental conditions, the glucose sensing was tested for human plasma and saliva samples (Fig.25).

In plasma testing, PBS buffer was used at pH 11.2, since from previous studies it has been proved to exhibit a good compromise between sensitivity and bio-compatibility versus biological media; pre-diluted human plasma sample (10 µl, PBS pH 10.5) was loaded to cell 1 and, after current stabilization, various aliquots of glucose solution were added to obtain a concentration range from 3.0 µM to 33.4 µM.

Fig.25a reports the plot of current density *versus* the glucose amounts in plasma media. Data were interpolated by a linear fit giving the equation Y=2.62 +0.693*X (R2=0.9751). This gives a sensitivity value of about 0.7 µA mM-1 cm-2.

This value is about 20 times lower than that previous observed in the experiment with analytical sample in the same experimental condition (Fig.24 at pH 10.5). This can be reasonably attributed to the interferences gave by the complexity of the plasma biological media.

To confirm the effectiveness of our sensor, we carried out a measurement with a real sample consisting in a human plasma diluted 1:1 with PBS pH 11.2. A current density value of about 3.8 µA/cm2 was recorded, corresponding to a glucose amount of about 1.71 mM (61.56 mg/dl) by using the previous calibration curve above discussed. The glucose amount in the same blood sample was measured by the commercial PoC system ACCU-CHECK Aviva, giving a value of 75 mg/dl. It is noteworthy this value is quite comparable with what found with the Ni EC device here presented, confirming the effectiveness of the device.

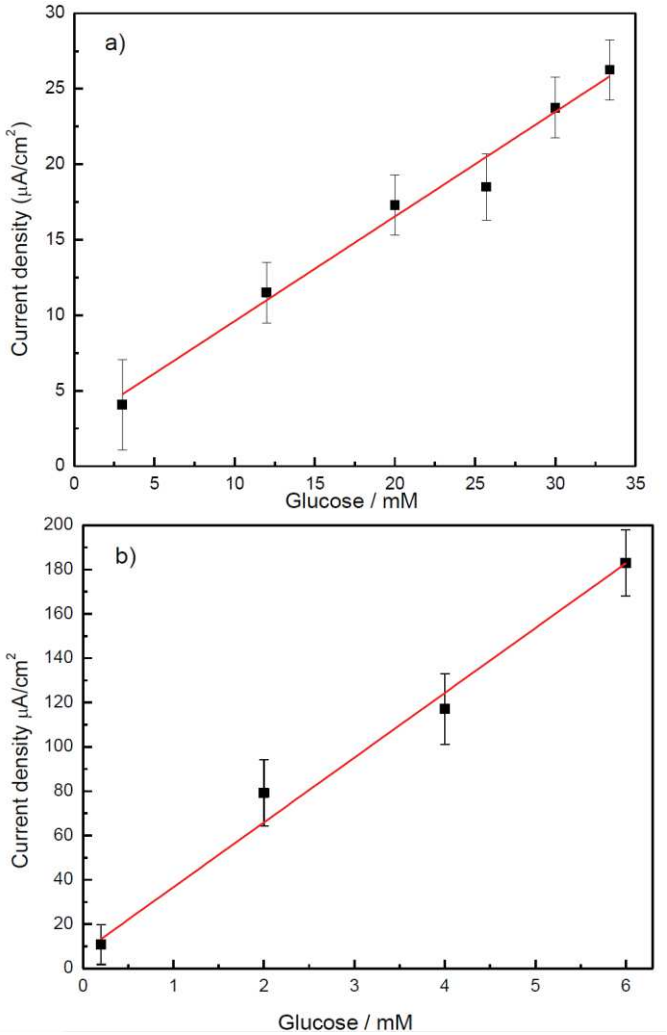


**Fig.25.** Cell 1-Ni EC device Glucose sensing tests in (a) human plasma and (b) saliva.

For the saliva testing, instead, PBS buffer was used at pH 13 (higher than that used for plasma) to increase the sensitivity of the device since the concentration of glucose in the saliva is lower than in the blood [10]. With the same approach employed for the plasma, the salivary glucose was detected after collection and dilution 1:1 with solution of PBS pH 13 (calculated final pH 12.7). Fig.25b illustrates the current density *versus* glucose concentration spiked in the saliva sample.

The linear fit of the data gives the equation Y=7.47+29.22*X; (R2=0.9853), with sensitivity value of about 29.2 μA $mM^{-1}cm^{-2}$. This value is about the half of that observed in the experiment with analytical sample (Fig.24 at pH 12.7). Also in this case, this difference can be probably attributed to the interference of the saliva media that, apparently, is less effective than plasma interference. The study was concluded with the measure of glucose in a real saliva sample. The results give a glucose amount of about 0.31 mM calculated by the calibration curve above reported. This correspond to about 5.41 mg/dL that is under the LoD of ACCU-CHECK Aviva (11 mg/dL).

### *4.3.2 – Aminoacids sensing*

The reversible mechanism ($NiOOH \rightarrow Ni(OH)_2 \rightarrow NiOOH$) of the Ni-based sensor, described above, can be applied to other redox active analytes such as aminoacids (AAs).

Recently, AAs monitoring is receiving a great interest from the scientific community due to their key role on metabolic diseases such as phenylketonuria [11].

In order to evaluate the versatility of the Ni-EC sensor device, the detection of the urinary Phe has been tested.

The sensing test was performed by adding various aliquots of Phe stock solution to diluted urine (1:1 PBS pH 11.2) obtaining final concentrations of 30 μM, 60 μM, 120 μM and 150 μM. Fig.26 (black square) shows the obtained results. A linear response of current density *vs* Phe

concentration was found and the data interpolation gives the following equation y=147.74+0.21*X (R2=0.99291), corresponding to a sensitivity of 0.21 μA $\mu M^{-1}$ $cm^{-2}$.

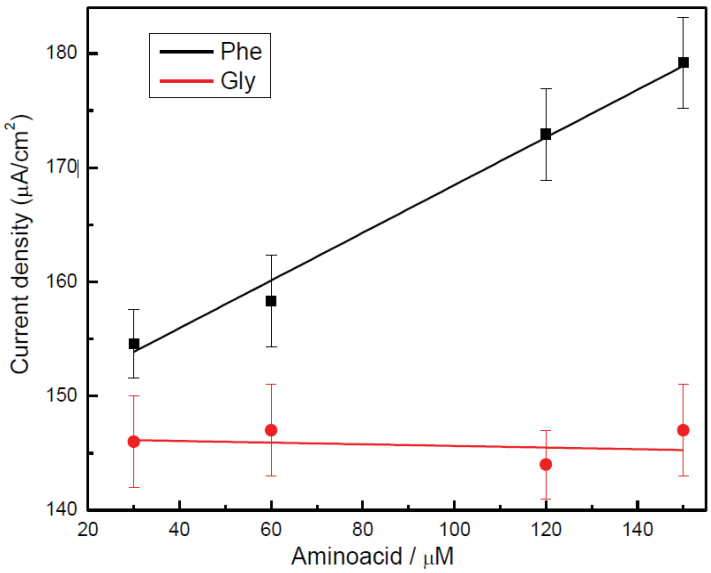


**Fig.26.** Ni-EC device urinary AAs detection (PBS pH 11.2): a) Phe and b) Gly.

To test the cross reactivity with another AAs molecule, Glycine (Gly) was used as probe analyte. Gly has higher potential oxidation value (anodic peak voltage is at 0.93 V at pH of 13.027) respect to the Phe (anodic peak voltage 0.33 V at pH 11.0). Therefore, it is expected to give no current signal at the potential of +0.8 V employed in the chronoamperometric experiment.

According to that, data reported in Fig.26 (red circle) show negative sensing response versus various amount of Gly in the range of 30-150 μM. The finding indicates a good specificity of this method to detect Phe in urine sample.

## Experimental Part

### 4.1 – CDC Silicon chip Technology for Real-Time PCR.

The Real Time PCR System is composed by the following components: (a) a disposable Chip that contains reaction chambers for the real time PCR process; (b) a portable and customized thermacycler instrument (Q3 reader) that thermally and optically drives the chip during the real time PCR process; (c) a Software Package that manages the PCR process and carried out the data analysis. The following figure reports the picture of the platform.


**Fig.27.** CDC platform: Q3 reader and smart-software.

*Microchip fabrication.*

The miniaturized disposable chip has been manufactured by using silicon VLSI (Very-large-scale integration) technology on a six inch silicon wafer (Figure 2). The chip (1.2 x 1.7 mm) contains temperature sensors and heaters integrated on the bottom of the device. They consist in AlCu metal strips (size 4.0 ± 0.1, spaced 5.0 ± 0.1 µm for the temperature sensor, size 115.0 ± 0.1 µm spaced 30.0 ± 0.1 µm for the heater). (b) a top part (ring) made in polycarbonate. A polycarbonate plastic ring, manufactured by molding technology, is glued onto the silicon part by silicone glue. This ring creates an architecture of 6 reaction chambers (3mm of radius) with cylindrical shape

featured by a total volume of 25 µL. The microchip is finally mounted on a plastic holder to facilitate the chip handling.

During the PCR cycles the thermal sealing is guarantee by 15 ul of paraffin wax dispensed on each chamber.

The device performs thermal cycling in combination with the driving Instrument (Q3-reader below described) with the following performances: temperature sensor maximum power consumption 55 mW, heater maximum power consumption 10 mW, temperature control accuracy of ± 0.2 °C, heating rate of 15 °C/s, cooling of rate: 8 °C/s and temperature resolution: 0.1 °C.

*Q3 Reader.*

The Q3 instrument reader was developed by STMicroelectronics (Fig.27). It thermally and optically drives the chip during the real time PCR process. It has a size of 14 L x 7.1 W x 8.7 H (cm) (weight: 322 g). The optical module contains up to 2 independent optical channels, for multiple Fluorescent reporters (FAM, VIC®). The LED light sources are centered at wavelength 470, 530 nm, respectively. The emission is detected by a CMOS camera that contains a high-pass filter at 520 nm or 20 nm wide band-pass filter centered at 556. Finally, the thermal Module drives the temperature sensor and heater of the chip to reach the Temperature Performance Characteristics.

*Smart-Software for image analysis.*

The Smart-Software was properly developed for the image analysis, it is based on three main core modules: 1) Fully automatic image quantification: a set of algorithms for the digital image analysis process; 2) Numerical computation: a set of algorithms for the numerical analysis of raw

data coming from Real time PCR, 3) Graphical output: a graphical user interface to show the fluorescence curves for the PCR.

*Chemicals.*

Hepatitis B virus (HBV) clone (ref. product CLO-05960116 HBV Complete Genome) and all the reagents for the HBV Real time PCR were purchased from Clonit (kit ref. product CLO-FO2 HBV MMIX KIT 48) and used according to the Instruction for Use.

*RTPCR experimental set up.*

Real time PCR experiments were performed using a Master Mix solution (volume 10 µL) containing Clonit buffer (1×) and Taq DNA polymerase, 0.5 µM of each forward and reverse primers, 2 µL of HBVclone ($10^5$ copies/µL). Different amount of probe (0.01, 0.05, 0.1 and 0.2 µM) were tested. The PCR cycling was performed in the portable Q3-thermocycler– reader by using the following thermal program: preheating period of 10 min. at 95 °C, followed by a maximum of 45 cycles of 95 °C for 15 s and 60 °C for 60 s. Different temperature of annealing were used for testing (60-63°C). Negative samples were prepared substituting the HBV clone with the same amount of water. Each experiment was repeated 10 times.

Same Real Time PCR experiments (10 µL of the above reported Master Mix) were executed on standard 96 well reaction plate in gold standard Applied Biosystem 7500 real time PCR equipment as reference.

**4.2 – PCR free electrochemical detection of DNA.**

*Materials.*

P1 probe (sequence: 5' HS-C6-GGT GAG TGA TTG GAG GTT) and P2 probe (sequence: 5'HS-C6-CAC ATC AGG ATT CCT AGG) were purchased from MWG (Germany). Hepatitis B virus (HBV) clone complete genome was purchased from Clonit (ref. 05960467) and consists in HBV genome 3.2 kbps and a plasmid PBR322 vector 3.8 kbps provided in a TE (Tris 10 mM, EDTA 1 mM, pH = 8) solution. Hybridization buffer, for electrochemical HBV assay, is a 20 mM sodium phosphate buffer, 1M NaCl, 5.2mM KCl, 0.1% Tween 20, 2x Denhardt's solution. Mycobacterium Tubercolosis (MTB) clone complete genome was purchased from Clonit (ref. 05960564) provided in a TE (Tris 10 mM,EDTA 1 mM, pH = 8) solution. Qiagen QIAamp DNA Mini Kit (Ref. 51306) was purchased by Qiagen KCl powder and 11-mercaptoundecane were purchased from Sigma Aldrich. All reagents used for the synthesis of $[Os(bpy)_2DPPZ]Cl_2$ were purchased by Sigma Aldrich.

*Microchip fabrication.*

The miniaturized device has been manufactured using the VLSI (Very Large Scale Integration) technology on a 6" silicon substrate. To electrically isolate the electrodes from the substrate e silicon oxide has been thermally grown. Then a platinum film has been sputtered and lithographically defined in the electrodes areas and contact zones (PAD). A passivation layer is then deposited (Silicon oxide by PECVD) to isolate the first metallization (Pt) form the second one (Au). A dry etch has been performed to connect the first and the second metallization where necessary (i.e. on interconnection tracks). The second metallization (Au) is then sputtered and lithographically defined in complementary electrodes regions and contacts areas. The final device is composed by four integrated electrochemical cells with three planar electrodes. In our study we used the cell featured by a working electrode (WE) made in Platinum with size 1000 × 2000 µm, a counter and a reference electrode (CE, RE) made both of gold with size 800 × 500 and 800 × 1250

µm, respectively. The electrode-to electrode distances are 100 µm. Each electrode was electrically isolate from the substrate by a silicon oxide layer thermally grown. The silicon device was mounted on a polycarbonate ring (size 1.3 cm x1.5 cm, thickness 3mm) to create 4 testing chambers (size 2.6 mm x 2.6 mm, thickness 3mm) of 20 µL each that contains on their floor the electrochemical electrodes. The complete structure is fixed on a plastic holder for easily handling (Fig.6).

*Working electrode chemical treatment.*

The Platinum WE surface, were properly chemically modified as follows: the WE was firstly cleaned by Oxygen plasma, 1000 watt for 5 min. After that, 10 µl of a solution containing sodium phosphate buffer (150 mM at pH 9.0) and two specific thyol 5'-terminated Forward and Reverse probes at final concentration of 20 µM were microdeposed (Perking Elmer Piezo array) on the WE surface and incubated in a climatic chamber at 30 °C, 90% RH for 4 hours. After several cleanings with deionized water to remove the unbinding P1 and P2 probes, the WE-modified surface was passivated (by microdeposition) with an ethanolic solution of 11-mercaptodecane (10 mM). Then, several ethanol washings followed by three washing in water of the electrode were carried out. All reactions were performed in a 1000 clean room. The contact angle measurements confirmed the goodness of each chemical treatment step, showing the wettability changes of the WE surface.

*Electrochemical measurements.*

Cyclic (CV) and Square-wave (SW) voltammetry measurements were carried out by a Parstat 2273 equipment (Princenton Applied Research). The CV and SW experiments were executed in the device microchamber (volume 20µl) using Potassium Chloride 5 mM as buffer with the follow conditions: scan rate of 10mV/s, pulse high/pulse width 0.025V for 0.05s and stop height 12mV.

Before each test, the Platinum substrate has been activated by about 50 sweeps of cyclic voltammetry in KCl. Both experiments were carried out by a Parstat 2273 equipment (Princenton Applied Research).

*SEM and AFM analysis.*

AFM analysis were performed with a Veeco-Innova microscope operating in amplitude mode, and ultra-sharpened Si tips were used (MSNL-10 from Veeco Instruments, with anisotropic geometry, radius of curvature ~2 nm, tip height ~2.5 μm, front angle ~15°, back angle ~25°, side angle 22.5°). AFM images were analyzed by Gwyddion free software. SEM images were obtained by using high performance Schottky field emission LEO 1550 SEM. Instrument operating at 5 kV in secondary electron imaging mode.

*Hybridization Experiments (HBV genome)*

The HBV genome hybridization on Pt-WE modified surface with P1 and P2 probe was carried out for 30 minutes at 50 °C in 20 μL of total volume containing various amount of the DNA target HBV clone (2000, 200, 20 and 2 copies) in 20mM sodium phosphate buffer, 1M NaCl, 5.2mM KCl, 0.1% Tween 20, 2x Denhardt's solution. After hybridization the electrode was washed three times with deionized water.

*Cross-reactivity with Mycobacterium tuberculosis (MTB)*

The cross-reactivity of our system assay was investigated by testing the Pt-WE modified with P1 and p2 probes specific for HBV-clone with unspecific target consisting in Mycobacterium tuberculosis clone (MTB complete genome purchased from Clonit (ref. 05960564)). The hybridization was carried out according the procedure described in the "Hybridization Experiments (HBV genome)" section. The electrochemical results (Fig.19) shows negligible SW signal for the

hybridization carried out with a total amount of 2000 copies of MTB-clone (blu line). For comparison SW signal before hybridization is also reported (orange line).

*Real Time PCR Experiments.*

Real Time PCR experiments were executed on standard 96 well reaction plate using Applied Biosystem 7500 real time PCR equipment. Experiments were performed using a Clonit kit ref product CLO-FO2 HBV MMIX KIT 48 and used according to the Instruction for Use. 10 µL of a Master Mix solution (purchased by Clonit) containing PCR buffer (1×), Taq DNA polymerase, 0.5 µM of each forward and reverse primers and 2 µL of standard HBVclone (2, 20 200 and 2000 total copies). The PCR cycles were: denaturation step 10 min. at 95°C, followed by 45 cycles of 95°C for 15s and 60°C for 60s. Negative samples were prepared substituting the HBV clone with the same amount of water. Each experiment was replicated 3 times.

*Real Sample DNA extraction.*

HBV genome extraction from human blood was carried out using the commercial kit Qiagen QIAamp DNA Mini Kit (Ref. 51306), according their Instructions for Use. All experiments were performed in compliance with the Approved Guideline *MM13-A: Collection, Transport, Preparation, and Storage of Specimens for Molecular Methods*, by Clinical and Laboratory Standards Institute (CLSI), recognized as consensus guideline by the U.S. Food and Drug Administration (FDA). The extraction experiments we executed in laboratories certified under ISO 9001 and ISO 13485.

**4.3 – Other applications of electrochemical detection technology.**

*Chemicals and Materials*.

All reagents used for sensing tests, Potassium Chloride, sodium hydroxide, PBS tablet and glucose were purchased by Sigma Aldrich and used as received. Phenylalanine (Phe) and glycine (Gly) were

purchased by Sigma Aldrich and used as received. Test slide (1cm x 3cm) for contact angle measurements was obtained by sputtering a Ni layer (nominally 10nm) on silicon substrate.

*Electrochemical device preparation.*

The Ni electrochemical device was manufactured using the VLSI technology on a 6" silicon wafer substrate. To electrically isolate the electrodes from the substrate, a silicon oxide layer has been firstly thermally grown (first passivation layer) [12]. Then a Nickel film has been sputtered and lithographically defined in the electrodes areas. A second passivation layer was then deposited (Silicon oxide by PECVD) to isolate the first metallization (Ni) form the second one (Au). A dry etch was performed to connect the first and the second metallization (i.e. on interconnection tracks). The second metallization (Au) was then sputtered and lithographically defined in complementary electrodes regions and contacts areas. The final device is composed by 4 electrochemical cells each containing three planar microelectrodes, working electrode (WE) in Nickel, a counter (CE) and a reference (RE) electrode made in gold. The geometrical features of four electrochemical cell typologies are the same reported in Table 1.

*Electrochemical measurements.*

Cyclic voltammetry (CV) and chronoamperometry measurements were carried out by a Parstat 2273 equipment (Princenton Applied Research), The CV experiments were executed using the follow conditions: scan rate 10mV/s, voltage range -0.1 V/ +1.0V. The chronoamperometry were performed at a fixed voltage of 0.78-0.8V. All measurements were carried out in PBS at various pH values. (7.4, 9.2, 11.2 and 13.0). Before each testing the Nickel substrate has been activated by about 60 sweep of cyclic voltammetry in NaOH 0.1M. Both experiments were carried out by a Parstat 2273 equipment (Princenton Applied Research).

*Electrode surface characterization.*

*Rutherford Backscattering Spectrometry (RBS) analysis.* The RBS spectra were acquired using a 2.0 MeV $He^+$ beam, with normal incidence and detection mode (165° backscattering angle, 3.5 MV HVEE Singletron accelerator system). RBS spectra were simulated through SimNRA software [13].

*Contact angle (CA) measurement*.

The static water contact angle measurements were performed by KRUSS contact angle meter with a water drop volume of 10ul. The test slide composed by Ni 10 nm thickness layer on Silicon substrate (size 1x3 cm) were manufactured with the same technology process for electrode preparation.

*X-ray Photoelectron Spectroscopy (XPS) characterization.*

The XPS analysis was performed using a Kratos AXIS-HS spectrometer. The Mg K1,2 of 1253.6 eV was used at the conditions of 10 mA and 15 keV with a pass energy of 40 eV. During the analysis the residual pressure in the chamber was $10^{-7}$ Pa. The spectra were acquired from 2 mm × 2 mm square area. Survey spectra were acquired at step energy of 1 eV and 300 ms of dwell time; core level spectral regions were acquired at step energy of 0.05 eV and 300 ms of dwell time. Quantitative composition was obtained using experimental atomic sensitivity factors. Spectra acquiring, processing and calculation of quantitative chemical composition were done employing the Vision 2 software by Kratos Analytical.

*Glucose Sensing.*

A stock solution of glucose at concentration of 60mM in PBS at pH 11.2 was prepared and used for all tests. Mock sample has been prepared using human plasma and saliva.

The fresh human blood was centrifuged (3500 rpm 5 min) to remove the blood cells portion and the plasma was diluted with the same volume of PBS (pH 11.2). The 1$^{st}$ type of mock sample was prepared directly into electrochemical device adding to 10 µl of 1:1 diluited plasma sample (calculated pH ~10.5) various aliquots of 3 µL of glucose stock solution obtaining final

concentration of 3.0mM, 12.0mM, 20.0mM, 25.7mM, 30.0mM and 33.4mM. Chronoamperometry measurements at +0.8V were recorded after each glucose aliquot addition.

Similarly, a volume of about 0.1 mL of saliva sample (2$^{nd}$ type of Mock) was collected and diluted with same volume of PBS pH 13 buffer. Also in this case the final mock sample was prepared directly into electrochemical cells adding to 10 µl of saliva various aliquots of glucose stock solution (volume 3 µL), obtaining a final concentration of 0.2mM, 2.0mM, 4.0mM, 6.0mM. The current values from chronoamplerometry at +0.78V were recorded after each glucose additions.

For comparison, glucose measurements from real human blood was carried out with the commercial ACCU-CHECK Aviva POC system from ROCHE.

*Aminoacids Sensing*.

A stock solution of Phe at concentration of 60 mM in PBS at pH 11.2 was prepared and used for all tests. An aliquot of 1 ml of fresh collected urine sample (containing endogenous Phe) was diluted with the same volume of PBS pH 13. 10 µl of this solution was loaded on the electrochemical device and the chronoamperometry measurements carried out at +0.78 V. After current stabilization, various aliquots of 3 µl of Phe stock solution were added, obtaining a final concentration of 30 µM, 60 µM, 120 µM, 150 µM. The current intensities from chronoamperometry at +0.78V were recorded after each phenylalanine additions. The sensing test for Glycine was carried out with the same procedure above described.

Endogenous Phe in the urine sample was measured by Tandem mass (MS-MS) spectrometry method using the NeoBase Non-derivatized MSMS kit (PerkinElmer 3040-0010) in the *Centro di riferimento per le malattie metaboliche ereditarie*" (AOU Policlinico–VE Catania, Italy).

## References


1. Lazzara A, Castagna ME, Giuffrida R, Conoci S (2015) Miniaturised LabonChip for Bio-Chem Analysis.
2. T. Defever, M. Druet, D. Evrard, D. Marchal and B. Limoges, Anal. Chem., 2011, 83, 1815–1821.
3. S. Petralia, M. E. Castagna, E. Cappello, F. Puntoriero, E. Trovato, A. Gagliano and S. Conoci, Sens. Biosensing Res., 2015, 6, 690.
4. A. Ulianas, Y. H. Lee, A. H. Sharina and L. Tan Ling, Sensors, 2011, 12, 5445–5460.
5. A. Ulianas, Y. H. Lee, A. Musa, L. Han-Yih, I. Zamri and L. L. Tan, Sens. Actuators, B, 2014, 190, 694–701.
6. Tian K., Prestgard M. and Tiwari A. (2014), "A review of recent advances in nonenzymatic glucose sensors", Materials Science and Engineering C 41, 100–118.
7. Fleischmann M., Korinek K., and Pletcher D. (1971), "The oxidation of organic compounds at a nickel anode in alkaline solution", J Electroanal Chem. 31-39.
8. Iwu K.O., Lombardo A., Sanz R., Scirè S. and Mirabella S. (2016), "Facile synthesis of Ni nanofoam for flexible and lowcost nonenzymatic glucose sensing", Sensors and Actuators B, 224, 764–771.
9. Petralia S., Mirabella S., Strano V. and Conoci S. (2017), "A Miniaturized Electrochemical System Based on Nickel Oxide Species for Glucose Sensing Applications", Bionanoscience 7, 58-63.
10. Zhang W., Du Y., Wang M.L. (2015), "Non Invasive Glucose Monitoring using Saliva nano-biosensor", Sens Biosensing Res 4, 23-29.
11. Donlon J., Sarkissian C., Levy H.L. and Scriver C.R. (2015), "Hyperphenylalaninemia: Phenylalanine Hydroxylase Deficiency", Scriver's Online Metabolic and Molecular Bases of Inherited Disease, doi: 10.1036/ommbid.97.

12. S. Petralia, M. E Castagna, E. Cappello, F. Puntoriero, E. Trovato, A. Gagliano and S. Conoci, A miniaturized silicon based device for Nucleic Acids electrochemical Detection. Sens Biosensing Res 6 (2015) 90–94

13. M. Mayer (1999), SIMNRA, Simulation Program for the Analysis of NRA, RBS and ERDA, Proceedings of the 15th International Conference on the Application of Accelerators in Research and Industry, J. L. Duggan and I.L. Morgan (eds.). AIP Conf. Proc. 475 541–544

# 5. DNA CLONING IN THE ELECTROCHEMICAL DETECTION OF ENVIRONMENTAL ANALYTES.

This chapter reports the activity carried out during a visiting period at the University of Lausanne (Switzerland, February-August 2017), working in the scientific group of Professor Jan Roelof Van der Meer. The research has been devoted to the development of a molecular method consisting in a genetic cloning that has been coupled with the electrochemical device, described in the chapter 4, for the detection of environmental analytes in liquid matrix.

**5.1 – Whole-cell environmental biosensor.**

The great potential of both the proposed electrochemical device and the molecular methods stimulate a new study towards other possible sensing applications. In particular, I focused on the detection of Arsenite (AsIII) in potable water, using a specific bacterial bioreporter strain in combination with the EC device. This strain was obtained by a molecular cloning experiment performed on Escherichia coli enterobacteria, in order to be sensitive to the AsIII analyte.

**5.2 – Molecular cloning procedure.**

During the visiting period at the University of Lausanne, I have been learning and improving my expertise in molecular cloning and genetic recombination process, necessary to obtain a modified bacterial strain for biosensing applications.

The molecular cloning is a series of biological methods and reactions used together to insert a recombinant DNA fragment (one or more fused genes) into a molecular vector to be replicated in

a host bacterial organism; in this way, the recombinant fragment will be expressed into the host, carrying new biological features.

In the cloning process, two, or more, DNA fragments to be fused (A and B) are isolated from a prokaryotic genome. Subsequently, both vector and inserts must be cut and purified. The purified fragments are, finally, joined together and with the vector, so that they can be transferred into the host (Fig.1).

The molecular vector I used for the cloning experiment, was a plasmid DNA that can replicate in bacterial cells and is easy to be manipulated.

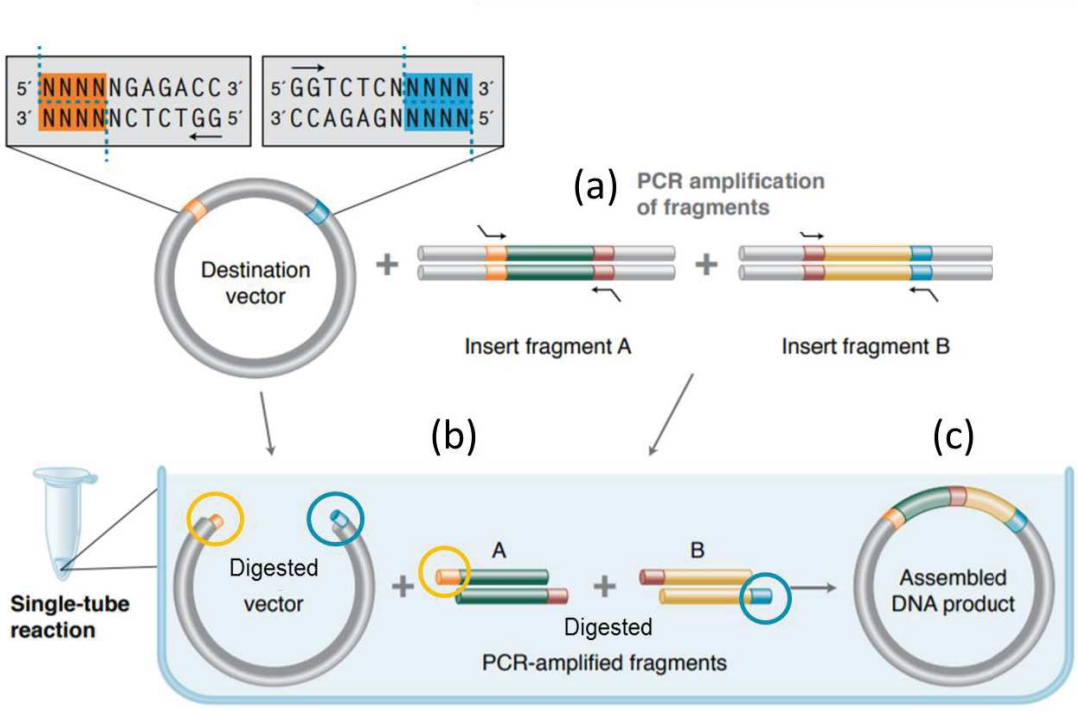


**Fig.1.** Molecular cloning experiment: (a) PCR on DNA fragments; (b) vector and fragments digestion; (c) plasmid ligation. Orange and blue ring highlight the linker region between vector and inserts. Arrows indicate the linker regions added to the DNA fragments.

To purify the insert DNA from the original genome, is necessary a first cutting step called *digestion,* performed by specific restriction enzymes; these are able to cut immediately outside the DNA fragment of interest without damaging the sequence and the instructions contained in the insert itself.

There exist many different restriction enzymes (such as EcoRV, BamHI, HindIII, etc.) with different DNA cutting sites that allow a very precise cut and insertion of a DNA fragment into the vector; these sequences are, mostly, concentrated within multiple cloning site (MCS) regions and plasmids containing MCS are, normally, preferred as cloning vector. Once digested, the insert DNA is collected in a test-tube in order to be fused with other inserts to create new recombinant fusion gene/polypeptides. The fusion process is obtained starting from a PCR reaction (Fig.1a) based on specific modified primers that, after a certain number of amplification cycles, create linker regions inside the DNA fragments able to stick each other (compatible ends). These insert-linker PCR products and the vector are, then, digested (Fig.1b) to open the fusion sites for the final *ligation* step; restriction enzymes for digestion are used in couples, so that can digest the DNA fragments in such a way that they can only be inserted in one possible direction into the vector plasmid (orange and blue ring in Fig.1b). For the final ligation step, then, a ligase enzyme links together the inserts and these with the digested vector, completing the inserts cloning. The recombinant assembled plasmid (Fig.1c) is, finally, introduced into the host bacterial cell to be expressed, through a process called *transformation*. In this process, E. coli cell membrane is permeabilized, through heat shock treatment or electroporation, to allow the plasmids to enter. After the transformation, host cells are let growing overnight to obtain a new bacterial generation, i.e. the bioreporters expressing a phenotype carried by the recombinant plasmid (Fig.2).

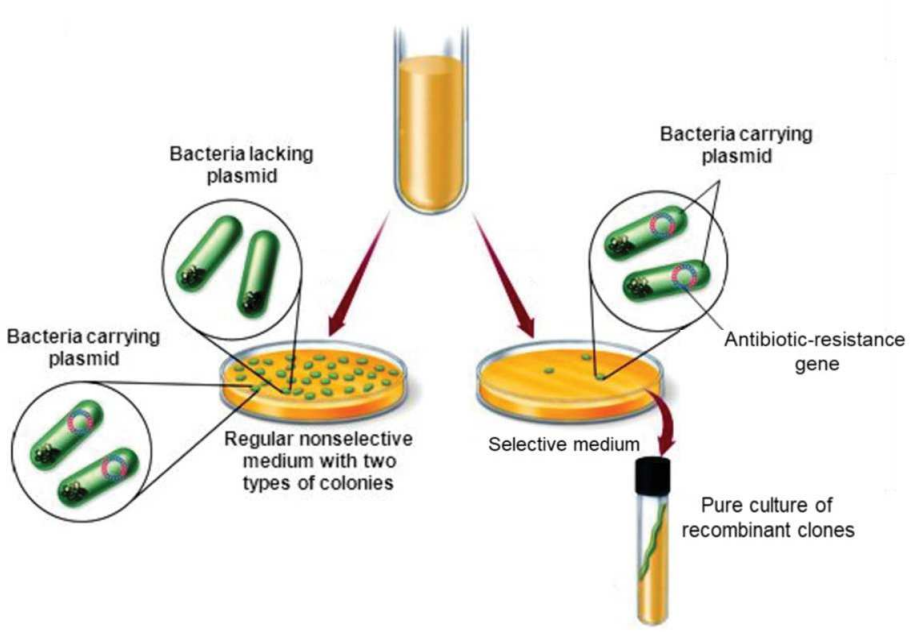


**Fig.2.** Growth and selection of clones containing the recombinant plasmid.

A selective growth medium is prepared with specific antibiotic, such as ampicillin, to select the clones of interest; among the phenotypes carried by the plasmid, in fact, the antibiotic resistance allows only the recombinant clones/bioreporters to growth. Finally, a pure culture of them is prepared so that the bioreporters can be used in the biosensing test.

**5.3 – Electrochemical detection of Arsenite in potable water by using the E. coli bioreporter.**

The AsIII bioreporter, obtained by using the molecular cloning technique described in section 5.2., is an E. coli modified strain that contains a plasmid (pMV132-arsR-ABS) in which the *ars* operon promoter sequence[1] ($P_{ars}$) is fused, downstream, to the *ars*R[2] and *lac*Z[3] gene.

[1] Promoter is a region of DNA that initiates the transcription of a gene; $P_{ars}$ promoter is specific for the cluster of genes encoding the detoxification system of arsenate (*ars* operon).
[2] ArsR is a regulatory protein that repress $P_{ars}$ activity if bound to DNA.
[3] The *lac* (lactose) operon is a genetic cluster required for the transport and metabolism of lactose in E. coli; *lac*Z gene encodes β-galactosidase enzyme.

Thanks to this genetic modification, when the AsIII enters the cell, the ArsR protein releases from its DNA binding site, downstream the $P_{ars}$ sequence, to bind AsIII similar as for the original arsenate resistance mechanism [1]; in this way, $P_{ars}$ is free to increase the expression level of *lac*Z gene, resulting in the synthesis of β-galactosidase (Fig.3A). This enzyme is able, then, to cleave the para-aminophenyl-glucuronidase (PAPG) producing para-aminophenol (PAP), Fig.3B [2,3].

Once released by the cell, PAP can interact with the Pt-WE, in the EC device, and trigger a redox process producing a current signal that is electrochemically detectable and quantifiable by CV measurements.

In this way, depending on the presence and amount of AsIII in water, the PAP is more produced, and the pollutant is detectable. How much PAP (so β-Gal) is synthesized is dependent on how much AsIII is encountered by the cells and how long the cells are exposed to it.

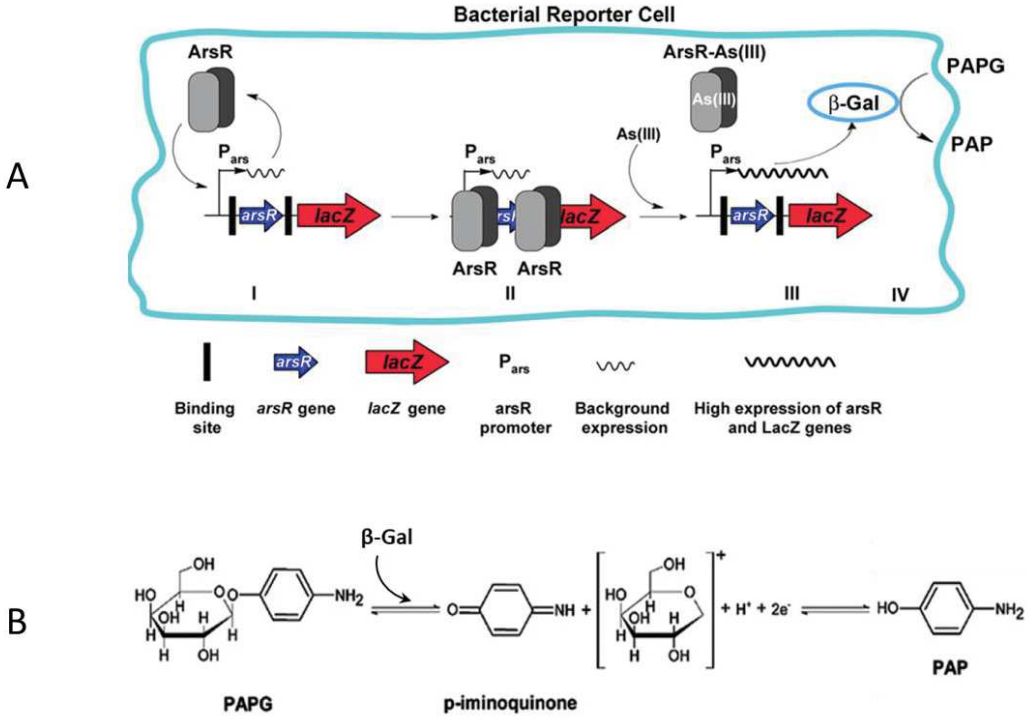


**Fig.3.** A) Genetic pathway in E. coli AsIII bioreporter. B) PAPG transformation in PAP by β-galactosidase.

E. *coli* bioreporter samples were prepared according the procedure reported in the *Experimental Part* at the end of this chapter.

The system described in Figure 4 was used for the CV measurements. Basically, the Pt-EC device (described in chapter 4) was interfaced to an integrated and miniaturized board and MATLAB software.

A

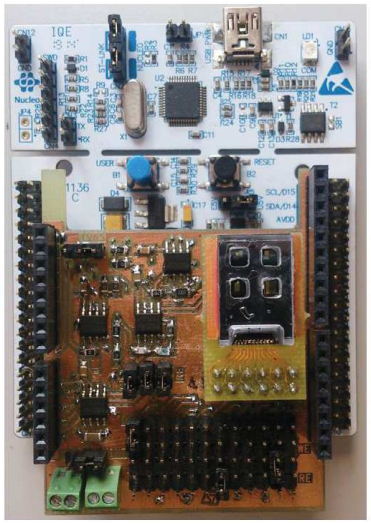

B

**Fig.4.** A) EC board and device for CV measurements. B) Laptop connection for analysis.

The first CV measurements on reference samples gave the expected peaks at +0.8 V for PAPG (Fig.5A) and +0.45 V for PAP (Fig.5B), proving the functioning of the EC board.

A

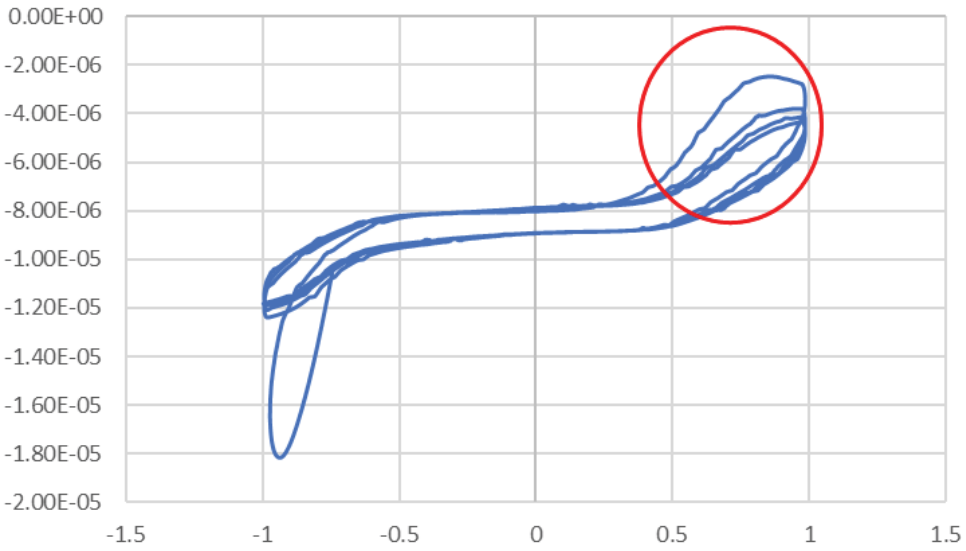

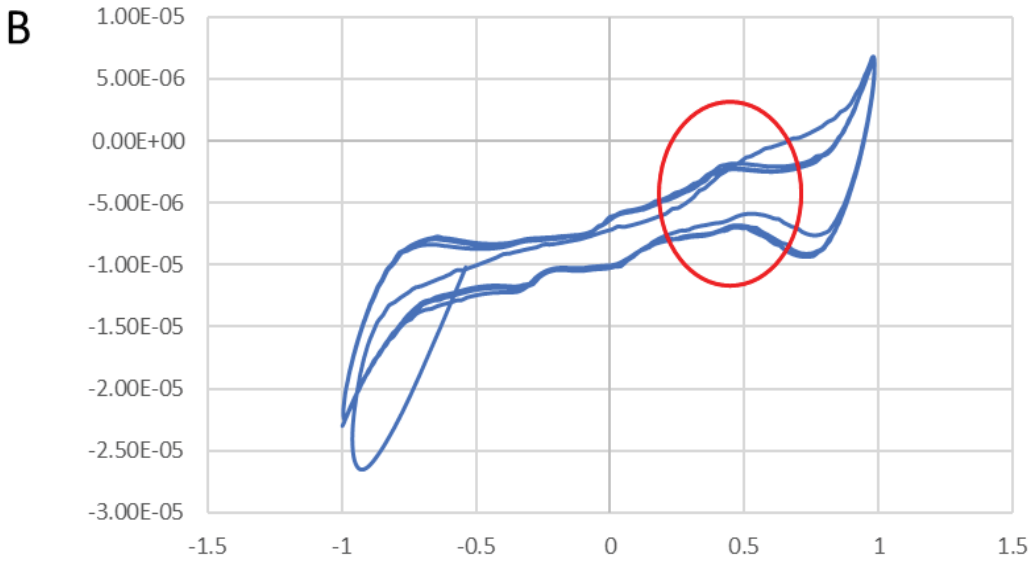


**Fig.5.** PAPG (A) and PAP (B) CV plot. Red rings highlight the anodic peak for both analytes.

Then, CV measurements of pre-treated E. coli cells with water at different AsIII concentrations were performed. In this case, the anodic peak of PAP appeared again with a trend directly related to the specific amount of AsIII in water sample (Fig.6A-B).

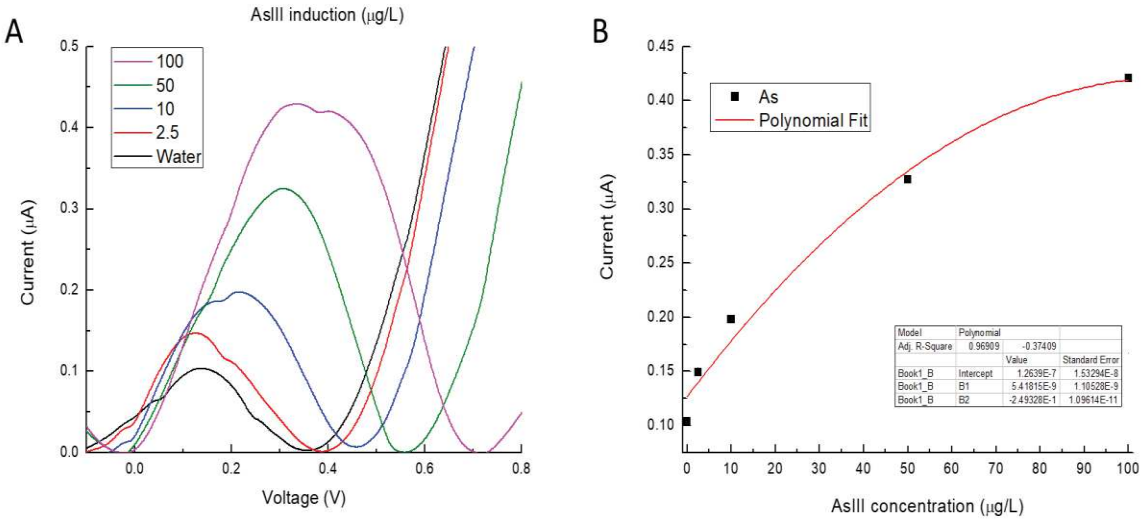


**Fig.6.** A) CV curves of PAP current signal from E. coli sample. B) Plot of PAP peaks.

To test the specificity of this detection system, a cross reactivity experiment by substituting the Arsenite analyte with Mercury (HgII) was performed. The experimental conditions (cells preparation and CV measurements) were the same used for the AsIII electrochemical detection.

Results of cross reactivity test are reported in Fig.7. It can be noticed that, notwithstanding the exposure to increasing concentrations of HgII, E. coli bioreporters didn't increase the PAP expression level, since are sensitive only to AsIII; no anodic peaks intensity trend, in fact, is visible in the HgII CV plot (red line in figure) compared to that one from the AsIII induction of PAP expression (black line).

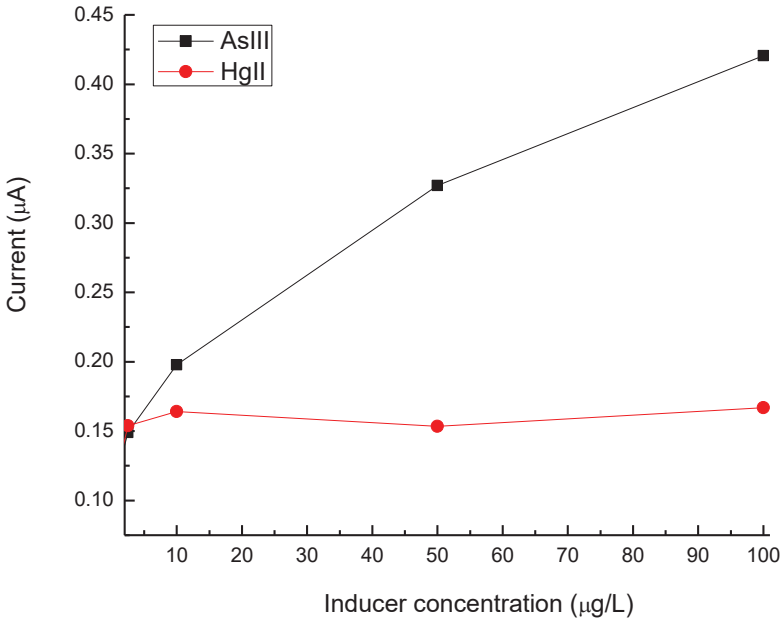


**Fig.7.** AsIII-HgII induction comparison.

These results, all together, proved that, thanks to the proposed EC system, AsIII contamination in water is detectable with high precision and sensitivity (up to 10 μg/L). Moreover, miniaturization and integration in the EC device and board remove the requirement of a laboratory that is an ideal condition to perform an in situ AsIII monitoring in water.

## Experimental Part

*E. coli bioreporter sample preparation.*

To prepare the cell suspension for the assay, the E. coli strain was plated in LB-agar + ampicillin 100 µg/ml. Subsequently, a culture in 20 mL LB + ampicillin 100 µg/ml was prepared and kept at 21°C overnight. The day after, the culture was diluted 2X in tap water (or MOPS without glucose), in a final volume of 4 mL, up to an optical density of 0.6-1. The dilution has been incubated, then, with $NaAsO_2$ at concentration of 0-2.5-10-50-100 µg/L and incubated at 30°C for 2 h. Subsequently, induced cells have been added with 20 mM of PAPG, in order to trigger the PAP production, and samples have been immediately used for the final electrochemical assay. In parallel, PAPG/PAP 10 mM standard solutions have been prepared and used as reference samples.

*Electrochemical measurements.*

To perform the CV measurements, the EC device was interfaced to an integrated and miniaturized board, developed by STMicroelectronics (Fig.4A). The board was linked to a laptop via USB connection (Fig.4B) and the RealTerm and MATLAB software were used to manage, respectively, the electronic settings for CV experiments and the data output/post-processing.

## *References*


1. Cervantes C., Ji G, Ramírez JL, Silver S (1994), Resistance to arsenic compounds in microorganisms, FEMS Microbiol Rev. 1994 Dec;15(4):355-67.
2. Stocker J., Balluch D., Gsell M., Harms H., Feliciano J., Daunert S., Malik K.A., Van der Meer J.R. (2003), Development of a set of simple bacterial biosensors for quantitative and rapid measurements of arsenite and arsenate in potable water, Environmental Science and Technology 37 (20), 4743–4750.
3. Cortés-Salazar F., Beggah S., Van der Meer J.R., Girault H.H. (2013), Electrochemical As(III) whole-cell based biochip sensor, Biosensors and Bioelectronics 47 (2013) 237–242.

# 6. CONCLUSIONS.

The present Ph.D. project was focused on the development of innovative and easy-to-use Point-of-Care (PoC) technological platforms for DNA analysis (from extraction to detection), implemented into portable and miniaturized devices. The genetic PoC are systems integrating all steps necessary for the molecular analysis such as sample preparation (extraction and purification of DNA) and detection (*i.e.* PCR or real time PCR) and they should be able to perform *in vitro* genetic analysis by unskilled personnel near to the patient, in hospital, in the physician office, clinic or home with rapid answer and low cost.

In this view, my research activity addressed three main modules:

1. **Development and characterization of a miniaturized platform for DNA extraction.**
2. **Development and characterization of miniaturized systems for DNA detection with both optical transduction methods (via RT-PCR) and electrical methods (electrochemical detection).**
3. **Development of molecular methods for the detection of environmental analytes.**

In a first module, two DNA extraction technologies were studied and characterized in terms of analytical performances. The first of them was the *DNA-on-disk technology*, which is an advanced magnetic beads-based technological platform in which all steps and reagents, required for the DNA isolation, are integrated in a plastic disk. By using a microfluidic system and a series of rotations, this PoC technology is able to extract Hepatitis B Virus genome at a concentration of $10^5$ copies/reaction (typical of infectious diseases), as confirmed by Real Time PCR quantification data. The extraction was performed with an extreme simplification of manual skill and time but, at the

same time, with a partial loss of DNA caused by the magnetic beads absorption process and the plastic material used to assemble the disk. This issue was overcome by the second technological platform employed for the DNA extraction. This platform was based on silicon material offering several advantages related to its physical properties (low heat capacity, good thermal conductivity, etc.). More specifically, the second DNA extraction platform consisted in a miniaturised biofilter composed by silicon micropillars. This device was able to extract analytical samples of HBV genome at the same concentration used in the previous experiment ($10^5$ copies/reaction), but without loss of DNA and with a high extraction efficiency; this was about 16% higher than that measured with a commercial kit (such as Qiagen and Magazorb), which is probably the result of a synergy between the filter structure, the material and the experimental protocol adopted.

The second module of my Ph.D. project was focused on the development and functional characterization of miniaturized devices for the DNA detection. The first device was a miniaturised silicon microchip for Real Time PCR analysis. The core of the device was a hybrid-chip composed by a silicon part containing integrated temperature sensors and heaters and a polycarbonate portion mounted on the plastic ring. The experiments were performed on HBV target genome using different annealing temperatures and different HBV probe amounts. Results showed an improvement of sensitivity of about 1 Log (3.3 Ct), if compared to conventional PCR technologies (Applied Biosystems).

However, the silicon device didn't solve the issue of the experimental procedure, in terms of costs and time, required by the PCR analysis itself. For this reason, I have been working, in parallel, on the introduction of a first example of PCR-free technology integrated in a miniaturized electrochemical device. The functional testes, with analytical and real sample of HBV genome, proved that this integrated miniaturized platform can detect the pathogen DNA without any amplification step; 200 copies/reaction of HBV genome were detected with a LoD comparable to

the standard real-time PCR method and a high specificity, as confirmed by the cross-reactivity test with Mycobacterium Tuberculosis genome. These results were described in a paper published on Analyst journal awarded by the Cover Page.

Moreover, the miniaturized electrochemical device proposed for the PCR-free DNA detection was found to be very versatile in the detection of other redox active species such as amines, glucose and aminoacids analytes.

Actually, it was used for the detection of the heavy metals. A sensing activity towards the para-aminophenol (PAP), for the heavy metals contamination monitoring in water was proved by using genetically modified E. *coli* AsIII bioreporters in combination with the miniaturized EC device. It was possible to measure and quantify the arsenate amount in water sample, with high specificity (no trend for HgII analyte) and sensitivity (up to 10 µg/L).

The glucose sensing tests, performed on real samples (human plasma and saliva) and upon a Nickel modification of the EC device, showed, also, positive results comparable to the commercial PoC system ACCU-CHECK Aviva (for plasma glucose sensing, 61.56 mg/dl from Ni-EC device *versus* 75 mg/dl from ACCU-CHECK Aviva).

For the aminoacids sensing, the Ni-EC device measured Phenylalanine, an important marker for the phenylketonuria disease, in real urine sample with very reliable results. Additionally, the device showed a good specificity for this aminoacids respect to Glycine, as reported from the cross-reactivity test.

These findings, all together, encourage to start a systematic study on organic compounds detection, paving the way to future development of versatile PoC biochemical sensors.

# 7. PUBLICATIONS AND EDUCATION

## 7.1 Published Papers

1. Libertino S, Conoci S, Santangelo MF, Pagano R, **Sciuto EL**, Sinatra F, Sanfilippo D, Fallica G and Lombardo S, "*Optical and Electrical Si-Based Biosensors: Fabrication and Trasduction Issues*", Analytical & Bioanalytical Techniques, 2014, *S12*- ISSN: 2155-9872, DOI: 10.4172/2155-9872.S12-007
2. M.F. Santangelo, **E.L.Sciuto,** A.C.Busacca, S.Petralia, S. Conoci, S. Libertino, "*SiPM as miniaturized optical biosensor in DNA-microarray applications*", Sensing and Bio-Sensing Research, Elsevier, vol.6, pp. 95-98, 2015
3. M. Favetta, A. Valletta, G. Fortunato, M.E. Castagna, S. Conoci, **E.L. Sciuto,** T. Cosentino, F. Sinatra, S. Libertino, "*Development of Si-based Electrical Biosensors: simulations and first experimental results*", Sensing & Bio-Sensing Research, Elsevier vol.6, pp. 72–78, 2015.
4. **E.L. Sciuto**, M.F. Santangelo, G. Villaggio, F. Sinatra, C. Bongiorno, G. Nicotra, S. Libertino, "*Photo-physical characterization of fluorophore* $Ru(bpy)_3^{2+}$ *for optical biosensing applications*", Sensing and Bio-Sensing Research, Elsevier, vol.6, pp. 65-71, 2015
5. M.F. Santangelo, **E.L. Sciuto,** S. Lombardo, A.C. Busacca, S. Petralia, S. Conoci, S. Libertino, "*Si photomultipliers for bio-sensing applications*", Journal of Selected Topics in Quantum Electronics, 2016 (doi: 10.1109/JSTQE.2015.2504979).
6. S. Petralia, **E.L. Sciuto**, S. Conoci, "*A Novel Miniaturized Biofilter based on Silicon Micropillars for Nucleic Acid Extraction*", Analyst, November 2016 (doi: 10.1039/C6AN02049F).
7. S. Petralia, **E.L. Sciuto,** S. Mirabella, M.L. Di Pietro, M. Zimbone, S. Conoci, "*Innovative Chemical Strategy for PCR-free Genetic Detection of Pathogens by an Integrated Electrochemical Biosensor*", Analyst, March 2017 **(Cover Page)**.

8. S. Petralia, T. Cosentino, F. Sinatra, M. Favetta, P. Fiorenza, C. Bongiorno**, E.L. Sciuto,** S. Conoci and S. Libertino, "*Silicon Nitride Surfaces as Active Substrate for Electrical DNA Biosensors*", Sensors and Actuators B Chemical, June 2017
9. Salvatore Petralia, Francesco Rundo, Sabrina Conoci, **Emanuele L. Sciuto**, Salvatore Mirabella and Francesco Priolo, "*Miniaturized Electrochemcial Cells for Sensing Applications*", Proceedings of the IEEE journal, 2017.
10. Salvatore Petralia, Francesco Rundo, Sabrina Conoci, Maria L. Di Pietro, **Emanuele L. Sciuto** and Salvo Mirabella, "*Electrochemical Biosensor for PCR free Nucleic Acids Detection*", Proceedings of the IEEE journal, 2017.
11. S. Petralia, **E.L. Sciuto**, M.A. Messina, A. Scandurra, S. Mirabella, F. Priolo and S. Conoci, "*Miniaturized and Multi-Purpose Electrochemical Sensing Device based on thin Ni Oxides*", submitted for publication to Sensor and Actuator B: Chemical (Elsevier)
12. S. Petralia, **E. L. Sciuto**, M. F. Santangelo, S. Libertino, M. A. Messina, and S. Conoci, A miniaturized Silicon photomultiplier for optical monitoring of sulphide species in water samples submitted for publication to Analytical Method (RSC)

## 7.2 Conferences

1. S. Petralia, E.L. Sciuto (poster presentation), M.L. Di Pietro, M. Zimbone, Maria G. Grimaldi and S. Conoci, "*Electrochemical Biosensor for PCR free Nucleic Acids Detection*", FisMat 2017, Trieste, Italy, October 1-5, 2017.
2. S. Petralia, S. Mirabella, E. L. Sciuto (poster presentation), F. Priolo and S. Conoci, "*NiO based nanostructures for sensor devices*", FisMat 2017, Trieste, Italy, October 1-5, 2017

3. Salvatore Petralia, Francesco Rundo, Sabrina Conoci, Maria L. Di Pietro, Emanuele L. Sciuto and Salvo Mirabella, "*Electrochemical Biosensor for PCR free Nucleic Acids Detection*", ECCTD 2017 - European Conference on Circuit Theory and Design, Catania, Italy, September 4-6, 2017
4. Salvatore Petralia, Francesco Rundo, Sabrina Conoci, Emanuele L. Sciuto, Salvatore Mirabella and Francesco Priolo, "*Miniaturized Electrochemcial Cells for Sensing Applications*", ECCTD 2017 - European Conference on Circuit Theory and Design, Catania, Italy, September 4-6, 2017
5. S. Petralia, E. L. Sciuto (oral presentation), T. Cosentino, F. Sinatra, P. Fiorenza, C. Bongiorno, S. Conoci and S. Libertino, "*Silicon Nitride surface for Biosensing applications*", E-MRS conference, Strasbourg, May 2017.
6. S. Petralia, E. L. Sciuto (oral presentation), T. Cosentino, F. Sinatra, P. Fiorenza, C. Bongiorno, S. Conoci and S. Libertino, "*Silicon Micropillars for pathogen Nucleic Acids isolation from biological sample*", E-MRS conference, Strasbourg, May 2017.
7. S. Petralia, E.L. Sciuto (oral presentation), S. Mirabella, M.L. Di Pietro, M. Zimbone, S. Conoci, "*A novel electrochemical biosensor for PCR-free nucleic acids detection*", 5th International Conference on Bio-Sensing Technology, Riva del Garda (TN), Italy, May 2017.
8. E. L. Sciuto (poster presentation), S. Petralia, M. Urso, F. Priolo, S. Mirabella, S. Conoci**,** "*Ni(OH)/Ni electrochemical biosensor for high sensitive glucometer*", 5th International Conference on Bio-Sensing Technology, Riva del Garda (TN), Italy, May 2017.
9. E. L. Sciuto (oral presentation), S. Petralia, T. Cosentino, M. Favetta, M. F. Santangelo, F. Sinatra, P. Fiorenza, C. Bongiorno, S. Conoci and S. Libertino, "*Comparison between thermal Silicon Oxide and Silicon Nitride surfaces for Biosensing applications*", Materials.it, Catania, Italy, December 2016.

10. S. Petralia, E.L. Sciuto (oral presentation), S. Mirabella, M.L. Di Pietro, M. Zimbone, S. Conoci, "*DNA electrochemical detection strategy on miniaturized silicon sensor*", Materials.it, Catania, Italy, December 2016.
11. S. Petralia, E.L. Sciuto (poster presentation) and S. Conoci, "*Silicon Miniaturized micropillars for Nucleic Acid Extraction*", Materials.it, Catania, Italy, December 2016.
12. E.L. Sciuto (poster presentation), M.F. Santangelo, G. Villaggio, F. Sinatra, C. Bongiorno, G. Nicotra, S. Libertino, "*Photo-physical characterization of fluorophore* $Ru(bpy)_3^{2+}$ *for optical biosensing applications*", 4th International Conference on Bio-Sensing Technology, Lisbon, Portugal, May 2015.

## 7.3 Courses attempting and schools

- "Lausanne Genomics Days 2017", Course & Workshop. Lausanne, Switzerland, February 2017.
- "Corso di Scientific Writing", Dipartimento di Scienze Chimiche, Catania, June 9-10 2016.
- "Materiali e Dispositivi a base di Silicio per l'analisi del DNA", CNR-IMM sede, Catania, May 16-19 2016.
- "La simulazione di sistemi complessi nella scienza dei materiali", CNR-IMM sede, Catania, May 16-19 2016.
- "Ph.D. Days, per una ricerca di qualità", Università degli Studi di Catania, Catania, April-June 2015.

## 7.4 Education and training

- Science & Technology Seminar at the IBM Research – Zurich, "*Novel electrochemical biosensors for PCR-free pathogen nucleic acids detection and glucose sensing*", July 12th, 2017, Zurich - Säumerstrasse 4, CH-8803 Rüschlikon, Switzerland.

- Visiting period at the University of Lausanne, "*Development of Escherichia coli genetic bioreporters for heavy metals monitoring in water*". February 1st - August 1st, 2017, Lausanne, Switzerland. Technical skills:
    - molecular cloning for the development of recombinant plasmid;
    - electrochemical assay of the E. *coli* mutant strains.
- Materiali e Dispositivi a base di Silicio per l'analisi del DNA (Dr. Sabrina Conoci). May 16-19, 2016, CNR-IMM sede, Catania – 3 CFU.
- La simulazione di sistemi complessi nella scienza dei materiali (Dr. Antonino La Magna). May 16-19, 2016, CNR-IMM sede, Catania – 3 CFU.
- Proprietà meccaniche dei materiali massivi e nano strutturati (Prof. Antonino Pollicino). July 13-14-15, 2015, Catania– 3 CFU.
- Metodologie di preparazione e modifica di nano strutture (Prof. Antonio Terrasi). June 29-30/July 1, 2015, Catania – 2 CFU.
- Tecniche spettroscopiche per l'analisi dei materiali, Palermo – 6 CFU:
    - luminescenza risolta in tempo (Prof. Marco Cannas), January 27, 2015;
    - spettroscopia Raman (Dr. Simonpietro Agnello), January 28, 2015;
    - simulazione computazionale (Dr. Francesco Ferrante), January 29, 2015;
    - assorbimento raggi X (Dr. Francesco Giannici), January 30, 2015.

# Acknowledgments

*I would like to thank Prof. Maria Grazia Grimaldi for the great opportunity, she gave me, to improve my scientific background and knowledges during these 3 years Ph.D. project.*

*Thank to Dr. Sabrina Conoci and Dr. Salvatore Petralia who taught me everything was necessary to work in this beautiful multidisciplinary scientific field of Nanotechnologies.*

*Thank to my kind colleagues Giuseppe Tosto and Dr. Maria Grazia Amore who I shared this beautiful experience and funny lab moments with.*

*Thank to Prof. Jan Roelof Van der Meer and Dr. Siham Beggah Möller for the beautiful work and life experience in Lausanne, where I had the opportunity to improve my scientific skills working with a wonderful team.*

*Last but not least, thank to my beautiful family, composed by my girlfriend and lifemate Federica, my sister Valentina, my mom Pinuccia and my dad Giuseppe who taught me how to face life adversities believing in myself and my abilities.*

*Thank you.*